UNIVERSITÉ DU QUÉBEC À MONTRÉAL

PROPRIÉTÉS MAGNÉTIQUES, MINÉRALOGIQUES ET SÉDIMENTOLOGIQUES DES SÉDIMENTS PROFONDS DE LA BAIE DE BAFFIN: CHRONOLOGIE ET DYNAMIQUE DES GLACIERS OUEST GROENLANDAIS, INNUITIENS ET LAURENTIDIENS AU COURS DE LA DERNIÈRE GLACIATION

THÈSE

PRÉSENTÉE

COMME EXIGENCE PARTIELLE

DU DOCTORAT EN SCIENCES DE LA TERRE ET DE L'ATMOSPHÈRE

PAR

QUENTIN SIMON

MARS 2013

«What makes you think she is a witch?
- Well, she turned me into a newt.
- A newt?
- I got better. Burn her anyway! Burn her! Burn! Burn her!...
- Quiet! Quiet! Quiet! Quiet! There are ways of telling whether she is a witch.
- Are there? Ah? Tell us! Tell us!... Do they hurt?
- Tell me. What do you do with witches?
- Burn! Burn! Burn! Burn them up! Burn!...
- And what do you burn apart from witches?
- More witches! Shh! Wood!
- So, why do witches burn?
- B--... 'cause they're made of... wood?
- Good! Heh heh. So, how do we tell whether she is made of wood?
- Build a bridge out of her.
- Ah, but can you not also make bridges out of stone?
- Oh, yeah. True. Uhh...
- Does wood sink in water?
- No, it floats! It floats!
- Throw her into the pond! The pond! Throw her into the pond!
- What also floats in water?
- Bread! Apples! Uh, very small rocks! Cider! Uh, gra--gravy! Cherries! Mud!...
- A duck!
- Oooh.
- Exactly. So, logically...
- If... she... weighs... the same as a duck,... she's made of wood.
- And therefore?
- A witch! A witch! A witch! A witch!...
- Here is a duck. Use this duck.
- Very good. We shall use my largest scales. Right. Remove the supports!
- A witch! A witch! A witch!
- It's a fair cop.
- Burn her! Burn her! Burn her! Burn her! Burn! Burn!...
- Who are you who are so wise in the ways of science?
- I am Arthur, King of the Britons."
- My liege!
- Good Sir knight, will you come with me to Camelot, and join us at the Round Table?
- My liege! I would be honored.
- What is your name?
- Bedevere, my liege.
- Then I dub you Sir Bedevere, Knight of the Round Table.»
Monty Python and the Holy Grail

AVANT-PROPOS

Cette thèse a été rédigée sous forme de trois articles en anglais formant chacun un chapitre. Le premier article a été publié en 2012 dans Geochemistry, Geophysics, Geosystems (doi:10.1029/2012GC004272), revue à comité de lecture (éditeur en chef,. éditeur associé et 2 réviseurs). Le deuxième article a été soumis à Paleoceanography (2012PA002397), revue à comité de lecture (éditeur en chef et 2 réviseurs). Le troisième article est en révision après acceptation avec corrections à Journal of Quaternary Science (doi:10.1002/jqs.2648), revue spécialisée à comité de lecture (éditeur en chef, éditeur invité et 2 réviseurs). La mise en page de ces trois chapitres respecte les directives propres à chaque revue. Pour cette raison, les titres et figures de chaque chapitre ne sont pas spécifiquement numérotés selon l'usage et les recommandations du *Guide de présentation des mémoires et thèse* ; les numéros tels qu'apparaissant dans les articles ont été conservés. De plus, les formats des références sont différents d'un chapitre à l'autre afin de respecter les codes de publications des revues dans lesquelles ils ont été ou seront publiés.

Ma contribution aux publications qui constituent le développement de cette thèse couvre la totalité du domaine analytique à l'exception de la granulométrie laser. J'ai participé à la mission qui a collecté la séquence sédimentaire étudiée. J'ai collecté et interprété l'ensemble des données, ainsi que rédigé les manuscrits sous la supervision et les conseils de mes directeurs de thèse, Claude Hillaire-Marcel et Guillaume St-Onge. La contribution de John T. Andrews en tant que co-auteur sur le troisième chapitre est motivée par une série d'analyses complémentaires permettant de discuter une problématique méthodologique, et par la discussion et l'interprétation des résultats.

Le premier chapitre est publié par la revue Geochemistry, Geophysics, Geosystems (doi:10.1029/2012GC004272) et a pour titre « Late Quaternary chronostratigrapic Framework of deep Baffin Bay glaciomarine sediments from high-resolution paleomagnetic data », avec pour co-auteurs Guillaume St-Onge (UQAR-ISMER) et Claude Hillaire-Marcel (UQAM-Geotop). Ce chapitre porte sur l'établissement d'une chronologie dans un bassin océanique (i.e., la Baie de Baffin) où les méthodes traditionnelles de datation des sédiments sont peu ou prou impossibles à appliquer de manière fiable. Ce chapitre propose un nouveau cadre chronostratigraphique sur base d'une approche paléomagnetique, et discute des précédentes tentatives d'établissement d'un modèle d'âge régional.

Le deuxième chapitre est un article soumis à la revue Paleoceanography (2012PA002397) et ayant pour titre « Detrital carbonate events in Baffin Bay during the last climatic cycle: Their timing vs. the Greenland Dansgaard-Oeschger cycles and North Atlantic Heinrich-events », avec pour co-auteurs Claude Hillaire-Marcel (UQAM-Geotop) et Guillaume St-Onge (UQAR-ISMER). Ce chapitre propose une interprétation des dépôts sédimentaires grossiers carbonatés dans un contexte climatique, et notamment en lien avec les cycles de Dansgaard-Oeschger enregistrés dans les glaces du Groenland, et les événements de Heinrich enregistrés dans les séquences sédimentaires de l'Atlantique Nord.

Le troisième chapitre est un article accepté avec corrections à la revue Journal of Quaternary Science (doi:10.1002/jqs.2648) et ayant pour titre « Northeastern Laurentide, western Greenland and southern Innuitian ice stream dynamics during the last glacial cycle », avec pour co-auteurs Guillaume St-Onge (UQAR-ISMER), Claude Hillaire-Marcel (UQAM-Geotop) et John T. Andrews (University of Colorado-INSTAAR). Ce chapitre propose une interprétation de la provenance des sédiments au cours du dernier cycle glaciaire. Il permet une interprétation temporelle et causale expliquant la dynamique des différents glaciers qui encerclent la baie de Baffin, et confronte ces résultats avec les résultats de modélisations récentes.

REMERCIEMENTS

Suis-je le seul à toujours débuter la lecture d'une thèse par le décryptage attentif des remerciements ? Cette rubrique unique laisse transparaitre l'émotion de l'auteur, qui, après avoir passé tant d'heures sur cette fichue thèse, laisse exhaler du chalut un souvenir de brise marine brassé de gratitude sincère envers les gens qui l'entourent et le supportent. Souvent drôles, toujours touchants, les remerciements constituent un « must read » incontournable.

Je veux commencer par remercier chaleureusement mes directeurs de thèse, Messieurs Claude Hillaire-Marcel et Guillaume St-Onge pour m'avoir guidé et fait confiance tout au long de ce projet. Merci pour toutes les discussions, le soutien (matériel et spirituel) et pour le temps consacré à cette thèse. Je vous remercie également de m'avoir permis de prendre part à 4 missions océanographiques qui furent pour moi de véritables révélations ; ainsi que de m'avoir soutenu afin de participer à des congrès scientifiques toujours plus intéressants au fur et à mesure de l'évolution de la thèse.

Je tiens à exprimer ma gratitude à Madame Anne de Vernal pour les discussions scientifiques et le défi artistique, à Monsieur John Andrews pour le temps consacré à la lecture de mon devis, et pour les discussions scientifiques, notamment lors de la rédaction du 3^{e} chapitre. D'un point de vue analytique, cette thèse fut une véritable promenade dans la Belle Province. La première et plus importante halte fut sans conteste Rimouski, et le laboratoire de Paléomagnétisme sédimentaire, merci à Jacques Labrie pour ses tours de magie magnétique, et au petit peuple des caves de l'ISMER. En remontant le fleuve, une halte s'est imposée à Québec, merci à Pierre Francus et Arnaud de Coninck pour leur aide lors des analyses Itrax, et à Guillaume pour le gîte et le couvert. Enfin, à Montréal, les analyses XRD n'auraient pas été possibles sans l'aide et le sens de l'humour de Michel Preda, merci à lui.

Je remercie chaleureusement les officiers et membres d'équipages des missions auxquelles j'ai eu la chance de participer sur le CCGS Hudson, le James Clark Ross (British Antarctica Survey), et le Coriolis II (Reformar). Ces missions m'ont permis de vivre intensément les plaisirs de la mer. Merci tangages et roulis pour tout ce bonheur. Merci aussi aux membres des équipes scientifiques pour les jeux dans la *bouette*. Des remerciements particuliers vont à l'équipe du « sweatshop JCR175 » (Anne, Aoibheann et Mariah) pour les nuits de travail intense à zigzaguer entre les cubes de glaces (i.e., icebergs).

Au Geotop, j'ai eu la chance et le bonheur de rencontrer des gens extrêmement plaisants à côtoyer au quotidien, ou lors des congrès étudiants. Merci à la grande famille du Geotop, et aux gens qui peuplent ses couloirs. Toutes les heures passées avec vous ont été savourées jusqu'à la dernière goutte, merci pour cet arrière-goût de brosse amicale. Aussi, comment ne pas froisser la susceptibilité de chacun en vous remerciant dans un ordre qui sera, au mieux approximatif, au pire, aléatoire. Les souvenirs des moments passés avec vous s'entrechoquent dans un joyeux désordre, et le tri de ces souvenirs est quasi impossible à énumérer ici par le détail. J'ai donc décidé de faire voter une loi spéciale interdisant toutes plaintes relatives à l'ordre établi ci-dessous (par contre, vous avez le droit de vous en câlisser... ça me ferait même un peu plaisir...). Merci à Alice, Marie-Pier, Jacques, Manu, Sandrine, André, Bassam, JF, Taoufik, Maryse, les tourbeux (c'est un prix de groupe), Hervé, Stelly, Guillaume, Emilie, Nicolas V., Christelle, Benoit, Ursule, Chantal, Pauline, Nicolas Van, Audrey, Olivia, Laurence, Jenny, Jean - I'm sexy and I know it - Baptiste (aka JB) et tous les autres que j'oublie et qui m'en voudront probablement un peu. Un merci tout particulier aussi à Agathe (aka maman), Milan et Ariane (aka la petite). Merci à tous pour votre amitié, pour les soirées, et autres ~~virées~~ discussions plus ou moins ~~arrosées~~ animées. Merci aussi à Josée, Diane et Nicole pour le soutien administratif certifié conforme durant mes années à errer au 7^{e}.

Merci à tous les artistes qui ont l'amabilité de performer tous les jours dans ma playlist iTunes. Sans eux, l'écriture de cette thèse n'aurait pas été possible, et la vie serait bien moins distrayante.

Merci à ma formidable colocataire Véro et à son Xav.

Un énorme bedankt-merci-danke à la Belgian Team de Montréal. Jamais, ou très rarement, je n'ai eu le mal du pays, et je suis certain que c'est en majeure partie grâce à vous. Merci pour ces WE chalets, soirées, resto, 5 à 7, tours de chants, BBQ, randonnées et j'en passe... Si tous ces moments passés avec vous ont été à moitié aussi agréables pour vous que le quart de ce qu'ils m'ont procuré comme moments de joie, mille remerciements n'y suffiront pas. On peut remercier une fois mille personnes, mais pas mille personnes une fois, enfin si... bref, mille fois merci à Cécile, Raph, Cath, Loic, FX, Isa, Sandra (assimilée belge), Nicolas (li flamin dè gattes), Renaud, Céline (aka DJ Césto), Laurence (aka Lolotje), Dimitri (aka Fort) et à la plus merveilleuse des amoureuses : Claire. Vous fûtes de merveilleux compagnons des plus chaudes heures du jour, jusqu'aux lueurs de l'aube. Bises.

Merci aux amis en Belgique, je vous aime les mecs. BDV all the way! Big up!

Enfin je finirai ce long panégyrique par des remerciements affectueux pour mes parents qui m'ont toujours soutenu tout au long de ces années, et qui, malgré la distance et mon sens de l'humour plus que douteux, ont continué à m'encourager. Un baudet qui fait à s'mode, c'est l'mitan de s'nourriture. Merci msieu, dame. The Dude abides.

Merci au Benelux.

Merci, bedankt, thanks, grazie, gracias, takk, спасибо, Arigatō, etc...

And Now for Something Completely Different...

TABLES DES MATIÈRES

LISTE DES FIGURES

LISTE DES TABLEAUX

LISTE DES ABRÉVATIONS

PC16	HU2008-029-016 Piston Core
AMOC	Atlantic Meridional Overturning Circulation
ARM	Anhysteretic Remanent Magnetization
BBDC-	Baffin Bay Detrital Carbonate
BC	Box Core
CAA	Canadian Arctic Archipelago
CAT-Scan	Computerized Coaxial Tomography-Scan
ChRM	Characteristic Remanent Magnetization
CIE	Commission International de l'éclairage
DC	Detrital Carbonate (facies)
D/O	Dansgaard Oeschger
DSR	Diffuse Spectral Reflectance
FORC	First Order Reversal Curve
GAD	Geocentric Axial Dipole
GIS	Greenland Ice Sheets
GISP	Greenland Ice Sheet Project (GISP2: Greenland Ice Sheet Project 2)
H-events	Heinrich events (e.g., H1, H2: Heinrich event 1, Heinrich event 2)
Hc	Coercive force
Hcr	Coercivity of remanence
HU2008-029	Hudson cruise # 29, 2008 (August 28 – September 23)
IIS	Innuitian Ice Sheets
IS	Interstadial (Greenland)
IRD	Ice Rafted Debris
IRM	Isothermal Remanent Magnetization
JCR175	James Clark Ross cruise #175, 2009 (August 4 – September 11)
LDC	Low Detrital Carbonate (facies)
LGM	Last Glacial Maximum

LIS	Laurentide Ice Sheets
MAD	Maximum Angular Deviation
MD	Multi Domain
MDF	Medium Destructive Field
MIS	Marine Isotope Stages
Mrs	Saturation remanence
Ms	Saturation magnetization
MSCL	Multi Sensor Core Logger
NADW	North Atlantic Deep Water
NAPIS	North Atlantic relative Paleointensity Stack
NRM	Natural Remanent Magnetization
OC	Olive Clay (facies)
ODP	Ocean Drilling Program
PCA	Principal Component Analysis (PC: Principal Component)
PSD	Pseudo-Single Domain
PSV	Paleomagnetic Secular Variation
SAR	Sedimentation Accumulation Rate
SD	Single Domain
RDL	Rapidly Deposited Layers
RPI	Relative Paleointensity
RSL	Relative Sea Level
SIRM	Saturation Isothermal Remanent Magnetization
TMF	Trough-Mouth Fans
TWC	Trigger Weight Core
UB	Uppermost Brown (facies)
XRD	X-Ray Diffraction
μXRF	micro X-Ray Fluorescence

RÉSUMÉ

Les interactions entre les océans, l'atmosphère et les calottes glaciaires constituent la clé de voûte de la compréhension du système climatique global. Deux méthodes croisées sont possibles afin de dénouer les fils de cette trame complexe : la modélisation des processus et l'étude des fluctuations passées. Dans cette thèse, nous nous sommes intéressés à la seconde alternative et, plus précisément, aux interactions entre les marges glaciaires et les changements climatiques et océanographiques du dernier cycle glaciaire. La reconstitution et la compréhension de la dynamique des marges glaciaires exigent une connaissance précise de leur instabilité dans le temps afin d'appréhender les processus intrinsèques. Cependant, l'érosion des traces géologiques directes des fluctuations des marges glaciaires contraint à l'étude d'empreintes indirectes, les sédiments marins, comme unique source d'information. La localisation de la séquence sédimentaire étudiée ici (HU2008-029-016PC) est idéale puisque le régime sédimentaire du site a été influencé par la dynamique des calottes glaciaires régionales (i.e., laurentidienne, innuitienne et groenlandaise) durant les dernières glaciations. Cependant, l'analyse de cette archive sédimentaire présente des difficultés de datation. En effet, les méthodes traditionnelles chronostratigraphiques, telles que la stratigraphie isotopique ($\delta^{18}O$ sur les tests de foraminifères) ou la datation par le radiocarbone (^{14}C), ne permettent pas l'établissement de modèles d'âges concluants dans cette région. L'approche paléomagnétique utilisée dans cette thèse a dès lors été guidée par cette problématique chronostratigraphique, avant de permettre une lecture environnementale de la variabilité des lithofaciès sédimentaires et de leurs origines.

Dans le premier chapitre de cette thèse, nous proposons une chronostratigraphie originale sur base de mesures paléomagnétiques, plus précisément à partir de l'enregistrement de la paléointensité relative du champ magnétique terrestre par les sédiments. Toutefois, l'identification d'une modulation lithologique (e.g., taille des grains, concentration) des propriétés magnétiques nous a obligé à filtrer les données pour éliminer la composante "environnementale" du signal magnétique. Pour ce faire, nous avons conduit des analyses détaillées afin de caractériser les minéraux magnétiques présents. Les résultats nous ont permis de définir que l'aimantation rémanente naturelle était portée majoritairement par des grains de magnétite dans une gamme de taille adéquate pour un enregistrement optimal du champ magnétique terrestre existant au moment de leurs dépôts. Aussi, ces analyses ont permis l'identification de certaines couches non représentatives, ayant surtout enregistré une lithologie particulière; elles ont dès lors été écartées de l'enregistrement paléomagnétique proprement dit. Nous avons reconstruit le signal de paléointensité relative en normalisant l'aimantation rémanente naturelle par l'aimantation rémanente anhystérétique induite, afin de réduire significativement l'empreinte magnétique environnementale secondaire. Le signal obtenu se compare avec succès aux enregistrements et compilations existants ce qui a permis de dériver un modèle d'âge

fiable couvrant le dernier cycle glaciaire (depuis 115 ka BP). La reconstruction des directions du champ magnétique terrestre a permis notamment l'identification de 2 excursions géomagnétiques (i.e., de Laschamp et de la mer de Norvège-Groenland) déjà bien connues et datées, renforçant ainsi la confiance dans le modèle d'âge proposé.

Dans le second chapitre, nous avons mis à profit le nouveau cadre chronostratigraphique afin d'interpréter l'origine des dépôts carbonatés. Sur base d'analyses minéralogiques des carbonates associées à des données granulométriques, de microfluorescence X et aux propriétés magnétiques des grains, nous avons identifié 14 couches carbonatées grossières. La composition minéralogique a permis de lier l'origine de ces dépôts aux glaciers du nord de la baie de Baffin (i.e., Laurentidien et Innuitien), tandis que les couches de sédiments fins riches en titane ont été associées à d'autres sources (Groenland et/ou est de l'île de Baffin). Le chronométrage des couches carbonatées a permis d'associer ces dépôts à la dynamique des glaciers nordiques, sensibles aux oscillations climatiques (ou océanographiques) de haute fréquence de type Dansgaard-Oeschger (dépôt bref, <1.5 ka), ou avec des avancées majeures (suivis pas des retraits progressifs) des glaciers nordiques à différentes périodes glaciaires (dépôt long, 3-6 ka). Nous concluons que ces dépôts sont distincts des événements de Heinrich enregistrés dans l'Atlantique Nord.

Dans le troisième chapitre, nous avons étudié les lithofaciès sédimentaires et les assemblages minéralogiques afin de retracer précisément les apports sédimentaires en provenance des marges groenlandaises et de l'île de Baffin. Pour ce faire, nous avons utilisé le programme SedUnMix afin d'estimer statistiquement les sources ayant contribué aux assemblages minéralogiques observés. Les sédiments en provenance de l'île de Baffin sont caractérisés par des dépôts rapides de sédiments grossiers transportés par la glace de mer et/ou des icebergs. Ils présentent également un synchronisme avec les dépôts carbonatés, ce qui suggère des réponses similaires des glaciers nordiques et de l'ouest de la baie de Baffin aux fluctuations et réorganisations océaniques de haute fréquence. Les sédiments en provenance du grand complexe glaciaire d'Uummannaq ont été mis en place durant de longs intervalles correspondant à des niveaux marins plus bas. Notamment, la signature sédimentaire singulière du dernier maximum glaciaire suggère une étendue de la marge glaciaire groenlandaise jusqu'à la marge du plateau continental. Des avancées plus réduites sur le plateau continental groenlandais ont également été identifiées durant les stades isotopiques 5b, 5d et 4.

Globalement, les résultats de cette thèse permettent de confirmer l'installation rapide de larges glaciers couvrant la région innuitienne immédiatement après le dernier interglaciaire, comme le suggèrent de récents efforts de modélisation.

Mots clés: Baie de Baffin, Dernier cycle glaciaire, Sédiments glaciomarins, Couches carbonatées, Paléocéanographie, Glaciers, Multi-proxy

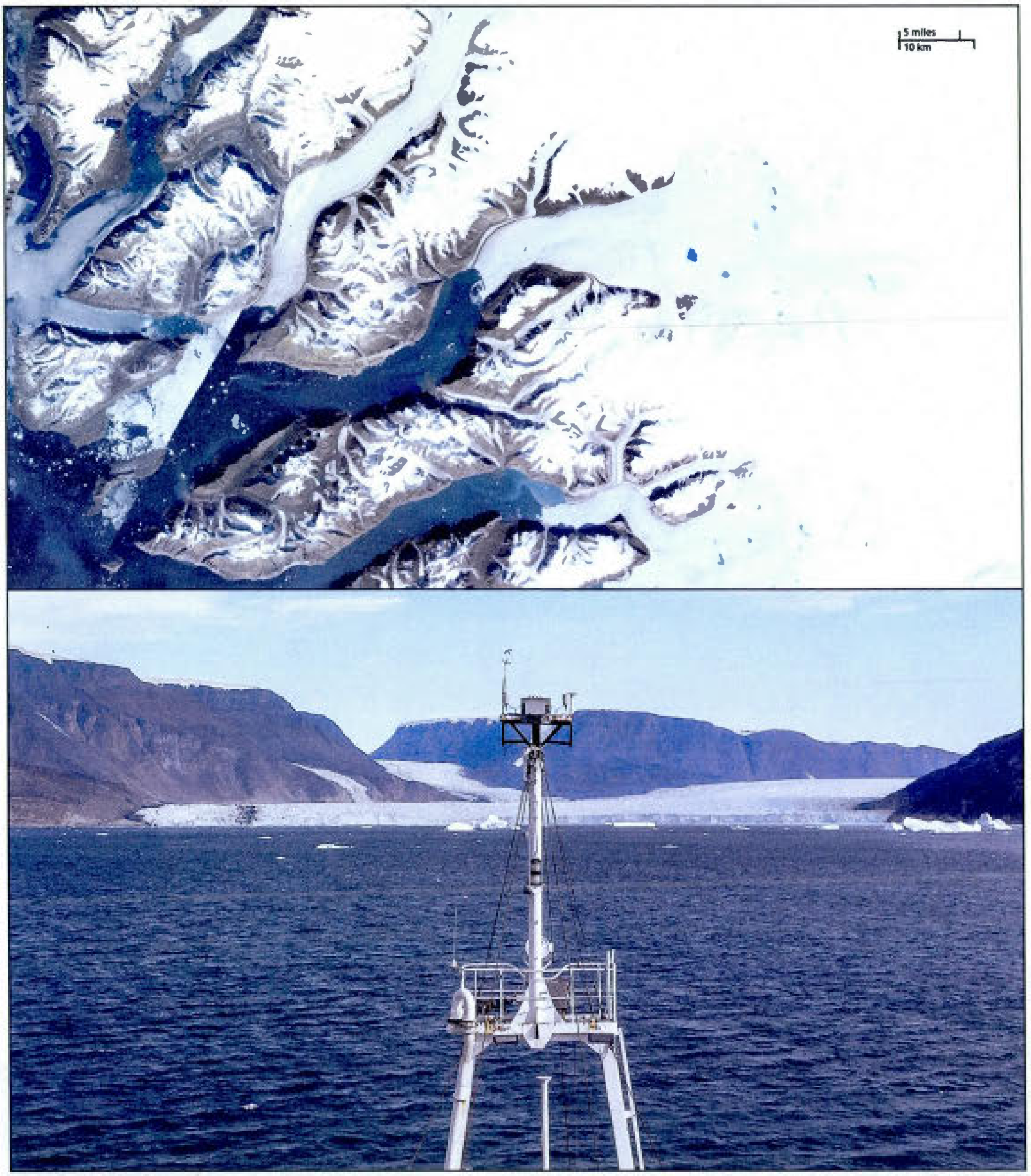

Rinks Isbrae glacier (Uummannaq). Image satellite : 2012 Google-Tele Atlas.
Photo: Quentin Simon (2009).

INTRODUCTION

Les dernières décennies ont vu naître une conscience internationale accrue des problématiques liées au changement climatique global et à son impact sur nos sociétés (comme en témoignent les travaux du GIEC par exemple). Cette prise de conscience se traduit par des efforts de compréhension du système climatique à travers l'étude des interactions complexes entre ses composantes (i.e., atmosphère, cryosphère, hydrosphère, biosphère, lithosphère, anthroposphère), et des forçages qui les régissent. Deux enjeux majeurs s'offrent à la communauté scientifique au vu de ces questions : 1) comprendre l'évolution et les échanges entre les différentes composantes gouvernant le système climatique ; et 2) intégrer ces connaissances dans des modèles éprouvés permettant de mieux appréhender leurs comportements, pour finalement pronostiquer l'évolution du climat à différentes échelles de temps et d'espace. Afin de répondre à ces enjeux, l'étude des changements passés enregistrés au travers des archives paléoenvironnementales s'avère un outil essentiel. Dans ce sens, l'étude de sédiments marins a permis de mieux cerner le rôle crucial de la circulation océanique sur le climat du Quaternaire récent, notamment à travers la circulation thermohaline (Broecker, 1987, 1991 ; Rahmstorf, 2002). Bien que récemment remis en question (Wunsch, 2010 ; Lozier, 2010), ce concept du « *great conveyor belt* » permet d'expliquer de manière synthétique le rôle de la redistribution thermique entre les différents réservoirs (i.e., océan – atmosphère) dans la mécanique climatique globale. Dans ce cadre, la région de l'Atlantique Nord présente un intérêt prépondérant en étant une des zones principales (avec les marges océaniques antarctiques) de production des masses d'eaux profondes. En effet, les mers nordiques et mer du Labrador engendrent la *North Atlantic Deep Water* (NADW), qui constitue l'un des moteurs majeurs de la dispersion thermohaline vers l'Atlantique Sud. Dans cette région, les interactions entre les masses d'eaux Atlantique chaudes salées et les masses d'eaux Arctique froides moins salées, combinées avec la présence de glace de mer, les eaux de fonte des glaciers, et la circulation atmosphérique, créent les conditions optimales de convection générant *in fine* les eaux profondes. L'influence de la composante « glace » fait donc partie à part entière de ce système de rétroaction thermique.

Cependant, cette composante cryosphérique subit actuellement des bouleversements majeurs, avec notamment la fonte de la banquise en Arctique (http://nsidc.org/), la fonte estivale de la glace superficielle de l'inlandsis groenlandais, et l'accélération du retrait des courants glaciaires rapides à bases marines. Ces courants glaciaires (*ice streams*) constituent les exutoires des calottes glaciaires (Rignot et Mouginot, 2012), leurs activités engendrent l'essentiel des pertes de masse de ces calottes glaciaires (Marshall et Koutnik, 2006). Par exemple, sur la côte occidentale du Groenland, le retrait du Jakobshaven Isbrae, drainant ~7% de la masse totale de la calotte groenlandaise et produisant ~10% des icebergs groenlandais (Weidick et Bennike, 2007) s'est intensifié récemment. Son bilan de masse (i.e., accumulation sur le bassin versant – décharge) est passé de -5.2 km^3/an en 1996 à -35.8 km^3/an en 2005 traduisant une accélération de la vitesse d'écoulement de la glace au front du glacier de 95% (Rignot et Kanagaratnam, 2006). Cette accélération s'explique aussi bien par une mobilité accrue de la base du glacier due à l'augmentation du drainage de l'eau de fonte produite durant les étés devenus plus chauds des deux dernières décennies, que par l'advection d'eaux chaudes atlantiques dans la baie de Baffin (Holland et al., 2008). Ces masses d'eaux chaudes atlantiques engendrent une augmentation de la fonte basale de la portion marine du glacier qui conduit à un amincissement de la marge flottante, à des vêlages accrus et, *in fine* à des pertes de masse importante de l'inlandsis groenlandais. Ces advections d'eaux chaudes atlantiques étant elles-même induites par des changements régionaux des circulation océanique et atmosphérique, donnent dès lors un aperçu de la complexité des processus qui gouvernent les instabilités glaciaires.

Pour tenter d'appréhender ces processus, les données instrumentales (données satellitaires par exemple) n'apportent que des réponses fragmentaires en étant largement limitées dans le temps, et ce, spécialement au niveau des hautes latitudes où les enregistrements climatiques, océanographiques et glaciologiques sont relativement récents. De plus, ces données (e.g., température, précipitation, couvert de glace de mer, vélage des icebergs, circulation océanique) peuvent être influencées largement par des modifications anthropiques posant la question de leurs empreintes naturelles. Afin de s'affranchir de cet aspect anthropique, les études paléoenvironnementales basées sur des enregistrements sédimentaires et/ou glaciaires s'avèrent essentielles pour retracer l'évolution climatique et en comprendre les interactions. En plus de l'interprétation paléoenvironnementale des résultats, ces données servent également à l'amélioration de la résolution des modèles et permettent de tester la validité des résultats de leurs simulations. Dans ce contexte, il est notamment capital de s'interroger sur la possibilité d'une disparition de l'inlandsis groenlandais et de l'impact de cette disparition sur la circulation océanique, donc sur le climat du globe (en plus des conséquences en ce qui a trait à la hausse des niveaux marins sur les sociétés humaines largement établies le long des côtes).

L'étude des séquences sédimentaires et des forages glaciaires a permis la reconnaissance d'oscillations rapides du climat, à des échelles inférieures (i.e., d'une durée comprise entre la décennie et le millénaire) à celles qui gouvernent les cycles astronomiques du climat (Berger, 1978) au cours du dernier cycle glaciaire (i.e., depuis le dernier interglaciaire il y a ~125 000 ans jusqu'au début de l'Holocène, ~10 500 ans). Ces fluctuations climatiques sont particulièrement bien enregistrées dans les carottes de glace (i.e., Groenland et Antarctique) et révèlent des réchauffements abrupts (5 à 10°C en quelques décennies), suivis de refroidissements graduels (quelques siècles à milliers d'années) se terminant par des refroidissements brutaux. Ces anomalies connues sous le nom de cycles de Dansgaard-Oeschger ou cycles de Bond (e.g., Dansgaard et al., 1993 ; Bond et al., 1992, 1995, 1997, 1999 ; Wolff et al.,

2010) présentent une certaine périodicité (entre ~950 et 1500 - 2000 ans, Obrochta, 2008). Elles sont accompagnées d'événements froids de plus grande amplitude et de moindre fréquence (un événement tous les ~7000 à 8000 ans environ), i.e., les événements de Heinrich, qui ont été abondamment identifiés dans les sédiments de l'Atlantique Nord (Heinrich, 1988 ; Broecker et al., 1992 ; Bond et al., 1992 ; Andrews et Tedesco, 1992). La plupart sont décelés par la présence de sédiments détritiques carbonatés, transportés par des armadas d'icebergs principalement associées à des épisodes de surtensions glaciaires dont l'exutoire a été localisé dans la région du détroit d'Hudson (Dowdeswell et al., 1995 ; Famer et al., 2003 ; Hemming, 2004). La présence de ces dépôts est actuellement expliquée couramment par des mécanismes internes (forçage interne) à la dynamique de l'inlandsis Laurentidien (i.e., hypothèse du *binge-purge cycle* ; MacAyal, 1993) provoquant l'effondrement soudain des marges glaciaires. Les larges quantités d'icebergs et d'eaux de fonte résultants ont entrainé de vastes réorganisations océaniques et climatiques (Rahmstorf, 2003). L'identification d'instabilités provenant d'autres calottes glaciaires synchrones ou antérieures aux instabilités laurentidiennes (Bond et al., 1993 ; Grousset et al., 2000) soulève toutefois la question du possible rôle de forçages externes (e.g., activité solaire, variation de l'insolation, large déstabilisation de banquises) qui ont pu contribuer à engendrer ces oscillations climatiques (Hulbe et al., 2004 ; Marcott et al., 2011 ; Wunsch, 2010). À ce jour, même si la théorie de la dynamique interne est toujours favorisée, de nombreuses questions restent en suspens, notamment concernant la coïncidence, ou non, des instabilités des différentes calottes glaciaires. Afin de répondre à ces questions, des défis scientifiques importants doivent encore être abordés. Parmi ceux-ci, relevons : (1) la nécessité d'améliorer la résolution chronologique des séries sédimentaires utilisées aux fins de reconstitution de la dynamique glaciaire, par exemple, indispensables pour détailler le synchronisme des événements ; et (2) la compréhension de la dynamique des différents inlandsis, notamment en ce qui a trait à leurs phases de croissance et de recul.

A cet égard, la baie de Baffin constitue une zone géographique privilégiée. En effet, les observations récentes identifient la baie comme le premier fournisseur d'icebergs dans l'Atlantique Nord. Les courants glaciaires ouest groenlandais sont également largement documentés ce qui permet d'obtenir des données sur les taux de retrait actuelles. De plus, la baie de Baffin constitue un exutoire majeur (avec le détroit de Fram) des eaux douces arctiques vers l'Atlantique Nord. Ces eaux douces contribuent à diminuer la convection dans la mer du Labrador et participent donc à la variabilité du climat global via la circulation thermohaline. Durant le dernier cycle glaciaire, la baie était presque entièrement circonscrite entre les inlandsis groenlandais, laurentidien et innuitien (ces 2 derniers ont aujourd'hui disparus) ce qui a modifié de manière importante les conditions de circulation océanique régionale. En conséquence, la dynamique de ces inlandsis entraine aujourd'hui (via le groenlandais), et hier (via les laurentidien et innuitien), un impact majeur sur la circulation océanique locale, régionale, mais aussi globale, contribuant dès lors à la variabilité climatique actuelle et durant le Quaternaire récent.

Baie de Baffin

La baie de Baffin est un bassin océanique étroit (~1300 km de long sur ~450 km de large, couvrant une superficie totale de ~690 000 km^2), semi-fermé, relié à l'océan Arctique par le détroit de Nares et par les chenaux de l'Archipel Arctique Canadien et, à l'Océan Atlantique, par le détroit de Davis. La baie est constituée d'une plaine abyssale (2000-2500 m de profondeur) entourée de plateaux continentaux. Le plateau continental groenlandais est large (>250 km) et profond (>300 m), tandis que le plateau de l'île de Baffin est plus étroit (25-50 km) et moins profond (~200 m). Les pentes de ces plateaux continentaux sont abruptes, tandis que la pente du plateau continental au nord de la baie est plus douce et s'étend progressivement jusqu'à la plaine abyssale. Au nord et à l'est de la baie, de larges deltas proglaciaires sont présents (Li et al., 2011 ; Ó Cofaigh et al., 2012) et signalent l'existence passée de complexes glaciaires au cours du dernier maximum glaciaire (Last Glacial Maximum, LGM) et probablement durant des phases de poussée glaciaire antérieures. Ce type de structure est absent du côté de l'île de Baffin (Ó Cofaigh et al., 2012).

La circulation de surface dans la baie est cyclonique (Tang et al., 2004). Les masses d'eaux atlantiques, relativement chaudes et salées (θ >0°C, S >34), s'écoulent vers le nord à l'est de la baie, entre 300 et 800 m de profondeur. Les eaux arctiques plus froides et peu salées (-1.5< θ >1°C, 31< S >33.5) s'écoulent en surface, vers le sud, le long des côtes de l'île de Baffin après avoir transité à travers les chenaux de l'Archipel Arctique Canadien. Enfin, la masse d'eau froide profonde est enclavée par des seuils dans le secteur abyssal (> 1200 m) ce qui limite fortement les échanges et taux de ventilation. Ces conditions océanographiques induisent une sous-saturation du carbonate de calcium à des profondeurs faibles (200-500 m pour l'aragonite et 1000-1500 m pour la calcite; Azetsu-Scott et al., 2010).

La glace de mer recouvre entièrement la superficie de la baie excepté durant les mois d'août et septembre. L'influence des masses d'eaux atlantiques relativement chaudes implique toutefois une asymétrie importante de ce couvert (Tang et al., 2004). La production d'icebergs est essentiellement attribuée aux glaciers groenlandais et, dans une moindre mesure, aux glaciers de l'Archipel Arctique Canadien (Weidick et Bennike, 2007). Cette production est estimée aujourd'hui à ~141 km^3/an pour le détroit de Nares et l'ouest groenlandais (Bigg et al., 1999). Durant le dernier cycle glaciaire, une estimation minimale propose un flux d'icebergs de l'ordre de ~$16.8 x 10^6$ km^3 (Marshall et Koutnik, 2006).

La baie est le prolongement septentrional de la branche occidentale du système du rift Nord Atlantique qui a contribué à séparer les cratons précambriens canadien et groenlandais durant le Crétacé et le Tertiaire. Dès lors, la géologie de la baie de Baffin est essentiellement caractérisée, sur ses flancs, par des affleurements de roches précambriennes (i.e., 3.2 – 1.7 Ga), tandis que des roches carbonatées paléozoïques affleurent au nord de baie. La phase de rift a aussi entrainé l'épanchement de basaltes dans la région de Disko Bugt et d'Uummannaq (une description détaillée de la géologie régionale est maintenant accessible via la carte géologique de l'Arctique, Harrison et al., 2011).

Durant le dernier cycle glaciaire, la baie était entourée par des inlandsis majeurs : les inlandsis groenlandais, laurentidien et innuitien. Des simulations récentes (Ganopolski et al., 2010 ; Stokes et al., 2012) montrent un développement rapide des inlandsis laurentidien et innuitien centré sur l'Archipel Arctique Canadien immédiatement après le dernier interglaciaire (entre 120 000 et 115 000 ans), en plus d'un développement rapide de l'inlandsis groenlandais. Ces inlandsis se sont ensuite développés jusqu'à leurs extensions maximales au dernier maximum glaciaire (Dyke, 2004 ; England et al., 2006 ; Funder et al., 2011). Leur destruction rapide s'est effectuée durant la période de déglaciation (il s'agit plutôt d'une diminution de volume dans le cas de l'inlandsis groenlandais, seul vestige du dernier cycle glaciaire dans l'hémisphère Nord). L'impact de ces phases de glaciation est repéré dans les sédiments marins de la baie, notamment par des couches de carbonates détritiques grossiers (i.e., *Baffin Bay Detrital Carbonate layers*, BBDC; cf. chapitre 2). L'interprétation des lithofaciès sédimentaires a permis d'identifier clairement une influence glaciaire sur le régime sédimentaire de la baie (Aksu, 1981 ; Aksu et Piper, 1979, 1987 ; Andrews et al., 1998). Toutefois, la chronologie et l'étendue de ces événements reste relativement floue à ce jour.

Problématique

Grâce à son emplacement, la baie de Baffin constitue un bassin idéal pour avoir enregistré la dynamique des inlandsis régionaux au cours du dernier cycle glaciaire.

Toutefois, la reconstitution de cette dynamique et des réponses des glaciers aux forçages internes ou externes est difficilement accessible. En effet, les traces géologiques et géophysiques directes (i.e., terrestres, plateaux continentaux) de la dynamique des inlandsis et des avancées des marges glaciaires, depuis le dernier interglaciaire jusqu'au maximum glaciaire, ont largement été érodées par l'action des avancées subséquentes des glaciers et par leurs retraits durant la phase de déglaciation. Les carottes de sédiments marins profonds constituent une alternative de choix afin de palier à ce manque de données.

De la difficulté d'établir des modèles d'âges fiables dans les sédiments profonds arctiques.

Toutes les études précédentes portant sur des sédiments marins profonds dans la baie de Baffin se sont butées à des difficultés chronostratigraphiques considérables, qui ont conduit à des interprétations radicalement différentes des signaux sédimentaires (Aksu, 1983 *versus* de Vernal et al., 1987). Il s'agit d'un problème étendu à l'ensemble des bassins arctiques profonds (Polyak et Jakobsson, 2011 ; Not, 2010). En effet, les conditions océanographiques dans ces bassins contribuent à une faible production et préservation des microfossiles calcaires, essentiels à l'utilisation des méthodes chronostratigraphiques usuelles (de Vernal et al., 1992). Cela implique des limitations importantes des méthodes de datation traditionnelle, tels que l'usage des isotopes de l'oxygène ou la datation radiocarbone (^{14}C), basées sur l'analyse des carbonates biogéniques comme les foraminifères. La présence de glace de mer réduit drastiquement leur production, tandis que les conditions de sous-saturation entrainent une dissolution des carbonates. Ces deux facteurs limitent fortement la présence et la diversité des carbonates biogéniques dans les sédiments. De plus, les entrées massives d'eaux douces et la distillation des saumures isotopiquement « légères » (issues de la formation de la glace de mer) produisent des décalages des teneurs en ^{18}O des foraminifères arctiques compliquant sérieusement les interprétations

(Hillaire-Marcel et de Vernal, 2008). Concernant la datation radiocarbone, elle est possible sur les rares microfossiles encore présents mais son usage précis est limité jusqu'à ~35-40 ka BP. De plus, l'incertitude associée aux âges réservoirs est encore très mal définie pour ces bassins. Enfin, cette incertitude a vraisemblablement connu une grande variabilité à travers diverses époques en fonction de la variabilité de la circulation océanique, spécialement lors d'événements abrupts comme le *Younger-Dryas* par exemple (Bard et al., 1994).

Au regard de ces difficultés, des méthodes chronostratigraphiques affranchies de ces problématiques doivent être envisagées afin de pouvoir circonscrire temporellement les enregistrements sédimentaires. Les objectifs de cette thèse s'alignent en droite ligne dans cette visée.

Objectifs de la thèse

Les objectifs de cette thèse concernent essentiellement (1) l'établissement d'un cadre chronostratigraphique fiable pour les sédiments profonds de la baie de Baffin et, (2) la reconstruction de l'évolution et de la dynamique des inlandsis régionaux au cours du dernier cycle glaciaire. Pour ce faire, les aspects développés dans les trois chapitres de cette thèse s'articulent autour de :

- L'établissement d'un modèle d'âge original et fiable dans la baie de Baffin sur base de mesures paléomagnétiques (chapitre 1) ;
- La compréhension de l'origine des couches carbonatées déposées dans la baie de Baffin en lien avec l'évolution glaciologique et climatique (notamment à l'échelle millénaire) (chapitre 2) ;
- L'identification de l'évolution distincte des marges et courants glaciaires sur le pourtour de la baie de Baffin, notamment en lien avec

les différentes échelles spatio-temporelles régissant leur évolution (chapitre 3) ;

Matériel et méthodes

Cette étude a été menée sur une séquence sédimentaire de 741 cm (voir les images et radiographies de la carotte, page 20) prélevée à l'aide d'un système de carottier à piston à une profondeur de 2063 m lors de la mission HU2008-029 à bord du CCGS Hudson (HU2008-029-016PC, 70°46.14N - 64°65.77O ; Campbell et de Vernal, 2009). Le site d'échantillonnage se situe dans la plaine abyssale à proximité du site de forage ODP645 (Srivastava et al., 1989), et d'une série d'autres carottes prélevées durant les années septante et quatre-vingts (Aksu, 1981, 1983 ; Andrews et al., 1998 ; de Vernal et al., 1987 ; Thouveny, 1988). Toutes les analyses et interprétations menées sur ces carottes ont permis de montrer une influence glaciaire sur les faciès sédimentaires (e.g., transport par la glace, courants de turbidité). Toutefois, une image claire et précise de l'influence de la dynamique glaciaire régionale n'a pas encore pu être établie, essentiellement à cause de l'absence d'une chronologie fiable et de bonne résolution (i.e., millénaire).

Afin de répondre aux problématiques et objectifs, l'approche méthodologique de cette thèse propose une étude multidisciplinaire. Ce type d'approche « multi-proxy », qui caractérise les études sédimentaires modernes, permet de cerner les différents processus qui entrent en jeu depuis l'érosion des roches jusqu'à la diagenèse, en passant par le transport et le dépôt des sédiments marins (Hillaire-Marcel et de Vernal, 2008).

Les analyses des propriétés magnétiques des sédiments permettent d'acquérir rapidement des données non destructives et de haute résolution retraçant, d'une part et qualitativement, les fluctuations du champ magnétique terrestre et, d'autre part et quantitativement, les fluctuations lithologiques enregistrées par les particules magnétiques des sédiments détritiques.

Les mesures paléomagnétiques permettent de reconstituer les variations d'intensité et d'orientation du champ magnétique terrestre qui régnaient au moment de l'enfouissement des sédiments magnétiques (Tauxe, 2010). Ces mesures sont réalisées sur des séquences sédimentaires à travers le monde et fournissent des enregistrements de référence précieux pour les corrélations (Stoner et al., 1995, 2000). Par exemple, la magnétostratigraphie permet de retracer rapidement les inversions de polarité magnétique et établit dès lors des cadres chronostratigraphiques fiables pour les échelles de temps géologiques. À des échelles plus courtes, les variations séculaires permettent également des corrélations entre les différents enregistrements (Stoner et St-Onge, 2007). Ces variations séculaires sont particulièrement intéressantes comme outils chronostratigraphiques dans les bassins arctiques (Barletta et al., 2008 ; Lisé-Pronovost et al., 2009).

Les variations lithologiques (i.e., minéralogie, concentration et taille des grains) et magnétiques ont été étudiées et sont expliquées par des variabilités des modes de transports des particules magnétiques détritiques depuis les sources géologiques, ainsi que par la dilution issue des flux matériel sédimentaires authigènes ou par les processus diagénétiques (e.g., Maher et Thompson, 1999 ; Gubbins et Herrero-Bervera, 2007 ; Butler, 2004 ; Dunlop et Özdemir, 1997 ; Stoner et al., 1996).

Dès lors, ces mesures ouvrent un champ d'étude très large, mais nécessitent une connaissance précise de l'origine des fluctuations enregistrées en préambule à toute interprétation des résultats.

Dans cette étude, nous avons réalisé des analyses paléomagnétiques de haute résolution sur des *u-channels* (tube en plastique de 150 cm de long par 2 cm x 2 cm de section) prélevés au centre des sections de la carotte sédimentaire. Ces *u-channels* permettent des mesures en continu au travers de magnétomètres cryogéniques adaptés, mesurant et induisant différents types de magnétisation. De cette façon, nous avons pu mesurer l'enregistrement de l'aimantation rémanante naturelle, mais aussi mesurer les réponses des sédiments magnétiques à différents types d'inductions magnétiques telles l'aimantation rémanente anhystérétique et isothermale (cf. Stoner et St-Onge, 2007 pour un aperçu de ces méthodes). Nous avons également effectué une étude détaillée des propriétés des grains magnétiques à partir d'échantillons représentatifs des différents facies. À cette fin, un magnétomètre à gradient alternatif est utilisé; il permet de mesurer la minéralogie et la granulométrie magnétiques (e.g., propriétés d'hystérésis, acquisition de l'aimantation isothermale). Enfin, nous avons mesuré la susceptibilité magnétique en fonction de la température (i.e., en chauffant de 24 à 700°C) sur des échantillons caractéristiques des différentes couches sédimentaires afin d'identifier des assemblages de minéraux magnétiques (notamment via la température de Curie des sédiments magnétiques). Ces types de mesures nous ont permis de caractériser précisément les minéraux ou grains porteurs de la rémanence magnétique à travers la carotte et d'évaluer leur fiabilité en tant qu'enregistreurs du champ magnétique terrestre (i.e., grains ferrimagnétiques de faible coercivité). Cette étape nous a permis de distinguer les informations relatives aux fluctuations du champ magnétique terrestre de celles relatives aux propriétés lithologiques.

Dans le premier chapitre de cette thèse, nous avons mis à profit ces données magnétiques afin de reconstruire le signal d'intensité relative (*paleointensity* ; Tauxe, 1993). Cette intensité relative nous a permis d'établir un modèle d'âge via la corrélation avec des enregistrements et compilations de références (Laj et al., 2000). Dans le second chapitre de cette thèse, nous nous sommes d'avantage concentré sur la variabilité des propriétés magnétiques en relation avec les modes de transport sédimentaire.

Nous avons également mené des études étendues des lithofaciès sédimentaires sur base d'une description de la carotte immédiatement après son ouverture, à bord, et des mesures telles que densité, susceptibilité magnétique, spectrophotométrie, radiographie (Cat-Scan), analyse laser de la taille des grains et, enfin, microfluorescence-X de haute résolution (*ITRAX™ core scanner*). Toutes ces méthodes sont décrites de manière détaillée dans les différents chapitres de cette thèse. Le lecteur intéressé peut aussi se rapporter à St-Onge et al. (2007) ou Stoner et St-Onge (2007), et références incluses, pour plus de détails. Ces études des faciès sédimentaires en relation avec le magnétisme environnemental nous ont permis d'identifier des faciès sédimentaires particuliers et de proposer des interprétations en ce qui a trait à leur mode de dépôt.

Enfin, afin de caractériser la provenance des sédiments, nous avons effectué des analyses minéralogiques par diffraction X (échantillons tous les 4 cm). Les assemblages minéralogiques ont été identifiés (chapitre 3) en utilisant le programme SedUnMix (Andrews et Eberl, 2012).

D'un point de vue thématique

Le premier chapitre porte sur l'établissement d'une chronologie dans un bassin océanique (i.e., la Baie de Baffin), où les méthodes traditionnelles de datation des sédiments se sont avérées inutilisables ou peu fiables. Ce chapitre propose un nouveau cadre chronostratigraphique et inclut une analyse critique des précédentes tentatives d'établissement d'un modèle d'âge régional.

Le deuxième chapitre propose une interprétation des dépôts sédimentaires grossiers carbonatés dans un contexte climatique, notamment en lien avec les cycles de Dansgaard-Oeschger enregistrés dans les glaces du Groenland et les événements de Heinrich enregistrés dans les séquences sédimentaires de l'Atlantique Nord.

Le troisième chapitre propose une interprétation de la provenance des sédiments au cours du dernier cycle glaciaire. Il permet une interprétation temporelle et causale expliquant la dynamique des différentes marges glaciaires entourant la baie de Baffin ; et confronte ces résultats avec les résultats de modélisations récentes.

Références

Aksu, A. E., and D. J. W. Piper (1979), Baffin Bay in the past 100,000 yr, *Geology,* 7, 245-248.

Aksu, A. E. (1981), Late Quaternary stratigraphy, paleoenvironmentology, and sedimentation history of Baffin Bay and Davis Strait, Ph.D. thesis, Dalhousie University, Halifax, NS, Canada.

Aksu, A. E. (1983), Short-period geomagnetic excursion recorded in Pleistocene sediments of Baffin Bay and Davis Strait, *Geology,* 11(9), 537-541.

Aksu, A. E, and D. J. W. Piper (1987), Late Quaternary sedimentation in Baffin Bay, *Can. J. Earth Sci.,* 24, 1833-1846.

Andrews, J. T. and K. Tedesco (1992), Detrital carbonate-rich sediments, northwestern Labrador Sea: implications for ice-sheet dynamics and iceberg rafting (Heinrich) events in the North Atlantic, *Geology,* 20, 1087-1090.

Andrews, J. T., M. Kirby, A. E. Aksu, D. G. Barber, and D. Meese, D. (1998), Late Quaternary Detrital Carbonate (DC-) layers in Baffin Bay marine sediments (67°-74° N): correlation with Heinrich events in the North Atlantic?, *Quaternary Science Reviews,* 17, 1125-1137.

Andrews, J. T., and D. D. Eberl (2012), Determination of sediment provenance by unmixing the mineralogy of source-area sediments: The "SedUnMix" program. *Marine Geology,* 291–294, 24-33.

Azetsu-Scott, K., A. Clarke, and K. Falkner (2010), Calcium carbonate saturation states in the waters of the Canadian Arctic Archipelago and the Labrador Sea, *J. Geophys. Res.,* 115, C11021, doi:10.1029/2009JC005917.

Bard, E., M. Arnold, J. Mangeruld, M. Paterne, L. Labeyrie, J. Duprat, M. A. Mélières, E. Sonstegaard, and J. C. Duplessy (1994), The North Atlantic atmosphere-sea surface ^{14}C gradient during the Younger Dryas climatic event, *Earth Planet. Sci. Lett.,* 126, 275-287.

Barletta, F., G. St-Onge, J. E. T. Channell, A. Rochon, L Polyak and D. Darby (2008), High-resolution paleomagnetic secular variation and relative paleointensity records from the western Canadian Arctic: implication for

Holocene stratigraphy and geomagnetic field behaviour. *Can. J. Earth Sci.*, 45,1265-1281.

Berger, A. (1978), Long-term variations of daily insolation and Quaternary climatic changes, *J. Atmos. Sci.*, 35(12), 2362–2367.

Bigg, G. R. (1999), An estimate of the flux of iceberg calving from Greenland, *Arctic, Antarctic, and Alpine Research,* 31(2), 174-178, doi:10.2307/1552605.

Bond, G., H. Heinrich, W. S. Broecker, L. Labeyrie, J. McManus, J. T. Andrews, S. Huon, R. Jantschik, S. Clasen, C. Simet, K. Tedesco, M. Klas, G. Bonani, and S. Simet (1992), Evidence for massive discharges of icebergs into the North Atlantic ocean during the last glacial period, *Nature*, 260(6401), 245-249.

Bond, G., W. S. Broecker, S. Johnsen, J. McManus, L. Labeyrie, J. Jouzel and G. Bonani (1993), Correlations between climate records from North Atlantic sediments and Greenland ice, *Nature*, 365(6442), 143-147.

Bond, G. and R. Lotti (1995), Iceberg Discharges Into the North Atlantic on Millennial Time Scales During the Last Glaciation, *Science*, 267(5200): 1005-1010.

Bond, G., W. Showers, M. Cheșeby, R. Lotti, P. Almasi, P. deMenocal, P. Priore, H. Cullent, I. Hajdas and G. Bonani (1997), A Pervasive Millennial-Scale Cycle in North Atlantic Holocene and Glacial Climates, *Science*, 278(1257): 1257-1266.

Bond, G., W. Showers, M. Elliot, M. Evans, R. Lotti, I. Hajdas, G. Bonani and S. Johnson (1999), The North Atlantic's 1-2 kyr climate rhythm: Relation to Heinrich events, Dansgaard/Oeschger cycles and the Little Ice Age, in : Mechanisms of Global Climate Change at Millennial Time Scales, edited by: O. U. Clark, R. Webb, and L. D. Keigwin, *Geophysical Monograph*, American Geophysical Union, Snowbird, UT, 35–58.

Broecker, W. S. (1987), The biggest chill, *Natural History,* 96, 74-82.

Broecker, W. S. (1991), The great ocean conveyor, *Oceanography,* 4, 79-89.

Broecker, W. S., G. Bond, M. Klas, E. Clark, and J. McManus (1992), Origin of the northern Atlantic's Heinrich events, *Climate Dynamics*, 6, 265-273.

Butler, R. F. (2004), Paleomagnetism: Magnetic Domains to Geologic Terranes, University of Portland, Portland, Oregon, USA, pp. 238.

Campbell, D. C., and A. de Vernal (2009), CCGS Hudson Expedition 2008029: Marine geology and paleoceanography of Baffin Bay and adjacent areas, Nain, NL to Halifax, NS, August 28- September 23; *Geological Survey of Canada*, Open File 5989, 1 DVD.

Dansgaard, W., S. J. Johnsen, H. B. Clausen, D. Dahl-Jensen, N. S. Gundestrup, C. U. Hammer, C. S. Hvidberg, J. P. Steffensen, A. E. Sveinbjörnsdottir, J. Jouzel and G. Bond (1993), Evidence for general instability of past climate from a 250-kyr ice-core record, *Nature*, 363(6434), 218-220.

de Vernal, A., C. Hillaire-Marcel, A. E. Aksu, and P. Mudie (1987), Palynostratigraphy and chronostratigraphy of Baffin Bay deep sea cores: climatostratigraphic implications, *Palaeogeogr., Palaeoclimatol., Palaeoecol.*, 61, 97-105.

de Vernal, A., G. Bilodeau, C. Hillaire-Marcel, and N. Kassou (1992), Quantitative assessment of carbonate dissolution in marine sediments from foraminifer linings vs. shell ratios: Davis Strait, northwest North Atlantic, *Geology* 20, 527-530.

Dowdeswell, J., M. Maslin, J. T. Andrews and I. McCave (1995), Iceberg production, debris rafting, and the extent and thickness of Heinrich layers (H-1, H-2) in North Atlantic sediments, *Geology*, 23, 301-304.

Dunlop, D. J., and Ö. Özdemir (1997), *Rock Magnetism: Fundamentals and Frontiers*, Cambridge University Press, New York, London and Cambridge.

Dyke, A. (2004), An outline of North American deglaciation with emphasis on central and northern Canada, *Developments in Quaternary Science*, 2, 373-424.

England, J., N. Atkinson, J. Bednarski, A. Dyke, D. A. Hodgson, and C. Ó Cofaigh (2006), The Innuitian Ice Sheet: configuration, dynamics and chronology, *Quat. Sci. Rev.,* 25, 689-703.

Farmer, G., D. G. Barber and J. T. Andrews (2003), Provenance of Late Quaternary ice-proximal sediments in the North Atlantic: Nd, Sr and Pb isotopic evidence, *Earth and Planetary Science Letters*, 209, 227-243.

Funder, S., K. K. Kjeldsen, K. H. Kjær, and C. Ó Cofaigh (2011), The Greenland Ice Sheet During the Past 300,000 Years: A Review, in: *Developments in Quaternary Sciences*, *Quaternary Glaciations, Extent and Chronology*, Part IV, A Closer Look, vol. 15, edited by J. Ehlers, P. L. Gibbard and P. D. Hughes, Elsevier, Amsterdam, The Netherlands, 699-713, doi:10.1016/B978-0-444-53447-7.00050-7.

Ganopolski, A., R. Calov, and M. Clausen (2010), Simulation of the last glacial cycle with a coupled climate ice-sheet model of intermediate complexity, *Climate of the Past* 6, 229-244.

Grousset, F., C. Pujol, L. Labeyrie, G. Auffret and A. Boelaert (2000), Were the North Atlantic Heinrich events triggered by the behavior of the European ice sheets? *Geology*, 28(2), 123-126.

Gubbins, D. and E. Herrero-Bervera (2007), Encyclopedia of Geomagnetism And Paleomagnetism, Springer, Dordrecht, The Netherlands, pp. 1054.

Harrison, J. C., M. R. St-Onge, O. Petrov, S. I. Strelnikov, B. G. Lopatin, F. H. Wilson, S. Tella, D. Paul, T. Lynds, S. P. Shokalsky, C. K. Hults, S. Bergman, H. F. Jepsen, and A. Solli (2011), Geological map of the Arctic, *Geological Survey of Canada*, Map 2159A, scale 1:5000000.

Heinrich, H. (1988), Origin and consequences of cyclic ice rafting in the northeast Atlantic Ocean during the past 130,000 years, *Quaternary Research*, 29, 142-152.

Hemming, S. R. (2004), Heinrich events: Massive late Pleistocene detritus layers of the North Atlantic and their global climate imprint, *Rev. Geophys.*, 42(1), RG1005.

Hillaire-Marcel, C. and A. de Vernal (2007), Proxies in late Cenozoic paleoceanography, Developments in Marine Geology, Elsevier, Amsterdam, The Netherlands, pp. 850.

Hillaire-Marcel, C. and A. de Vernal (2008), Stable isotope clue to episodic sea ice formation in the glacial North Atlantic, *Earth Planet. Sci. Lett,* 268, 143-150.

Holland, D. M., R. H. Thomas, B. de Young, M. H. Ribergaard and B. Lyberth (2008), Acceleration of Jakobshavn Isbrae triggered by warm subsurface ocean waters, *Nature Geoscience* 1(10), 659-664.

Hulbe, C. L., D. R. MacAyeal, G. H. Denton, J. Kleman, and T. V. Lowell (2004), Catastrophic ice shelf breakup as the source of Heinrich event icebergs, *Paleoceanography* 19, PA1004, doi:10.1029/2003PA000890.

Laj, C., C. Kissel, A. Mazaud, J. E. T. Channell, and J. Beer (2000), North Atlantic palaeointensity stack since 75 ka (NAPIS-75) and the duration of the Laschamp event, *Phil. Trans. R. Soc. London, Series B*, 358, 1009-1025.

Obrochta, S. P. (2008), Glacial North Atlantic Millennial variability over the last 300,000 years, Ph.D Thesis, Division of Earth and Ocean Sciences, Duke University, Durham, NC, USA, pp. 132.

Rahmstorf, S. (2003), The current climate, *Nature*, 421, 699.

Lozier, M. S. (2010), Deconstructing the Conveyor Belt, *Science*, 328(5985), 1507-1511.

Li, G., D. W. Piper, and D. C. Campbell (2011), The Quaternary Lancaster Sound trough-mouth fan, NW Baffin Bay, *Journal of Quaternary Science* 26, 511-522.

Lisé-Pronovost, A., G. St-Onge, S. Brachfeld; F. Barletta and D. Darby (2009), Paleomagnetic constraints on the Holocene stratigraphy of the Arctic Alaskan margin, *Global and Planetary Change*, 68, 85-99.

MacAyeal, D. R. (1993), Binge-purge oscilla- tions of the Laurentide Ice Sheet as a cause of the North Atlantic's Heinrich events, *Paleoceanography*, 8, 775–784.

Maher, B. A., and R. Thompson (1999), *Quaternary Climates, Environments and Magnetism*, Cambridge University Press, Cambridge, UK.

Marcott, S. A., P. U. Clark, L. Padman, G. P. Klinkhammer, S. R. Springer, Z. Liu, B. L. Otto-Bliesner, A. E. Carlson, A. Ungerer, J. Padman, F. He, J. Cheng, and A. Schmittner (2011), Ice-shelf collapse from subsurface warming as a trigger for Heinrich events, *Proceedings of the National Academy of Sciences* 108 (33), 13415-13419, doi:10.1073/pnas.1104772108.

Marshall, S. J., and M. R. Koutnik (2006), Ice sheet action versus reaction: Distinguishing between Heinrich events and Dansgaard-Oeschger cycles in the North Atlantic, *Paleoceanography* 21, PA2021, doi:10.1029/2005PA001247.

Not, C. (2010), Les Actinides dans les sédiments Quaternaires de l'océan Arctique, Ph.D. thesis, UQAM, Montréal, Qc, Canada.

Ó Cofaigh, C., J. T. Andrews, A. E. Jennings, J. A. Dowdeswell, K. Hogan, A. A. Kilfeather, and C. Sheldon (2012), Glacimarine lithofacies, provenance and depositionnal processes on a West Greenland trough-mouth fan, *Journal of Quaternary Science*, doi:10.1002/jqs.2569.

Polyak, L., and M. Jakobsson (2011), Quaternary sedimentation in the Arctic Ocean: Recent advances and further challenges, *Oceanography* 24(3), 52–64, http://dx.doi.org/10.5670/oceanog.2011.55.

Rignot, E., and P. Kanagaratnam (2006), Changes in the Velocity Structure of the Greenland Ice Sheet, *Science*, 311(5763), 986-990.

Rignot, E., and J. Mouginot (2012), Ice flow in Greenland for the International Polar Year 2008, *Geophys. Res. Lett.*, 39(11), L11501.

Srivastava, S. P. (1989), *Proceedings of the Ocean Drilling Program, Scientific Results*, Baffin Bay and Labrador Sea, Leg 105, Sites 645-647, 1-17.

St-Onge, G., T. Mulder, P. Francus and B. Long (2007), Continuous physical properties of cored marine sediments, in: Developments in Marine Geology, vol. 2, Proxies in late Cenozoic paleoceanography, edited by C. Hillaire-Marcel and A. de Vernal, Elsevier, 63-98.

Stokes, C. R., L. Tarasov, and A. S. Dyke (2012), Dynamics of the North American Ice Sheet Complex during its inception and build-up to the Last Glacial

Maximum, *Quaternary Science Reviews* 50, 86-104, doi:10.1016/j.quascirev.2012.07.009.

Stoner, J. S., J. E. T. Channell and C. Hillaire-Marcel (1995), Late Pleistocene relative geomagnetic paleointensity from the deep Labrador Sea: Regional and global correlations, *Earth and Planetary Science Letters*, 134, 237-252.

Stoner, J. S., J. E. T. Channell and C. Hillaire-Marcel (1996), The magnetic signature of rapidly deposited detritai layers from the deep Labrador Sea: Relationship to North Atlantic Heinrich layers, *Paleoceanography*, 11 (3): 309-325.

Stoner, J. S., J. E. T. Channell, C. Hillaire-Marcel and C. Kissel (2000), Geomagnetic paleointensity and environmental record from Labrador Sea core MD95-2024: global marine sediment and ice core chronostratigraphy for the last 110 kyr, *Earth and Planetary Science Letters*, 183, 161-177.

Stoner, J.S. and G. St-Onge (2007), Magnetic stratigraphy in paleoceanography: reversals, excursions, paleointensity, and secular variation. in: Developments in Marine Geology, vol. 2, Proxies in late Cenozoic paleoceanography, edited by C. Hillaire-Marcel and A. de Vernal, Elsevier, 99-138.

Tang, C., C. Ross,T. Yao, B. Petrie and B. DeTracey (2004), The circulation, water masses and sea-ice of Baffin Bay, *Progress in Oceanography*, 63, 183-228.

Tauxe, L. (1993), Sedimentary records of relative paleointensity of the geomagnetic field: theory and practice, *Reviews of geophysics*, 31(3), 319-354.

Tauxe, L. (2010), *Essentials of Paleomagnetism*, University of California Press, San Diego, USA.

Thouveny, N. (1988), High-resolution palaeomagnetic study of Late Pleistocene sediments from Baffin Bay: first results, *Can. J. Earth Sci.,* 25, 833-843.

Weidick, A. and O. Bennike (2007), Quaternary glaciation history and glaciology of Jakobshavn Isbræ and the Disko Bugt region, West Greenland: a review, *Geological Survey of Denmark and Greenland Bulletin*, 14, pp. 78.

Wolff, E. W., J. Chappellaz, T. Blunier, S. O. Rasmussen and A. Svensson (2010), Millennial-scale variability during the last glacial: The ice core record, *Quaternary Science Review*, 29, 2828-2838.

Wunsch, C. (2010), Towards understanding the Paleocean, *Quaternary Science Reviews*, 29(17–18), 1960-1967.

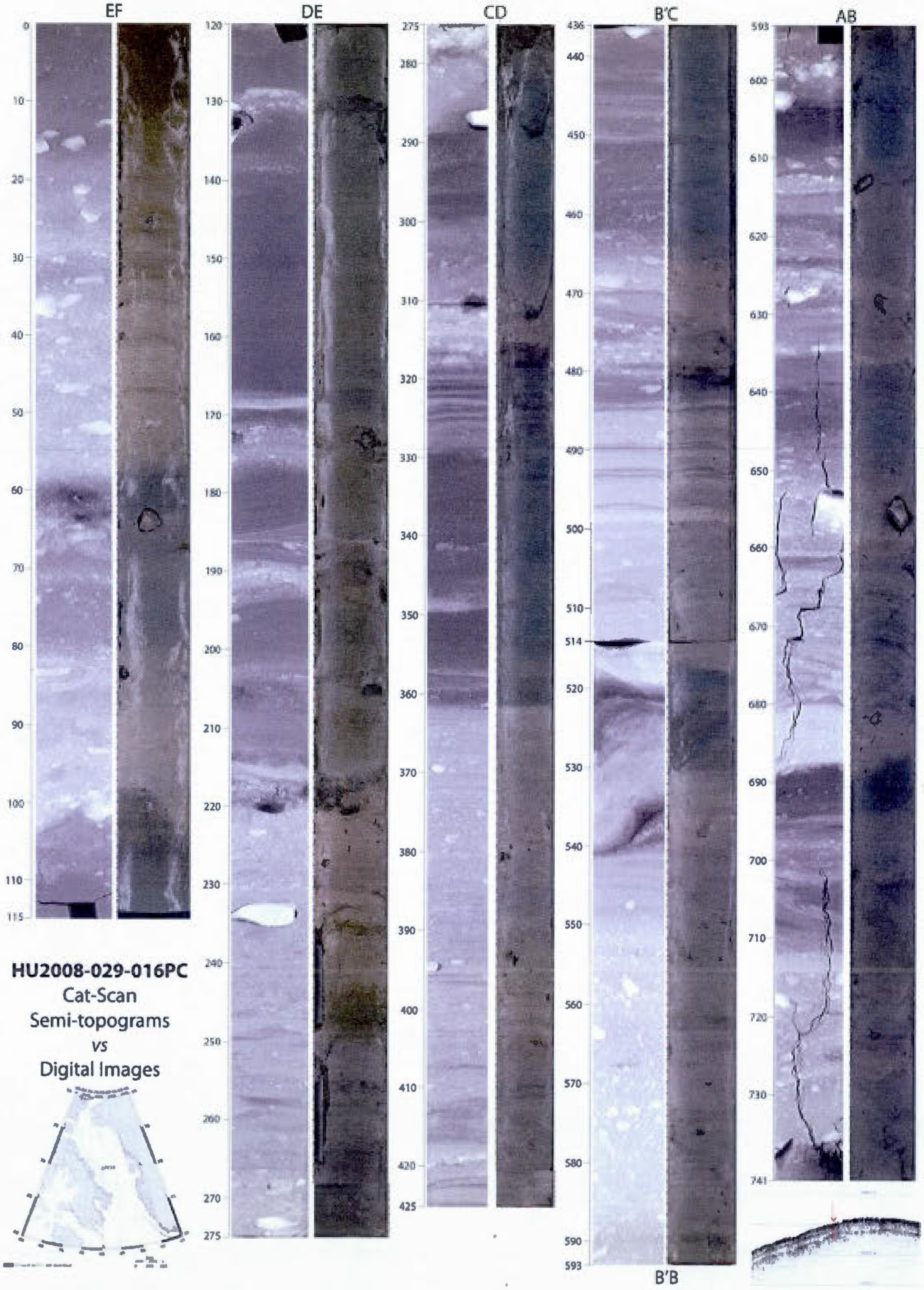

Images et radiographies (Cat-Scan) de la carotte HU2008-029-016PC

CHAPITRE I

Late Quaternary chronostratigraphic framework of deep Baffin Bay glaciomarine sediments from high-resolution paleomagnetic data

Quentin Simon[1,2], Guillaume St-Onge[1,3], Claude Hillaire-Marcel[1,2]

[1] Geotop Research Centre, Montréal, H3C3P8, Qc, Canada.

[2] Université du Québec à Montréal, Montréal, H3C3P8, Qc, Canada.

[3] Canada Research Chair in Marine Geology & Institut des sciences de la mer de Rimouski (ISMER), Université du Québec à Rimouski, Rimouski, G5L3A1, Qc, Canada.

Keywords: Baffin Bay; chronostratigraphy; geomagnetic excursions; late Quaternary; paleointensity; rock magnetism.

Key Points:

A late Quaternary stratigraphy is derived for central Baffin Bay

Relative paleointensity and two excursions support the chronostratigraphy

Sedimentation rates vary from ~3 up to 20 cm/ka during the last glacial cycle

Article publié dans Geochemistry, Geophysics, Geosystems

(doi :10.1029/2012GC004272)

Abstract

The late Quaternary Baffin Bay sediments provide exclusive records of Greenland, Innuitian and Laurentide ice sheet margin activities, as well as information about the Arctic and northern Atlantic ocean linkages through the Canadian Arctic Archipelago. Because of specific oceanographic conditions, foraminiferal $\delta^{18}O$-stratigraphies and radiocarbon ages fail to provide reliable chronologies. Here we propose an original chronostratigraphy spanning the last glacial cycle based on high-resolution paleomagnetic investigations on a 741-cm long core (HU2008-029-016PC) raised from the deep central Baffin Bay, near ODP site 645. Two major difficulties were encountered: (1) the high-frequency occurrence of rapidly deposited layers related to short ice sheet margin events (e.g., ice surges), and (2) the magnetic grain size variability. Physical and magnetic mineralogical properties were used to screen out unreliable magnetic sediment layers. The obtained relative paleointensity (RPI) proxy matches reference paleomagnetic stacks and regional records. Moreover, the resulting record depicts two major excursions which were assigned to the Laschamp and the Norwegian-Greenland-Sea events. It has thus been possible to derive a robust 115 ka chronology for the cored sequence. We concluded that even under such a dynamic sedimentary regime, magnetic properties of the sediments can provide a reliable chronostratigraphy, together with information on sedimentary processes.

1. Introduction

The Baffin Bay area constitutes a unique vantage point to study the ice margin dynamics of several of the largest late Quaternary ice sheets (i.e., Laurentide, Innuitian and Greenland). However, paleoceanographic studies in Baffin Bay, and more largely in the Arctic basins, have been proven highly challenging due to chronostratigraphic limitations. Biogenic carbonates are either scarce or dissolved in the terrigenous glaciomarine sediments of the central Baffin Bay, thus preventing the setting of reliable ^{14}C-chronologies or oxygen isotope stratigraphies [*Aksu*, 1981; *de Vernal et al.*, 1987; *Srivastava et al.*, 1989; *Andrews et al.*, 1998]. In addition, the production of isotopically light brines resulting from sea-ice formation often hinders the interpretation of foraminiferal oxygen isotope data when they exist [*Hillaire-Marcel et al.*, 2004; *Hillaire-Marcel and de Vernal*, 2008].

As a consequence, ambiguous and conflicting late Quaternary chronostratigraphies have been proposed for central Baffin Bay sediments. (1) *Aksu and Piper* [1979] proposed a chronology involving relatively high sedimentation rates (8 – 12 cm/ka) based on the identification of ash horizons and peaks of foraminifera abundance. (2) Later, *Aksu* [1983a] and *Mudie and Aksu* [1984] revisited this model and proposed a chronology presenting lower sedimentation rates (2 – 3 cm/ka) based on bulk ^{14}C dates and $\delta^{18}O$ interpretations. According to this chronology, *Aksu* [1983b] assigned a geomagnetic excursion recorded between 2.5 and 4.5 mbsf in Baffin Bay cores raised during the 1970s to the Blake event (~123±3 cal ka BP) [*Lund et al.*, 2006]. (3) Later on, *de Vernal et al.* [1987] presented new ^{14}C ages on foraminifera and dinocyst assemblages' interpretation that favored the high sedimentation rate scenario (8 – 12 cm/ka). (4) Magnetostratigraphic investigations carried out on Ocean Drilling Program (ODP) site 645 set the Brunhes/Matuyama boundary at 90 mbsf, thus in support of a mean sedimentation rate of 12 cm/ka [*Baldauf et al.*, 1989]. (5) *Thouveny* [1988] identified 2 intervals with anomalous inclinations possibly confirming the high sedimentation rate hypothesis (notably the possible recognition of the Mono Lake excursion around 2.5 mbsf, yielding a mean sedimentation rate of 10 cm/ka). In *Thouveny*'s [1988] study, two radiocarbon ages even suggested a higher sedimentation rate during MIS2 (~20 cm/ka). (6) Finally, *Andrews et al.* [1998] reviewed the chronology in central Baffin Bay based on 21 new AMS ^{14}C ages in 9 piston cores from central Baffin Bay [*Aksu et al.*, 1981]. They proposed a temporal correlation between Baffin Bay Detrital Carbonate layers (BBDC) and the onset of major interstadial $\delta^{18}O$ peaks recorded in the GISP2 ice core. That assumption ruled out the low sedimentation rate hypothesis. Thus, although the stratigraphy of Baffin Bay sediment is now better constrained (e.g., more radiocarbon ages, lithofacies, BBDC), the "climatostratigraphic" interpretations of deep-sea cores remain largely imprecise and insufficient to resolve the phase relationships between millennial-scale climate records.

Magnetic stratigraphy constitutes a valuable answer to resolve these chronological issues in such environments although some conditions have to be achieved to obtain reliable records [e.g., *Tauxe*, 1993, 2007; *Valet*, 2003; *Stoner et al.*, 1998, 2000; *Stoner and St-Onge*, 2007; *St-Onge and Stoner*, 2011; *Channell et al.*, 1997, 2002, 2009; *Xuan and Channell*, 2010]. In this paper, we revisit previous age model hypotheses and present an original age model for central Baffin Bay based on the combination of relative paleointensity (RPI) data, the identification of magnetic excursions and radiocarbon dating.

2. Regional setting

2.1. Hydrography

Baffin Bay (Figure 1) is a narrow oceanic basin (1300 km long and 450 km wide, ~690 000 km^2) nearly enclosed with shallow connections to the Arctic by Nares Strait and the Canadian Arctic Archipelago (CAA) channels, and a connection to the North Atlantic via Davis Strait (sill depth: 650 m). The morphology of the bay consists of a central abyssal plain (2000 – 2500 m) surrounded by continental shelves

(Figure 1). Surface current circulation is anti-clockwise [*Tang et al.*, 2004] (Figure 1). The modern specific oceanographic features of the bay lead to a very shallow lysocline resulting in poor preservation of calcareous microfossils [*Aksu*, 1983a; *de Vernal et al.*, 1992; *Azetsu-Scott et al.*, 2010]. Extensive sea-ice covers the bay except in August and September and does not allow for high productivity rates [*Tang et al.*, 2004].

2.2 Bedrock geology

The Baffin Bay geology is mostly characterized by a Precambrian crystalline basement overlain by a Lower Paleozoic succession dominated by shallow marine platform carbonates. Very limited outcrops of younger rocks are found. Tertiary rifting resulted in the development of a series of large grabens (sound, strait) and basaltic flows, observed along Canadian and Greenland Precambrian Shield margins [*Hiscott et al.*, 1989; *Korstgärd and Nielsen*, 1989; *Thiébault et al.*, 1989; *Aksu and Piper*, 1987; *MacLean et al.*, 1990]. Archean and Paleoproterozoic are the largest outcropping units on each side of the bay. Paleozoic carbonate, principally dolostones with some limestones, outcrops in NW Greenland and the Canadian Arctic Archipelago (Figure 1).

2.3. Quaternary geology and sedimentation

During the Last Glacial Maximum (LGM) the NE Laurentide Ice Sheet (LIS), the Innuitian Ice Sheet (IIS) and the western Greenland Ice Sheet (GIS) constituted a continuous ice belt surrounding Baffin Bay. The GIS probably extended westward at the inner shelf, and possibly as far as the shelf edge [*Ó Cofaigh et al.*, 2010; *Funder et al.*, 2011]. GIS and IIS were likely joined across Nares Strait [*England et al.*, 2006]. The LIS extended through Baffin Island, probably as far as the fjords mouths and possibly over part of the Baffin Island shelf [*Briner et al.*, 2003; 2006]. Deglaciation was on its way as early as ~15 – 16 cal ka BP [*Briner et al.*, 2006;

Funder et al., 2011; *Jennings et al.*, 2011]. However, Nares Strait was not deglaciated until 8.5 cal ka BP [*Dyke*, 2004; *Jennings et al.*, 2011].

The impact of the pre-LGM glaciations on Baffin Bay sediment delivery is poorly known because of weak chronostratigraphies [*Vincent and Prest*, 1987]. Nevertheless, sedimentary facies and the mineralogy of the late Quaternary sediments have been thoroughly described [e.g., *Marlowe*, 1966; *Piper*, 1973; *Aksu*, 1981; *Aksu and Piper*, 1987; *Hiscott et al.*, 1989; *Andrews et al.*, 1998]. Based on the mineralogy of detrital supplies and sediment textures, sedimentary processes were tightly controlled by glacial/interglacial (or stadial/interstadial) cycles and sediment facies could be discriminated from their deposition processes. For instance, deposition of coarser carbonate (dolomite-rich) ice-rafted sediments (i.e., Baffin Bay Detrital Carbonates layers, BBDC) suggest an axial source of ice-rafted debris, probably reflecting rapid breakup and melting of formerly dry-base ice shelves off Devon and Ellesmere Islands and in Lancaster Sound [*Aksu and Piper*, 1987; *Parnell et al.*, 2007]. According to *Andrews et al.* [1998], these BBDC layers may be broadly coeval with major interstadials $\delta^{18}O$ peaks of the GISP2 record and could be caused by or associated with the inflow of warm Atlantic Water into the western part of the bay [*Hiscott et al.*, 1989; *Andrews et al.*, 1998] causing rapid retreat of northern Baffin Bay ice streams. However, the age models and timing for these BBDC-events are insufficient to properly correlate them with Greenland interstadials or North Atlantic Heinrich events as well as to put forwards unquestionable relationships between both types of events.

3. Materials and Methods

Core HU2008-029-016PC (PC16 hereinafter) is a 741-cm long piston core raised from central Baffin Bay during the 2008-029 CCGS Hudson expedition (70°46.14 N/-64°65.77 W; water depth: 2063 m) [*Campbell and de Vernal*, 2009]. The core location (Figure 1) is within proximity of an ODP site previously drilled in

1985 (ODP 645, leg 105) [*Srivastava et al.*, 1989] and of several sites of cores raised from deep central Baffin Bay during the 1970s and 1980s [*Aksu*, 1981; *Aksu and Piper*, 1987; *Andrews et al.*, 1998].

3.1. Physical and geochemical properties

Physical properties such as wet bulk density (by Gamma Ray Attenuation) and low field volumetric magnetic susceptibility (k_{LF}) were measured on board using a GEOTEK Multi Sensor Core Logger (MSCL) at 1 cm intervals. Diffuse spectral reflectance data were acquired at 1 cm resolution immediately after splitting the core, using a Minolta CM-2600d handheld spectrophotometer and then converted into the *Commission Internationale de l'Eclairage* (CIE) color space (i.e., L*, a*, b*) [*St-Onge et al.*, 2007]. The core sections (1.5 m long) were described and sampled with u-channels (rigid u-shaped plastic liners, 2 x 2 cm cross section) from the center of the working halves for paleomagnetic and µXRF (ITRAX™ core scanner-see below) analyses. The archive halves were ran through a computerized coaxial tomography scanner (CAT-Scan) at 0.1 cm intervals at INRS-ETE in Québec City. The digital X-ray resulting images were displayed on grey scale and expressed as CT numbers, which primarily reflects changes in bulk density [*St-Onge et al.*, 2007; *Duchesne et al.*, 2009]. Grain size analyses were performed on sediment samples (1 – 2 g) at the *Institut des sciences de la mer de Rimouski* (ISMER) using a Beckman Coulter™ LS13320 laser diffraction grain size analyzer at 4 cm intervals. Wet sediment was mixed in a solution of 20 gL^{-1} of Calgon electrolytic solution (sodium hexametaphosphate) and water. The samples were rotated for 3 hours and then sieved at 2 mm prior to analysis. The grain size distribution and statistical parameters (mean, standard deviation) were calculated using the Gradistat software [*Blott and Pye*, 2001]. Relative content of calcium (Ca), titanium (Ti), iron (Fe), manganese (Mn), among others, were determined by micro X-ray fluorescence (µXRF) spectrometry on the u-channels at 0.5 cm intervals and a 50 s counting time using an ITRAX™ core scanner (Cox Analytical Systems). The measurements were carried out at the

GIRAS laboratory (Geochemistry, Imagery and Radiography of Sediment) of INRS-ETE, with a molybdenum anode tube that allowed the measurements of elements from Si to U. The output data represent relative concentrations, which are reported in peak area integrals for each element (dispersive energy spectrum). Ca contents were used to identify the BBDC layers in core PC16 assuming Ca was of detrital origin [*Polyak et al.*, 2009].

3.2. Mineralogy

Mineralogical assemblages were determined by X-ray diffraction (XRD) at UQAM using a Siemens D-5000 diffractometer (CoKα1,2 radiation and a Si detector). The analyses were performed on bulk sediments (<2 mm) from the top of the core to 115 cm at 4 cm intervals. Semi-quantitative estimations ($\pm 1\sigma \sim 5\%$) of the main mineral species were based on the height of the first diffraction peak for each mineral corrected for quartz [*Thorez*, 2003].

3.3. Magnetic remanence analyses

Paleomagnetic data were measured at the *Laboratoire de paléomagnétisme sédimentaire et géologie marine* at ISMER with a 2G-Enterprises™ u-channel cryogenic magnetometer allowing the continuous measurement, at 1 cm intervals, of the natural, anhysteretic and isothermal remanent magnetizations (respectively NRM, ARM, IRM). The response function of the magnetometer pick-up coils integrates measurements over several centimeters (~7 – 8 cm). To reduce the edge effect associated with the response function, the data from the last and first 5 cm of each u-channel were excluded. The NRM was measured using stepwise alternating field (AF) demagnetization at peak fields from 0 to 80 mT at 5 mT increments. Directions (inclination and declination) of the characteristic remanent magnetization (ChRM) were calculated by principal component analysis (PCA) with 9 AF demagnetization steps from 20 to 60 mT. The declination record was rotated in order to adjust the mean declination to zero. The precision of the best-fit procedure was estimated by the maximum angular deviation (MAD) [*Kirschvink et al.*, 1980]. MAD values lower than 5° are often considered as high quality directional data for paleomagnetic secular variations (PSV) and relative paleointensity (RPI) studies of Quaternary marine sediments [*Stoner and St-Onge*, 2007]. The ARM was induced at a peak AF of 100 mT with a 0.05 mT direct current (DC) biasing field, and then demagnetized and measured from 0 mT to 70 mT at 5 mT increments. The ARM was also expressed as the anyhsteretic susceptibility (k_{ARM}) by normalizing the ARM with the biasing field. An IRM was imparted to the z-axis of the u-channel with a DC pulse field of 0.3 T using a 2G Enterprises™ pulse magnetizer. The IRM was then demagnetized and measured from 0 mT to 70 mT at 5 mT increments. A second IRM corresponding to a saturated IRM (SIRM) was imparted with a higher DC field of 0.95 T and then demagnetized and measured at the same steps. We calculated the IRM/SIRM ratio (Pseudo-S ratio) after AF demagnetization at peak fields of 25 mT in order to measure the relative importance of the high coercivity component of the magnetic mineral assemblage [e.g., *Stoner and St-Onge*, 2007]. Values close to 1 are indicative of low coercivity magnetic carriers (e.g., magnetite), whereas lower values indicate a high coercivity magnetic mineralogy (e.g., hematite). Median destructive field (MDF, the value of the peak AF necessary to reduce the magnetic remanence to half of its initial value) of the NRM was calculated using the Mazaud Excel spreadsheet [*Mazaud*, 2005]. It reflects the mean coercivity state of the magnetic grain assemblage, which depends on both the grain size and mineralogy [e.g., *Dunlop and Özdemir*, 1997; *Dankers*, 1981]. The k_{ARM}/k_{LF} ratio was calculated to estimate the magnetic grain size variability throughout the core [*Banerjee et al.*, 1981; *King et al.*, 1982; *Maher and Thompson*, 1999].

3.4. Rock-magnetism

Magnetic assemblages were determined in 170 samples by measuring hysteresis properties, back-field remanence and IRM acquisition curves using an alternating gradient force magnetometer (AGM) MicroMag™ 2900 from Princeton

Measurements Corporation™. Hysteresis loops along with backfield remanence curves were used to determine saturation magnetization (Ms), coercive force (Hc), saturation remanence (Mrs) and coercivity of remanence (Hcr). The ratios Mrs/Ms and Hcr/Hc are used as magnetic grain size proxies and to identify the magnetic domain state [*Day et al.*, 1977; *Dunlop*, 2002a; *Tauxe et al.*, 1996, 2010]. In a biplot of these ratios, theoretical area for single (SD), pseudo-single (PSD) and multi domain (MD) magnetite grains and the mixing reference curves have been proposed by *Day et al* [1976] and then revisited by *Dunlop* [2002a, 2002b]. Along with these measurements, the temperature-dependence of magnetic susceptibility was measured on 24 samples using a MS2WF Bartington™ instrument. The measurements were made at 2°C steps from room temperature (~24°C) to 700°C and subsequent cooling to room temperature (air environment). The magnetic mineralogy can be determined using the specific Curie temperature of minerals [*Dunlop and Özdemir*, 1997].

3.5. Radiocarbon dating

Three radiocarbon ages were obtained (Table 1) from planktonic foraminifera (*Neogloboquadrina pachyderma* left-coiled (Npl)) samples by accelerator mass spectrometry measurements performed at the Lawrence Livermore National Laboratory Center for Accelerator Mass Spectroscopy (LLNL-CAMS). The ^{14}C ages were then calibrated using the CALIB 6.0 software [*Stuiver et al.*, 2010] using the Marine09 dataset [*Reimer et al.*, 2009]. Results are reported in calendar *kilo*-years before present (cal ka BP) at the 2σ-confidence level (95%) (Table 1). A regional reservoir correction of 0 yr (ΔR=0) was first applied based on ocean circulation and ventilation similar to today [*Coulthard et al.*, 2010]. However, ΔR values during the last deglaciation, i.e., the interval dated here, probably departed from 0 yr. Therefore, we applied the bayesian calibration technique using the BCal online program [*Buck et al.*, 1999] based on radiocarbon ages and prior information (i.e., stratigraphical order) as a way to encompass this dilemma. The posterior age depth model presents the radiocarbon ages as the highest posterior density function (HPDF) within the sequence using the Marine09 and a $\Delta R=200\pm200$ to append a marine reservoir effect (Figure 12). It enables significant improvement in terms of precision using HPDF outputs compared with the traditional calibration method of CALIB 6.0. The resulting calibrated ages are consistent with individual ages calibrated with a ΔR close to 400 yrs. This is also consistent with high ΔR previously estimated for the North Atlantic during the last deglaciation [*Bard et al.*, 1994; *Waelbroeck et al.*, 2001; *Bondevik et al.*, 2006; *Cao et al.*, 2007; *Austin et al.*, 2011]. Moreover, a high regional ΔR (> 200 yrs) during that period is probably appropriate considering the low ventilation between the ocean and the atmosphere due to (1) the presence of sea ice toward the bay [*de Vernal et al.*, 1987] and (2) meltwater inputs that reduced convection.

4. Results

4.1. Stratigraphy

The photographs and CAT-Scan images (Figures 2, 3 and 12) reveal a highly variable lithology throughout the core. Likewise the grain size distribution shows a broad size range from very fine clay material to coarse sand and up to gravel intervals (Figure 2). Clay content (<2 μm) is relatively stable with values between 20 to 30 % except within the 130 – 170 cm interval where peaks up to 40 % and close to 60 % are observed. Silt content (2 μm – 63 μm) has an average of 45 – 50 % and exhibits a significant increase from 70 cm to the top of the core (60 to >80 %). Sandy layers (63 μm – 2 mm, Figure 2) are numerous throughout the core with sand percentages of 20 to 30 % in distinct intervals and up to 50 % between 210 – 225 cm. Gravel contents (>2 mm) between 10 to 30 % occur at very specific depth-intervals. The gravel peaks are associated with sandy layers supporting an ice rafted debris (IRD) transport mode. Between 20 to 100 cm, gravel percent oscillates between 5 and 20 %. This is most probably concomitant to the last deglaciation with larger IRD release and meltwater pulses related to the collapse of the large regional ice sheets (IIS, GIS and Baffin Island's ice caps). Grain size sorting (not shown) varies from poorly sorted to very poorly sorted sediment with a trimodal to polymodal mode that demonstrates multiple sediment transport and deposition processes (i.e., hemipelagic, sea-ice, IRD, meltwater pulses, turbidites). Grayish-brown layers (5Y $^5/_2$ - 7.5 YR $^5/_2$) are associated with gravelly sandy mud, higher L* (white) values, high Ca and low Fe and Ti contents (Figure 2). The very top of the core (0 – 20 cm) is characterized by a brown to dark brown color (10YR $^3/_4$ - 7.5 YR $^4/_2$) illustrated by increasing a* values (red) and a very large increase of the Mn/Ti ratio possibly related to changes in redox conditions (Figure 2) [*Croudace et al.*, 2006], and to increases in Mn-rich sediments that could be synchronous of the Holocene period in the Arctic regions [*Polyak et al.*, 2009]. Mud- to slightly sandy mud layers are dark gray (5Y $^4/_1$) to olive-gray (5Y $^5/_2$), which is reflected by lower L* (black) and a* (green) values coinciding with higher Fe and Ti contents. Pebbles are recognizable on the CAT-Scan images and are most often associated with gravelly sandy mud grayish-brown layers (see lithostratigraphic log on Figures 2, 3 and 12). The density profiles (GRA density and CT number, Figure 2) reveal layers of increased density associated with higher L* values, corresponding to higher Ca and lower Fe contents and lower k_{LF} values. These grayish brown, gravelly to sandy mud decimetric layers (20 to 60 cm) correspond to intervals of higher carbonate content (Figures 2, 3 and 12). These layers are in accordance with the BBDC layers previously reported [*Aksu et al.*, 1981; *Aksu and Pipper*, 1987] and summarized by *Andrews et al.* [1998] (see section 2.3).

Based on the core description, physical properties, grain size and previous studies of Baffin Bay marine sediments [e.g., *Aksu and Pipper*, 1987; *Andrews et al.*, 1998], we define 4 major sediment facies that broadly characterize central Baffin Bay sediments and more precisely core PC16 sediments: (1) Uppermost Brown (UB) – brown to dark brown silty muds; (2) Olive Clay (OC) – brownish-black and olive-black silty muds to clayey muds; (3) Detrital Carbonate (DC) – carbonate-rich yellowish-brown to dark brown very poorly sorted gravelly sandy muds (corresponding to the BBDC-layers); (4) Low Detrital Carbonate (LDC) – olive-gray to dark grey poorly sorted sandy muds to slightly gravelly sandy muds.

4.2. Magnetic properties

The different lithological facies questions the reliability of a straightforward magnetostratigraphy approach. Accordingly, an extended rock-magnetic description of these lithological facies is needed to assess their magnetic reliability for the recording of a genuine geomagnetic signal.

4.2.1. Magnetic Mineralogy

IRM acquisition curves saturated below 300 mT (Figure 4b), together with the typical shape of hysteresis loops (Figure 4a) suggest that the NRM is carried by low-coercivity magnetic mineral such as magnetite and/or titanomagnetite [*Tauxe*, 1996]. Thermomagnetic analyses (Figure 4c) point out three distinct behaviors during heating: (1) an increase in susceptibility from 200 to 300°C, (2) a weak and continuous loss in susceptibility following the 300°C peak and (3) a significant drop in susceptibility at roughly 580°C (= Curie temperature of magnetite) [*Dunlop and Özdemir*, 2007] in almost all samples. The drop at the Curie temperature indicates magnetite as the main remanence carrier along the core. The increase in susceptibility during heating together with the higher susceptibility values after the cooling and the asymmetry of the heating and cooling curves are indicative of alteration, transformation and growth of magnetic minerals during the course of the analysis [*Dearing*, 1999; *Maher and Thompson*, 1999]. The decrease in magnetic susceptibility at 300 – 350°C could be associated with a change of maghemite to hematite [*Dearing*, 1999; *Butler*, 1992], or with some alteration of greigite and/or pyrrhotite [*Maher and Thompson*, 1999] within specific depth-intervals. The presence of greigite is confirmed by gyroremanence (GRM) in the AF demagnetization data of NRM [*Roberts et al*, 2011] at a few intervals (0-4 cm, 58-88 cm, 102-115 cm, 217-235 cm, 520-535 cm), while pyrrhotite may probably be present within the 130-160 cm depth-interval (olive-black clay sediments, facies "OC") according the values of $SIRM/k_{LF}$ >20 kAm^{-1} (not shown) and k_{ARM}/k_{LF} >15 [*Maher and Thompson*, 1999]. The recovery of the transition temperature near 350°C on the cooling curves (Figure 4c) suggests a Curie temperature for titanomagnetite [*Butler*, 1992]. Within the "Uppermost Brown facies" (upper part of the core), some susceptibility remains after 600°C, hinting at the presence of hematite within the magnetic assemblage at this specific interval which is also characterized by the highest MDF_{NRM} (Figure 3) and a* (red) values (Figure 2). As a whole, the Pseudo-S ratio varies between ~0.8 and 1 (Figure 3). Values higher than 0.9 are observed from the top to 130 cm and from 215 cm to the bottom of the core (except within specific layers, see below), indicating that much of the saturation of the magnetic assemblage is achieved in a 0.3 T field, which is consistent with the presence of magnetite and/or titanomagnetite as main remanence. Between 130 and 215 cm, the Pseudo-S ratio shows values close to 0.8 indicating the possible presence of higher coercivity minerals in this interval (i.e., goethite, greigite, pyrrhotite, hematite). MDF_{NRM} values ranging from ~25 – 30 mT are found from 250 cm to the bottom of the core which again suggests the presence of low coercivity minerals such as magnetite and/or titanomagnetite in this interval [*Dankers*, 1981] (Figure 3). From 80 cm to the top of the core, MDF_{NRM} values sharply increase with values up to 90 mT except very low values (close to 5 mT) within the 45 – 60 cm and 90 – 105 cm layers corresponding to larger magnetic grain size (MD grains, Figures 3 and 5) also associated with a gravel peak (Figure 2). These high MDF_{NRM} values could be characteristic of the presence of high-coercivity minerals such as hematite within the mineralogical assemblage. Between 90 to 105 cm, low Pseudo-S ratio values of ~0.7 suggest the apparent presence of higher coercivity minerals such as goethite or hematite. However, when looking at the same ratio but at 0 mT, the values are close to 0.9 (not shown), which are indicative of low coercivity minerals. The difference between the Pseudo-S ratio at 0 and 25 mT thus reflects changes in magnetic grain size and not mineralogy in this specific interval characterized by the presence of gravel. Altogether these results point to magnetite and/or titanomagnetite as being the dominant remanence carriers throughout the core, although iron sulfides, maghemite and hematite may be present within specific depth-intervals.

4.2.2. Magnetic grain size and concentration

Magnetic concentration parameters such as NRM, ARM, IRM, SIRM and k_{LF} (Figure 2 and 3) show increases in the intensity of the remanence and magnetic susceptibility in the Low Detrital Carbonate facies suggesting an increase in the concentration of ferrimagnetic minerals within this facies. Low Detrital Carbonate facies are also characterized by higher k_{ARM}/k_{LF} (Figure 3) values corresponding to finer magnetic grains. The coarsening of magnetic grain size within carbonate layers suggests a distinct origin (or transport process, e.g., IRD) and/or a dilution of the finer ferrimagnetic minerals. Moreover, the lowest k_{ARM}/k_{LF}, NRM, ARM, IRM, SIRM, MDF_{NRM} values indicate the occurrence of somewhat coarser magnetic grain intervals within some specific Detrital Carbonate layers (Figure 3). Such coarse intervals are well illustrated by MD grains within the Day plot (Figure 5). High values of NRM, ARM, IRM, SIRM, k_{ARM}/k_{LF} together with low k_{LF} suggest a relative increase of finer grains (Figure 2 and 3) rather than an overall concentration increase within the "Olive Clay facies". This is also illustrated by a close match between the clay percent and k_{ARM}/k_{LF}, which supports the presence of finer magnetic grains throughout the Olive Clay facies. In addition, higher Mrs/Ms values (0.35 – 0.4) and wider hysteresis loops (Figure 4a) are found within the Olive Clay facies and are indicative of finer grains (PSD to SD domain; Figure 5), whereas Mrs/Ms values ranging between 0.1 and 0.3 characterize the bulk of the core and are typical of relatively coarser PSD titanomagnetite grains [*Day et al.*, 1977; *Tauxe*, 1993; *Dunlop*, 2002a] (Figure 5). Sediments from the Uppermost Brown, Olive Clay and Low Detrital Carbonate facies are well distributed ($r > 0.92$) along mixing lines within the PSD domain (1 – 15 μm; Figure 5), while some Detrital Carbonate layers are found in the MD domain according to the Day plot [*Day et al.*, 1977; *Dunlop*, 2002a]. DC-layers are also characterized by a more heterogeneous magnetic grain size distribution (r = 0.7). Uppermost Brown and Olive Clay facies' grains are slightly shifted upward toward the SD domain (also revealed by the hysteresis shape, Figure 4a) indicating finer ferrimagnetic grains.

In summary, the sedimentary sequence is composed of 4 distinct magnetic assemblages:

(1) low coercivity ferrimagnetic minerals within the PSD range, which characterize a "background" facies corresponding to the Low Detrital Carbonate facies;

(2) finer magnetic minerals within the SD – PSD range characterizing the Uppermost Brown (upper 20 cm) and Olive Clay (130 - 215 cm) facies, possibly containing a fraction of higher coercivity minerals;

(3) low coercivity ferrimagnetic minerals in the coarse PSD range with lower magnetic concentration, characterizing the main fraction of the Detrital Carbonate layers;

(4) low coercivity ferrimagnetic minerals in the MD domain associated with magnetic dilution and coarse grains.

4.3. Natural remanent magnetization

The vector end-point diagrams [*Zijderveld*, 1967] reveal the presence of two magnetic components that characterize the magnetic recording (Figure 6): a very low coercivity component (viscous magnetization) easily removed after a AF demagnetization between 5 – 15 mT, and a stable well-defined characteristic remanent magnetization (ChRM). The maximum angular deviation (MAD) values are lower than 5° for most of the core (87.5% of the whole core, Figure 7a), which is considered as excellent quality data [*Stoner and St-Onge*, 2007]. MAD values between 8 and 12°, which are still considered as good quality data [*Butler*, 1992; *Opdyke and Channell*, 1996], are only found in very few Detrital Carbonate layers (2.3% of the total measurements) characterized by MD magnetic grain and/or edges of the u-channels (Figure 5 and 7a) while the remaining MAD values are found between 5 to 8°. As a whole, the Characteristic remanent magnetization (ChRM) inclinations (Figure 7b) fluctuate around the expected inclination based on a geocentric axial dipole (GAD) model for the latitude of the coring site (I_{GAD} = 79.9°), indicating a well-preserved and high-quality paleomagnetic signal [e.g., *Stoner and St-Onge*, 2007].

To summarize all magnetic data, most of the sedimentary sequence is characterized by a well-defined and strong ChRM carried by low coercivity minerals within the PSD range and following a magnetite mixing line. Nonetheless, the presence of secondary magnetic minerals such as iron sulfides, hematite and/or maghemite may be found in specific intervals, but these intervals represents only ~16 % of the core and are not associated with key intervals such as the RPI peaks and throughs used for the establishment of the age-model (see below). In addition, several thin layers corresponding to the sandiest intervals (Figure 2 and 8) are identified by a larger grain size in the MD domain (Figures 3 and 5) and will have to be taken with caution (especially when corresponding to MAD >5°, Figure 7) for relative paleointensity (RPI) reconstruction. Concentration and grain size variability remain below a factor 10 (reliable for RPI study) if such specific DC layers are excluded (gray shaded areas on Figure 7 and 8). Nonetheless, as noted by *Stoner et al.* [2000], thin sand layers (with MD grains) within a sediment sequence could still be suitable for paleomagnetic studies as they may not significantly influence the rock magnetic properties of the remanence carriers. Moreover, *Spassov and Valet* [2012] demonstrated that the depositional remanent magnetization (DRM) of carbonate-rich sediments is linearly related to the field intensity, confirming their reliability for RPI studies. Their experiments also suggest that down-core changes in carbonate content do not affect the response of the magnetization to the field.

4.4. Relative paleointensity (RPI) determination

Estimation of the relative paleointensity (RPI) of the geomagnetic field in sedimentary sequences is a function of the natural remanent magnetization carried by the detrital ferrimagnetic grains [see *Tauxe* 1993, 2007 and *Valet* 2003 for extended reviews]. However, the intensity of the remanence is also influenced by changes in the magnetic mineralogy, concentration and grain size. Thus the NRM must be normalized by an appropriate magnetic parameter in order to compensate for these "non-geomagnetic field" imprints. Concentration dependant parameters such as laboratory-induced magnetizations (ARM, IRM and SIRM) or k_{LF} are commonly employed as normalizers in literature [e.g., *King et al.*, 1983; *Tauxe*, 1993, 2007].

To validate the reliability of the RPI proxy, several criteria must be satisfied:

(1) The NRM must be characterized by a strong, stable and single component magnetization carried by low coercivity ferromagnetic grains (e.g., magnetite) within the SD – PSD range [*King et al.*, 1983; *Tauxe*, 1993]. Moreover, changes in the magnetic concentration should not vary by more than a factor 10 [*Tauxe*, 1993]. As discussed earlier, with the exception of some specific intervals (not used for RPI determination), the magnetic mineralogy for the bulk of the core is well-suited for paleointensity determination with the presence of magnetite in the PSD grain size range with a strong, stable and well-defined ChRM (Figures 4, 5 and 6).

(2) The normalizer should activate the same grains that carried the NRM [*Levi and Banerjee 1976*]. k_{LF} being sensitive to large MD magnetite grains as well as superparamagnetic (SP) grains, which do not carry a magnetic remanence, it was considered as an inappropriate normalizer in this environment heavily impacted with coarse ice rafted debris layers. In addition, the presence of coherency (high values of

the Blackman-Tuckey cross-spectral analysis using a Bartlett window at 95% confidence level), and a linear correlation coefficient of -0.33 between NRM/k_{LF} and k_{LF} (supplementary materials, S2-a) reveal an incomplete normalization or an over correction [*Tauxe*, 2007]. The next possible normalizers are the ARM and IRM. The ARM is often chosen as a normalizer because it activates PSD grains of magnetite, whereas IRM can also activate a large fraction of magnetic grains (MD) that do not carry the NRM [*Levi and Banerjee*, 1976]. To select the demagnetization interval and normalizer that best mimics the coercivity spectrum of the NRM, we compared the slope of the NRM, ARM and IRM intensity from several demagnetization steps [*Levi and Banerjee*, 1976]. Linear correlation coefficients (r) were calculated in order to quantify the relationship throughout the whole core [*Channell et al.*, 2002]: r-value close to 1 being indicative of well-defined slopes with coercivity of the normalizer that activates the same coercivity than the NRM. The best r-values were found for the 25 – 35 mT AF demagnetization interval (supplementary materials, S1) for both ARM and IRM. The r calculated against ARM present very few values <0.99, while correlations with IRM show r <0.95 for some specific intervals (45 – 60 cm, 95 – 105 cm, 245 – 250 cm and 535 – 560 cm) corresponding to intervals of low MDF_{NRM}, high MAD values and/or presence of secondary magnetic minerals such as greigite or maghemite. Within these intervals, and more largely for the whole core, the ARM coercivity spectra seem to best mimic the NRM than the IRM ones.

(3) The RPI proxy cannot be correlated with its normalizer or with any lithological proxy [*Tauxe and Wu*, 1990]. Here, the relative paleointensity estimates (RPI) do not correlate with their normalizer (r <0.2) (supplementary material, S2-a). Furthermore, we tested the coherence between both RPI estimates and their respective normalizers using a Blackman-Tuckey cross-spectral analysis with a Bartlett window at 95% confidence level [*Paillard et al.*, 1996]. The cross-spectral analysis reveals that the RPI proxies are not coherent with their normalizers for the majority of the core but present some coherency over few specific intervals

(supplementary materials, S2-a). We also tested the coherence of NRM/ARM and NRM/IRM with lithological proxies such as MDF_{NRM}, k_{ARM}/k_{LF} and IRM/SIRM (supplementary material, S2-b, S2-c). NRM/IRM is not coherent nor correlated with these proxies ($r < 0.1$), while NRM/ARM is slightly more coherent with NRM_{MDF} ($r = 0.28$). When comparing both NRM/ARM and NRM/IRM proxies (Figure 8), the same variability is observed from 120 cm to the bottom of the core, while RPI estimates present distinct features from 115 cm to the top of the core. When removing the section 0 – 115 cm, NRM/ARM presents no coherency or correlation ($r = 0.05$) with NRM_{MDF}. The clear mismatch between both RPI curves and the extreme MDF_{NRM} and IRM/SIRM fluctuations at the top of the core (0 – 115 cm) lead to a doubtful recording of the genuine geomagnetic field in that specific interval.

Based on these results, we selected the $ARM_{25\text{-}35\ mT}$ as the best normalizer. It activates the same magnetic assemblages than the $NRM_{25\text{-}35mT}$ and presents no correlation with lithological proxies. However, some problematic layers will have to be treated with caution or removed from the record as their coarser (e.g., MDF_{NRM} <5) magnetic grains may have diminished the effectiveness of the normalization (shaded area in Figures 7, 8 and 9).

5. Discussion

5.1. Age/depth relationship

In order to establish an original age-depth relationship in central Baffin Bay, an environment characterized by significant calcium carbonate dissolution and the problematic use of ^{18}O stratigraphies (see sections 1 and 2.1), we compared the core PC16 RPI record with several well-dated RPI records and stacks (Figure 9). Nonetheless, the establishment of an age-depth relationship for the top of the core based on RPI correlations still presented some difficulties due to the lower quality of the remanence carrier that characterizes the interval 0 – 115 cm (see sections 4.2 and 4.4). Therefore, in order to propose an original age model for that period we correlated the relative percentages of calcite between the PC16 record and a nearby well-dated box core from Baffin Bay (core JCR175-BC06) studied by *Andrews and Eberl* [2011] (Figure 11). The records from BC06 and PC16 were correlated (r = 0.975) with 10 tie points using the AnalySeries program [*Paillard et al.*, 1996]. It enables to transfer the chronology of core BC06 to core PC16 (Figure 11). The robust correlation between both mineralogical signals together with the good fit between the interpolated age model and the 3 available radiocarbon ages allow a pretty strong chronology for that problematic interval even if it is set from an indirect approach (changes in sediment mineralogy).

Between 125 and 478 cm, the age model was established by correlating core PC16 to the North Atlantic relative paleointensity stack (NAPIS-75) [*Laj et al.*, 2000] (between 22 to 75 ka) with 21 tie points (peaks and troughs, Figure 9 and Table 2) using the AnalySeries program. The best correlation coefficient (r = 0.8) was obtained by sliding the two curves with respect to each other (Figure 10). The incertitude in the age model for the 22 – 75 ka interval corresponds to the $\pm 2\sigma$ incertitude from the NAPIS bootstrap calculation (grey area on Figures 9, 10 and 12). The use of the NAPIS-75 stack, that compiled 6 North Atlantic marine cores spanning the last 10 - 75 ka [*Laj et al.*, 2000], as the main reference is particularly interesting because (1) the stacking process has removed the variability induced by the lithology or regional magnetic origins (i.e., non-dipole field), (2) post-depositional magnetization acquisition are considered negligible in the NAPIS-75 stack [*Kissel et al.*, 1999; *Laj et al.*, 2000], and (3) the NAPIS-75 age model was correlated at the millennial scale and placed on the GISP2 age scale, allowing a robust chronology. The RPI record from 480 to 741 cm was correlated using 14 tie-points with 6 well-dated individual records and stacks (Figure 9). The individual RPI reference curves are from (1) the Labrador Sea: cores MD95-2024 [*Stoner et al.*, 2000] and 094PC [*Stoner et al.*, 1996, 1998] and (2) the North Atlantic: ODP site 983 [*Channell et al.*, 1997]. The RPI marine stacks include (1) the high-resolution

Mediteranean & Somali region stack [*Meynadier et al.*, 1992] and (2) the low resolution Sint200 [*Guyodo and Valet*, 1996] and PISO-1500 [*Channell et al.*, 2009] stacks, from Atlantic, Mediterranean, Indian and western Pacific records. The temporal shifts observed between these records are represented by the standard deviation between the 6 references curves (grey area on Figure 12) and are due to their intrinsic chronological uncertainties. The different sedimentation rates and lock-in depths of the distinct records could explain part of the differences observed in the amplitude of relative paleointensity variations. Also, some non-dipole component (especially where very high sedimentation rates were recorded) could be part of individual records, possibly accounting for some relative differences between paleointensity features.

The RPI record of core PC16 is remarkably in agreement and present strong coherency (at 95% confidence level using Blackman-Tuckey cross-spectral analysis with a Bartlett window) with the NAPIS-75 stack (Figure 10 and supplementary materials, S3). Similarly, the relatively strong correlation coefficients obtained between core PC16 and several other individual high-resolution RPI records and stacks further supports the geomagnetic origin of the signal (Figure 9) in the 20 – 75 ka interval (Figure 9). Between 75 and 100 ka (where each dataset overlap), the overall agreement between the main RPI features in PC16 and other reference curves (Figure 9) also supports the age-model established. However, the correlation coefficients calculated in this interval present lower values, which can be explained by (1) low-resolution stacks (i.e., Sint200, PISO-1500) with low variability, (2) highly variable sedimentation rates between cores (for instance, the best correlation (r=0.71) is calculated with core ODP983, which have similar sedimentation rates with PC16 in this time period, i.e., ~10 cm/ka) [*Channell et al.*, 1997] and (3) uncertainty of the respective age models based on low-resolution isotopic stratigraphies [*Stoner et al.*, 1996, 1998, 2000; *Guyodo and Valet*, 1996].

5.2. Paleomagnetic secular variations and excursions in Baffin Bay

Two large declination changes are observed at 2 intervals that have been excluded based on rock-magnetism analyses (Figure 7c). The first one (46 – 62 cm) is located within a coarse sediment interval (MDF_{NRM} <5 and MD grain, Figures 3 and 5), while the second one is a remobilized facies (525 – 545 cm, CT image). It demonstrates the lithological influence on the declination in these specific intervals (note that these intervals have been removed for the RPI reconstruction, see sections 4.2 and 4.4). While the inclination record generally oscillates around the expected GAD values, 3 inclination lows (Figure 7b) present large deviations from the GAD (>40°) and are associated to low geomagnetic intensity (95 – 105 cm; 270 – 290 cm; 415 cm – section break). Such a pattern is commonly considered as a geomagnetic excursion [*Laj and Channell*, 2007]. The 95 – 105 cm (~14.8 – 15.5 cal ka BP) large deviation is recorded within a layer characterized by coarse magnetic grains (with MDF_{NRM} <5 and MD grain) and the paleomagnetic results are most likely attributed to lithological overprints. The 2 remaining large deviations are found in sedimentary layers that may be seen as reliable recorders of the genuine state of the geomagnetic field. Unfortunately, these potential excursions are located near section breaks and are characterized by 8 and 6 data points, respectively (excluding the deleted data at section break), hence questioning their magnetic origin. Yet the paths of the Virtual Geomagnetic Poles (VGPs, Figure 7d) toward the Southern Hemisphere during these 2 intervals are relatively similar to the ones observed for the Norwegian-Greenland Sea and Laschamp geomagnetic excursions except for the sense of looping [*Laj and Channell*, 2007; *Laj et al.*, 2006; *Lund et al.*, 2005]. The details of the field behavior (i.e., sense of looping and paths) during these excursions could have been poorly recovered considering the low sedimentation rates (<8 cm/ka) and the smoothing associated with post-depositional remanent magnetization acquisition [*Roberts*, 2008]. It might explain the discrepancy with the above references. These two large inclination lows are recorded at ca. 40.9 and 64.8 cal ka BP (respectively) according to the constructed age model. The timing is thus consistent with the Laschamp (41±1 ka) [*Lund et al.*, 2006] and the Norwegian-Greenland Sea (61±2 ka) [*Lund et al.*, 2006] excursions, which in turn supports their excursional origin. However, several low inclinations in sedimentary cores from the Arctic have been recently attributed to partially self-reversed CRM carried by titanomaghemite and acquired during the oxidation of detrital (titano)magnetite grains rather than representing genuine geomagnetic excursions [*Channell and Xuan*, 2009; *Xuan and Channell*, 2010; *Xuan et al.*, 2012]. Since oceanographic conditions in Baffin Bay are broadly similar to the Arctic Ocean and since no NRM thermal demagnetization experiments were carried out in this study, a partially self-reversed CRM carried by titanomaghemite cannot be excluded and could explain the low inclination values in Baffin Bay rather than representing real excursions. However, the correspondence and timing of the two excursions in core PC16 with previously published records together with the contemporaneous RPI lows support a geomagnetic origin.

Several excursions have already been observed in numerous Baffin Bay cores but previous age models based on lithological inter-core correlations did not permit a clear identification of these events [*Aksu*, 1983; *Thouveny*, 1988]. *Thouveny* [1988] identified two potential excursions dated around 18 and 24 cal ka BP (at ~0.9 and 2.5 m respectively) within a piston core (HU85-027-016PC) collected at ODP site 645. The large inclination deviation recognized in core PC16 between 95 – 105 cm (~14.8 – 15.5 cal ka BP) could possibly be related to the low inclination dated at 18 cal ka BP in core HU85-027-016PC considering uncertainties in the corresponding age model based on 2 radiocarbon ages and an open discussion on the oxygen isotopic stratigraphy. However, the corresponding pattern in PC16 is believed to be of lithological origin (Figure 7), which therefore questions the excursional nature of the inclination low in core HU85-027-016PC. We propose to relate this inclination low to a lithological imprint rather than representing an excursion as previously proposed [*Thouveny*, 1988]. The second large inclination deviation occurred at 2.5 mbsf (~24 cal ka BP) in core HU85-027-016PC. We do not observe any deviation of the inclination at this depth in core PC16 but according to the geographical proximity of these 2 cores (same site), and assuming the same sedimentation deposition regime, it is coeval with an intensity low recorded at 246 cm in core PC16 and dated at 34.5 ± 0.35 ka (tie-point: N10, Figure 9). We propose to adjust the age of the excursion observed in core HU85-027-016PC from 24 cal ka BP to ca. 34.5 cal ka BP to be synchronous with the Mono Lake excursion [*Lund et al.*, 2006]. According to our results, we believe that previous deep central Baffin Bay chronological frameworks [*Aksu* 1981, 1983a; *Aksu and Piper*, 1979, 1987; *de Vernal et al.*, 1987; *Thouveny*, 1988; *Hillaire-Marcel et al.*, 1989] were problematic due to the (1) scarcity of ^{14}C ages together with inaccurate $\delta^{18}O$ interpretations [*Hillaire-Marcel et al.*, 2008], and (2) false assumption of nearly constant sedimentation rates, all leading to an incorrect identification of geomagnetic excursions. We therefore propose to relate the excursions described by *Aksu* [1983b] in several cores collected in the 1970s (between 250 and 450 cmbsf) to the Mono Lake or the Laschamp events (33±1 cal ka BP or 41±1 ka cal BP) [*Lund et al.*, 2006] rather than the Blake event (123±3 cal ka BP) [*Lund et al.*, 2006]. Our findings here clearly rules out the low sedimentation rate model for Baffin Bay. As a general comment, this confirms the extreme caution to be taken before interpreting excursions in Arctic or sub-Arctic sediments [*St-Onge and Stoner*, 2011] because of (1) uncertain chronologies and (2) lithological or diagenetic effects [*Channell and Xuan*, 2009; *Xuan et al.*, 2012].

5.3. Chronostratigraphy in central Baffin Bay

The RPI correlations along with the recognition of two possible excursions strongly support the proposed chronostratigraphy for the last climatic cycle (~0 – 115 ka). The derived age-model (Figure 12) yields a mean sedimentation rate of ~6.5 cm/ka. This is slightly lower that the high sedimentation rate hypothesis estimated from previous studies of central Baffin Bay sediments (8 – 12 cm/ka) [*de Vernal et al.*, 1987; *Andrews et al.*, 1998] but still coherent considering (1) previous age models confidence, and (2) uncertainty on precise BBDC duration in the core. The low sedimentation rates in Baffin Bay reflect an overall dry-base character of ice-sheets in source areas [*Aksu*, 1981; *Andrews et al.*, 1985; *Aksu and Piper*, 1987; *Hiscott et al.*, 1989; *Hillaire-Marcel et al.*, 1989]. According to the proposed age model, the sedimentation rates varied largely from values <5 cm/ka to 20 cm/ka, and up to 35 cm/ka immediately after the Younger Dryas (Figure 12). While the "background" facies corresponds to lower sedimentation rates (3 to 6 cm/ka), the inter-bedded layers depict three to four fold higher rates. The 3 AMS ^{14}C dates support the higher sedimentation rates during the last Termination (Table 1, Figures 11 and 12). This non-linear sedimentation pattern is not surprising due to: (1) facies variability throughout the core; and (2) the core location within the confined Baffin Bay's sedimentary basin associated with a highly variable depositional environment (e.g., rapidly deposited layers) correlated with last glacial cycle short events (e.g., ice surges).

6. Conclusions

This high-resolution rock-magnetic and paleomagnetic analysis of a central Baffin Bay sedimentary sequence spanning the last climatic cycle indicates that the magnetic remanence is mainly carried by magnetite in the PSD range throughout most of the core. A strong relationship between lithological facies and magnetic signatures prevails. Detrital carbonate layers (BBDC) are characterized by coarse magnetic grain size (coarse PSD to MD domain) and a low ferrimagnetic concentration. Holocene and last glacial maximum (LGM) sediments contain fine magnetic grains (PSD to SD domain) and have a high ferrimagnetic concentration. Despite the identification of several sedimentary facies and high lithological variability, we were nonetheless able to derive a reliable RPI proxy for much of the core. The directional data also allowed the recognition of two geomagnetic excursions, the Laschamp and Norwegian-Greenland-Sea excursions. The relative paleointensity correlations with well-dated RPI records and stacks (notably the

NAPIS-75) yield a relatively robust chronostratigraphic framework for central Baffin Bay (from 0 to 115 ka BP). It helps the setting of more precise chronological benchmarks for the dating of major lithological changes and for the BBDC events. It will permit a refinement of paleoceanographic and paleoclimatic interpretations for the late Quaternary depositional history in the bay and thus help identifying ice margin instabilities of the three main regional ice-sheets that deliver sediments to the bay. These results also highlight the potential of the paleomagnetic approach to date sedimentary sequence in problematic areas such as Arctic basins.

Acknowledgements

We thank Jacques Labrie (ISMER) for his technical support during paleomagnetic measurements, Louis-Frédéric Daigle (INRS) for the CAT-scan analysis, Pierre Francus (INRS) and Arnaud de Coninck (INRS) for their help during the ITRAX™ core scanning, and Michel Preda (UQAM) for assistance with XRD measurements. Special thanks are due to Olivia Gibb (UQAM) for the picking of the few available foraminifera for ^{14}C ages, to Joseph Stoner (COAS) and Carlos Laj (LSCE) for sharing paleomagnetic data, and John Andrews (INSTAAR) for sharing JR06Bx mineralogical data. We are in debt to Agathe Lisé-Pronovost (ISMER), the anonymous associate editor, two anonymous reviewers and the editor-in-chief Dr. James Tyburczy for constructive comments that significantly improved this manuscript. We are grateful to the captain, officers, crew and scientists on board the CCGS Hudson during the HU2008-029 expedition. This study is part of the Canadian contribution to the Past4Future project. Support from MDEIE (Ministère du Développement Economique, de l'Innovation et de l'Exportation), NSERC (Natural Sciences and Engineering Research Council of Canada), FQRNT (Fonds Québécois de la Recherche sur la Nature et les Technologies) and the CFI (Canadian Foundation for Innovation) is acknowledged.

References

Aksu, A. E., and D. J. W. Piper (1979), Baffin Bay in the past 100,000 yr, *Geology,* 7, 245-248.

Aksu, A. E. (1981), Late Quaternary stratigraphy, paleoenvironmentology, and sedimentation history of Baffin Bay and Davis Strait, Ph.D. thesis, Dalhousie University, Halifax, NS, Canada.

Aksu, A. E. (1983a), Holocene and Pleistocene dissolution cycles in deep-sea cores of Baffin Bay and Davis Strait: paleoceanographic implications, *Mar. Geol.,* 53, 331-348.

Aksu, A. E. (1983b), Short-period geomagnetic excursion recorded in Pleistocene sediments of Baffin Bay and Davis Strait, *Geology,* 11(9), 537-541.

Aksu, A. E., and D. J. W. Piper (1987), Late Quaternary sedimentation in Baffin Bay, *Can. J. Earth Sci.,* 24, 1833-1846.

Andrews, J. T., A. E. Aksu, M. Kelly, R. Klassen, G. H. Miller, W. N. Mode, and P. Mudie (1985), Land/ocean correlations during the last interglacial/glacial transition, Baffin Bay, northwestern North Atlantic: A review, *Quat. Sci. Rev.,* 4(4), 333-355.

Andrews, J. T., M. Kirby, A. E. Aksu, D. G. Barber, and D. Meese, D. (1998), Late Quaternary Detrital Carbonate (DC-) layers in Baffin Bay marine sediments (67°-74° N): correlation with Heinrich events in the North Atlantic?, *Quat. Sci. Rev.*, 17, 1125-1137.

Andrews, J. T., and D. D. Eberl (2011), Surface (sea floor) and near-surface (box cores) sediment mineralogy in Baffin Bay as a key to sediment provenance and ice sheet variations, *Can. J. Earth Sci.,* 48, 1307-1328.

Austin, W. E. N., R. J., Telford, U. S. Ninnemann, L. Brown, L. J. Wilson, D. P. Small, and C. L. Bryant (2011), North Atlantic reservoir ages linked to high Younger Dryas atmospheric radiocarbon concentrations, *Global Planet. Change,* 79(3-4), 226-233.

Azetsu-Scott, K., A. Clarke, and K. Falkner (2010), Calcium carbonate saturation states in the waters of the Canadian Arctic Archipelago and the Labrador Sea, *J. Geophys. Res.,* 115, C11021, doi:10.1029/2009JC005917.

Banerjee, S. K., J. W. King, and J. Marvin (1981), A rapid method for magnetic granulometry with applications to environmental studies, *Geophys. Res. Lett.,* 8(4), 333-336.

Baldauf, J. G., B. Clement, A. E. Aksu, A. de Vernal, J. Firth, F. Hall, M. J. Head, R. Jarrard, M. A. Kaminski, D. Lazarus, A. L. Monjanel, W. A. Berggren, F. Gradstein, S. Knuttel, P. Mudie, and M. D. Russell (1989), Magnetostratigraphic and biostratigraphic synthesis of Ocean Drilling Program Leg 105: Labrador Sea and Baffin Bay, in *Proceedings of the Ocean Drilling Program, Scientific Results*, vol. 105, edited by S. P. Srivastava, M.

Arthur, and B. Clement, College Station, TX (Ocean Drilling Program), 935-956.

Bard, E., M. Arnold, J. Mangeruld, M. Paterne, L. Labeyrie, J. Duprat, M. A. Mélières, E. Sonstegaard, and J. C. Duplessy (1994), The North Atlantic atmosphere-sea surface ^{14}C gradient during the Younger Dryas climatic event, *Earth Planet. Sci. Lett.*, 126, 275-287.

Blott, S. J., and K. Pye (2001), GRADISTAT: a grain size distribution and statistics package for the analysis of unconsolidated sediments, *Earth Surf. Processes Landforms,* 26, 1237-1248.

Bondevik, S., J. Mangerud, H.H. Birks, S. Gulliksen, and P. Reimer (2006), Changes in North Atlantic Radiocarbon Reservoir Ages During the Allerod and Younger Dryas, *Science,* 312(5779), 1514-1517.

Briner, J. P., G. H. Miller, P. T. Davis, P. Bierman, and M. Caffee (2003), Last Glacial Maximum ice sheet dynamics in Arctic Canada inferred from young erratics perched on ancient tors, *Quat. Sci. Rev.,* 22, 437-444.

Briner, J. P., G. H. Miller, P. T. Davis, and R. Finkel (2006), Cosmogenic radionuclides from fiord landscapes support differential erosion by overriding ice sheets, *Geol. Soc. Am. Bull.,* 118, 406-420.

Buck, C. E., J. A. Christen, and G. N. James (1999), BCal: an on-line Bayesian radiocarbon calibration tool, *Internet Archaeology,* 7, (http://intarch. ac.uk/journal/issue7/buckS).

Butler, R. F. (1992), Paleomagnetism: Magnetic domains to geologic terranes, Blackwell Scientific Publications, 319p, Oxford, UK.

Cao, L., R. G. Fairbanks, R. A. Mortlock, and M. J. Risk (2007), Radiocarbon reservoir age of high latitude North Atlantic surface water during the last deglacial, *Quat. Sci. Rev.,* 26(5-6), 732-742.

Campbell, D. C., and A. de Vernal (2009), CCGS Hudson Expedition 2008029: Marine geology and paleoceanography of Baffin Bay and adjacent areas, Nain, NL to Halifax, NS, August 28- September 23; *Geological Survey of Canada*, Open File 5989, 1 DVD.

Channell, J. E. T., D. Hodell, and B. Lehman (1997), Relative geomagnetic paleointensity and δ^{18}O at ODP Site 983 (Gardar Drift, North Atlantic) since 350 ka, *Earth Planet. Sci. Lett.,* 153, 103-118.

Channell, J. E. T., A. Mazaud, P. Sullivan, S. Turner, and M. E. Raymo (2002), Geomagnetic excursions and paleointensities in the 0.9-2.15 Ma interval of the Matuyama Chron at Ocean Drilling Program Sites 983 and 984 (Iceland Basin), *J. Geophys. Res.,* 107(B6), doi:10.1029/2001JB000491.

Channell, J. E. T., and C. Xuan (2009), Self-reversal and apparent magnetic excursions in Arctic sediments, *Earth Planet. Sci. Lett.,* 284(1-2), 124-131.

Channell, J. E. T., C. Xuan, and D. Hodell (2009), Stacking paleointensity and oxygen isotope data for the last 1.5 Myr (PISO-1500), *Earth Planet. Sci. Lett.,* 283, 14-23.

Coulthard, R. D., M. F. A. Furze, A. J. Pieńkowski, F. C. Nixon, and J. H. England (2010), New marine Delta R values for Arctic Canada, *Quaternary Geochronology,* 5, 419-434.

Croudace, I., A. Rindby, and R. Rothwell (2006), ITRAX: description and evaluation of a new multi-function X-ray core scanner, in *New techniques in sediment core analysis*, Geological Society, Special Publications, 267, London, UK, 51–63.

Dankers, P. (1981), Relationship between median destructive field and remanent coercive forces for dispersed natural magnetite, titanomagnetite and hematite, *Geophys. J. R. Astron. Soc.*, 64, 447-461.

Day, R., M. D. Fuller, and V. A. Schmidt (1976), Magnetic hysteresis properties of synthetic titanomagnetites, *J. Geophys. Res.*, 81, 873-880.

Day, R., M. D. Fuller, and V. A. Schmidt (1977), Hysteresis properties of titanomagnetites: Grain-size and compositional dependence, *Phys. Earth Planet. Inter.,* 13, 260-267.

de Vernal, A., C. Hillaire-Marcel, A. E. Aksu, and P. Mudie (1987), Palynostratigraphy and chronostratigraphy of Baffin Bay deep sea cores: climatostratigraphic implications, *Palaeogeogr., Palaeoclimatol., Palaeoecol.*, 61, 97-105.

de Vernal, A., G. Bilodeau, C. Hillaire-Marcel, and N. Kassou (1992), Quantitative assessment of carbonate dissolution in marine sediments from foraminifer linings vs. shell ratios: Davis Strait, northwest North Atlantic, *Geology* 20, 527-530.

Dearing, J. A. (1999), Magnetic susceptibility, in *Environmental Magentism: A practical Guide*, edited by J., Walden, F. Oldfiel, and J.P. Smith, Quaternary Res. Assoc., London, UK, 35-53.

Duchesne, M., F. Moore, B. Long, and J. Labrie (2009), A rapid method for converting medical Computed Tomography scanner topogram attenuation scale to Hounsfield Unit scale and to obtain relative density values, *Engineering Geology,* 103, 100-105.

Dunlop, D. J., and Ö. Özdemir (1997), *Rock Magnetism: Fundamentals and Frontiers*, Cambridge University Press, New York, London and Cambridge.

Dunlop, D. J. (2002a), Theory and application of the Day plot (Mrs/Ms versus Hcr/Hc) 1. Theoretical curves and tests using titanomagnetite data, *J. Geophys. Res.,* 107(B3), 2056, doi:10.1029/2001JB000486.

Dunlop, D. J. (2002b), Theory and application of the Day plot (Mrs/Ms versus Hcr/Hc) 2. Application to data for rocks, sediments, and soils, *J. Geophys. Res.*, 107(B3), 2057, doi:10.1029/2001JB000487.

Dunlop, D. J., and Ö. Özdemir (2007), Magnetizations in rocks and minerals, in *Geomagnetism, Treatise on Geophysics*, vol. 5, edited by G. Schubert, Elsevier, Amsterdam, The Netherlands, 277-336.

Dyke, A. (2004), An outline of North American deglaciation with emphasis on central and northern Canada, *Developments in Quaternary Science*, 2, 373-424.

England, J., N. Atkinson, J. Bednarski, A. Dyke, D. A. Hodgson, and C. Ó Cofaigh (2006), The Innuitian Ice Sheet: configuration, dynamics and chronology, *Quat. Sci. Rev.*, 25, 689-703.

Funder, S., K. K. Kjeldsen, K. H. Kjær, and C. Ó Cofaigh (2011), The Greenland Ice Sheet During the Past 300,000 Years: A Review, in: *Developments in Quaternary Sciences, Quaternary Glaciations, Extent and Chronology*, Part IV, A Closer Look, vol. 15, edited by J. Ehlers, P. L. Gibbard and P. D. Hughes, Elsevier, Amsterdam, The Netherlands, 699-713, 10.1016/B978-0-444-53447-7.00050-7.

Guyodo, Y., and J. P. Valet (1996), Relative variations in geomagnetic intensity from sedimentary records: the past 200,000 years, *Earth Planet. Sci. Lett.*, 143, 23-36.

Hillaire-Marcel, C., A. de Vernal, A. E. Aksu, and S. Macko (1989), High-resolution isotopic and micropaleontological studies of upper Pleistocene sediment at ODP site 645, Baffin Bay, in P*roceedings of the Ocean Drilling Program, Scientific Results*, vol. 105, edited by S. P. Srivastava, M. Arthur, and B. Clement, College Station, TX (Ocean Drilling Program), 599-616.

Hillaire-Marcel, C., A. de Vernal, L. Polyak, and D. A. Darby (2004), Size-dependent isotopic composition of planktic foraminifers from Chukchi Sea vs. NW Atlantic sediments, implications for the Holocene paleoceanography of the western Arctic, *Quat. Sci. Rev.*, 23, 245-260.

Hillaire-Marcel, C., and A. de Vernal (2008), Stable isotope clue to episodic sea ice formation in the glacial North Atlantic, *Earth Planet. Sci. Lett*, 268, 143-150.

Hiscott, R. N., A. E. Aksu, and O. B. Nielsen (1989), Provenance and dispersal patterns, Pliocene-Pleistocene section at site 645, Baffin Bay, in P*roceedings of the Ocean Drilling Program, Scientific Results*, vol. 105, edited by S. P. Srivastava, M. Arthur, and B. Clement, College Station, TX (Ocean Drilling Program), 31-52.

Hughen, K., S. Lehman, J. Southon, J. T. Overpeck, O. Marchal, C. Herring, and J. Turnbull (2004), ^{14}C activity and global carbon cycle changes over the past 50,000 years, *Science*, 303(5655), 202-207.

Jennings, A. E., C. Sheldon, T. M. Cronin, P. Francus, J. Stoner, and J. T. Andrews (2011), The Holocene history of Nares Strait: Transition from glacial bay to Arctic-Atlantic throughflow, *Oceanography*, 24(3), 26–41.

King, J., S. K. Banerjee, J. Marvin, and Ö. Özdemir (1982), A comparison of different magnetic methods for determining the relative grain size of magnetite in natural materials: Some results from lake sediments, *Earth Planet. Sci. Lett.,* 59, 404-419.

King, J., S. K. Banerjee, and J. Marvin (1983), A new rock-magnetic approach to selecting sediments for geomagnetic paleointensity studies: application to paleointensity for the last 4000 years, *J. Geophys. Res.,* 88(B7), 5911–5921.

Kirschvink, J. L. (1980), The least-squares line and plane and the analysis of palaeomagnetic data, *Geophys. J. R. Astron. Soc.*, 62, 699-718.

Kissel, C., C. Laj, L. Labeyrie, T. Dokken, A. Voelker, and D. Blamart (1999), Rapid climatic variations during marine isotopic stage 3: magnetic analysis of sediments from Nordic Seas and North Atlantic, *Earth Planet. Sci. Lett.,* 171, 489-502.

Korstgärd, J. A., and O. B. Nielsen (1989), Provenance of dropstones in Baffin Bay and Labrador Sea, in P*roceedings of the Ocean Drilling Program, Scientific Results*, vol. 105, edited by S. P. Srivastava, M. Arthur, and B. Clement, College Station, TX (Ocean Drilling Program), 65–69.

Laj, C., C. Kissel, A. Mazaud, J. E. T. Channell, and J. Beer (2000), North Atlantic palaeointensity stack since 75 ka (NAPIS-75) and the duration of the Laschamp event, *Phil. Trans. R. Soc. London, Series B*, 358, 1009-1025.

Laj, C., C. Kissel, and A. P. Roberts (2006), Geomagnetic field behavior during the Iceland Basin and Laschamp geomagnetic excursions: A simple transitional field geometry?, *Geochem., Geophys., Geosyst.,* 7, Q03004, doi:10.1029/2005GC001122.

Laj, C., and J. E. T. Channell (2007), Geomagnetic Excursions, in: *Treatise on Geophysics*, vol. 5, edited by G. Schubert, Elsevier, Amsterdam, The Netherlands, 373-416.

Levi, S., and S. K. Banerjee (1976), On the possibility of obtaining relative paleointensities from lake sediments, *Earth Planet. Sci. Lett.,* 29, 219-226.

Lund, S. P., M. Schwartz, L. Keigwin, and T. Johnson (2005), Deep-sea sediment records of the Laschamp geomagnetic field excursion (~41,000 calendar years before present), *J. Geophys. Res.,* 110(B04101), doi:10.1029/2003JB002943.

Lund, S. P., J. S. Stoner, J. E. T. Channell, and G. Acton (2006), A summary of Brunhes paleomagnetic field variability recorded in Ocean Drilling Program cores, *Phys. Earth Planet. Inter.,*156, 194-204.

MacLean, B. (1985), Geology of the Baffin Island Shelf, in *Quaternary Environments : Eastern Canadian Arctic, Baffin Bay and Western Greenland*, edited by J. T. Andrews, Allent and Unwin, Boston, USA, 154-177.

MacLean, B., G. L. Williams, and S. P. Srivasatava (1990), Geology of the Labrador Shelf, Baffin Bay, and Davis Strait. Part 2. Geology of Baffin Bay and Davis Strait, in *Geology of the continental margin of eastern Canada, Geology of Canada,* 2, edited by M. J. Keen, and G. L. Williams, Ottawa, Ontario, Canada, 293–348.

Maher, B. A., and R. Thompson (1999), *Quaternary Climates, Environments and Magnetism*, Cambridge University Press, Cambridge, UK.

Marlowe, J. I. (1966), Mineralogy as an indicator of long-temr current fluctuations in Baffin Bay, *Can. J. Earth Sci.*, 3(2), 191-201.

Mazaud, A. (2005), User-friendly software for vector analysis of the magnetization of long sediment cores, *Geochem., Geophys., Geosyst.,* 6, Q12006, doi:10.1029/2005GC001036.

Meynadier, L., J. P. Valet, and R. Weeks (1992), Relative geomagnetic intensity of the field during the last 140 ka, *Earth Planet. Sci. Lett.,* 114(1), 39-57.

Moskowitz, B. (1991), Hitchhiker's Guide to Magnetism, in: *Environmental Magnetism Workshop (IRM),* vol. 279(1), 48 pp.

Mudie, P., and A. E. Aksu (1984), Palaeoclimate of Baffin Bay from 300,000-year record of foraminifera, dinoflagellates and pollen, *Nature,* 312, 630-634.

Ó Cofaigh, C., J. A. Dowdeswell, A. Kilfeather, K. Hogan, A. E. Jennings, D. McCarthy, J. M. Lloyd, J. Evans, R. Noormets, Q. Simon, and M. Walton (2010), West Greenalnd Ice Streams on the continental shelf of Baffin Bay during the Last Glacial Cycle: geomorphology, flow trajectories and chronology, 40st Arctic Workshop, Winter Park, Colorado.

Opdyke, N. D., and J. E. T. Channell (1996), *Magnetic stratigraphy*, San Diego, CA: Academic Press.

Paillard, D., L. Labeyrie, and P. Yiou (1996), Macintosh Program performs time-series analysis, *Eos Trans. AGU*, 77(39), 379, doi:10.1029/96EO00259.

Parnell, J., S. Bowden, J. T. Andrews, and C. Taylor (2007), Biomarker determination as a provenance tool for detrital carbonate events (Heinrich events?): Fingerprinting Quaternary glacial sources into Baffin Bay, *Earth Planet. Sci. Lett.,* 257, 71-82.

Piper, D. J. W. (1973), A late quaternary stratigraphic marker in the Central Basin of Baffin Bay. *Maritime Sediments,* 9, 62-63 .

Polyak, L., J. Bischof, J. D. Ortiz, D. A. Darby, J. E. T. Channell, C. Xuan, D. S. Kaufman, R. Lovlie, D. A. Schneider, D. D. Eberl, R. E. Adler, and E. A. Council (2009), Late Quaternary stratigraphy and sedimentation patterns in the western Arctic Ocean, *Global Planet. Change,* 68, 5-17.

Reimer, P.J., M. G. L. Baillie, E. Bard, A. Bayliss, J W. Beck, P. G. Blackwell, C. Bronk Ramsey, C. E. Buck, G. S. Burr, R. L. Edwards, M. Friedrich, P. M. Grootes, T. P. Guilderson, I. Hajdas, T. J. Heaton, A. G. Hogg, K. A. Hughen, K. F. Kaiser, B. Kromer, F. G. McCormac, S. W. Manning, R. W. Reimer, D. A. Richards, J. R. Southon, S. Talamo, C. S. M. Turney, J. van der Plicht, and C. E. Weyhenmeyer (2009), Intcal09 and Marine09 radiocarbon age calibration curves, 0-50,000 years cal BP, *Radiocarbon,* 51(4), 1111-1150.

Roberts, A. P. (2008), Geomagnetic excursions: Knowns and unknows, *Geophys. Res. Lett.,* 35(L17307), doi:10.1029/2008GL034719.

Roberts, A. P., L. Chiang, C. J. Rowan, C. –S. Horng, and F. Florindo (2011), Magnetic properties of sedimentary Greigite (Fe_3S_4): An update, *Rev. Geophys.*, 49, RG1002, doi:10.1029/2010RG000336.

Spassov, S. and J. –P. Valet (2012), Detrital magnetizations from redeposition experiments of different natural sediments, *Earth Planet. Sci. Lett.,* 351-352, 147-157.

Srivastava, S. P. (1989), *Proceedings of the Ocean Drilling Program, Scientific Results*, Baffin Bay and Labrador Sea, Leg 105, Sites 645-647, 1-17.

Stoner, J. S., J. E. T. Channell, and C. Hillaire-Marcel (1996), The magnetic signature of rapidly deposited detritai layers from the deep Labrador Sea: Relationship to North Atlantic Heinrich layers, *Paleoceanography,* 11, 309-325.

Stoner, J. S., J. E. T. Channell, and C. Hillaire-Marcel (1998), A 200 ka geomagnetic chronostratigraphy for the Labrador Sea: Indirect correlation of the sediment record to SPECMAP, *Earth Planet. Sci. Lett.,* 159, 165-181.

Stoner, J. S., J. E. T. Channell, C. Hillaire-Marcel, and C. Kissel (2000), Geomagnetic paleointensity and environmental record from Labrador Sea core MD95-2024: global marine sediment and ice core chronostratigraphy for the last 110 kyr, *Earth Planet. Sci. Lett.,* 183, 161-177.

Stoner, J. S., and G. St-Onge (2007), Magnetic stratigraphy in paleoceanography: reversals, excursions, paleointensity and secular variation, in *Developments in Marine Geology. Proxies in late Cenozoic paleoceanography*, vol. 1, edited by C. Hillaire-Marcel, and A. de Vernal, Elsevier, Amsterdam, The Netherlands, 99-137.

St-Onge, G., T. Mulder, P. Francus, and B. Long (2007), Continuous physical properties of cored marine sediments, in *Developments in Marine Geology. Proxies in late Cenozoic paleoceanography*, vol. 1, edited by C. Hillaire-Marcel, and A. de Vernal, Elsevier, Amsterdam, The Netherlands, 63-98.

St-Onge, G. and J. S. Stoner (2011), Paleomagnetism near the North Magnetic Pole: a unique vantage point to understand the dynamics of the geomagnetic field and its secular variations, Oceanography, 24(3), 42-50.

Stuiver, M. and H. A. Polach (1977), Discussion: reporting of ^{14}C data, *Radiocarbon*, 19, 355-363.

Stuiver, M., P. J. Reimer, and R. W. Reimer (2010), CALIB 6.0, Available from: http:// radiocarbon.pa.qub.ac.uk/calib/.

Tang, C., C. Ross, T. Yao, B. Petrie, B. DeTracey, and E. Dunlap (2004), The circulation, water masses and sea-ice of Baffin Bay, *Progress in Oceanography*, 63, 183-228.

Tauxe, L., and G. Wu (1990), Normalized remanence in sediments of the Western Equatorial Pacific: relative paleointensity of the geomagnetic field?, *J. Geophys. Res.*, 95(B8), 12,337-12,350.

Tauxe, L. (1993), Sedimentary records of relative paleointensity of the geomagnetic field: theory and practice, *Rev. Geophys.*, 31, 319-354.

Tauxe, L., T. Mullender, and T. Pick (1996), Potbellies, wasp-waists, and superparamagnetism in magnetic hysteresis, *J. Geophys. Res.*, 101, 571-583.

Tauxe, L., and T. Yamazaki (2007), Paleointensities. in: *Treatise on Geophysics*, vol. 5, edited by G. Schubert, Elsevier, Amsterdam, The Netherlands, 509-563.

Tauxe, L. (2010), *Essentials of Paleomagnetism*, University of California Press, San Diego, USA.

Thiébault, F., M. Cremer, P. Debrabant, J. Foulon, O. B. Nielsen, and H. Zimmerman (1989), Analysis of sedimentary facies, clay mineralogy, and geochemistry of the Neogene-Quaternary sediments in Site 645, Baffin Bay, in: P*roceedings of the Ocean Drilling Program, Scientific Results*, vol. 105, edited by S. P. Srivastava, M. Arthur, and B. Clement, College Station, TX (Ocean Drilling Program), 83–100.

Thorez, J. (2003), *L'argile, minéral pluriel*, Bulletin de la Société Royale des Sciences de Liège, 72(1), 19-70.

Thouveny, N. (1988), High-resolution palaeomagnetic study of Late Pleistocene sediments from Baffin Bay: first results, *Can. J. Earth Sci.*, 25, 833-843.

Valet, J. P. (2003), Time variations in geomagnetic intensity, *Rev. Geophys.*, 41(1), 1004, doi:10.1029/2001RG000104.

Vincent, J., and V. Prest (1987), The early Wisconsinan history of the Laurentide ice sheet, *Géographie physique et Quaternaire*, 41, 199–213.

Waelbroeck, C., J. C. Duplessy, E. Michel, L. Labeyrie, D. Paillard, and J. Duprat (2001), The timing of the last deglaciation in North Atlantic climate records, *Nature*, 412, 724-727.

Xuan, C., and J. E. T. Channell (2010), Origin of apparent magnetic excursions in deep-sea sediments from Mendeleev-Alpha Ridge, Arctic Ocean, *Geochem., Geophys., Geosyst.*, 11, Q02003, doi:10.1029/2009GC002879.

Xuan, C., J. E. T. Channell, L. Polyak and D. A. Darby (2012), Paleomagnetism of Quaternary sediments from Lomonosov Ridge and Yermak Plateau: implications for age models in the Arctic Ocean, *Quat. Sci. Rev.*, 32, 48-63.

Zijderveld, J. D. A. (1967), AC demagnetization of rock: analysis of results in: *Methods in Paleomagnetism*, edited by D. W. Collinson, K. M. Creer, and S. K. Runcorn, Elsevier, Amsterdam, The Netherlands, 254-286.

Table 1. Radiocarbon ages for core HU2008-029-016PC.

Depth (cm)	^{14}C Age[a] (yr BP)	ΔR	Calibrated age[b] (cal BP)	Dated material	Lab. Number[c]
66 - 67	11905±40	0	13355 (13254 - 13457)	planktonic foraminifera (Npl)	CAMS-151299
		400	12953 (12783 – 13124)		
79-80	12470±40	0	13859 (13738 - 13981)	planktonic foraminifera (Npl)	CAMS-151297
		400	13525 (13372 – 13678)		
111-112	13820±130	0	16361 (15835 – 16888)	planktonic foraminifera (Npl)	CAMS-151300
		400	15783 (15109 – 16458)		

[a] The age was determined by the AMS method and corrected for natural and sputtering fractionation ($\delta^{13}C$=~25% versus Vienna Pee-Dee Belemnite (VPDB)). The statistical uncertainty of the age determination is given as one standard deviation (Stuiver and Polach, 1977).
[b] Calibrated using the CALIB 6.0 software (Stuiver et al., 2009) using the the Hughen et al., (2004) marine dataset. A total marine reservoir correction of 400 yr (ΔR = 0 yr) and 800 yr (ΔR = 400 yr) were applied. The first and last ages, in parentheses, represent the 2σ cal age range.
[c] Center for accelerator mass spectrometry, Lawrence Livermore National Laboratory.
Npl = *Neogloboquadrina pachyderma* left-coiled

table legend (page 58)
[a] Tie-points age for: calcite correlation (yellow), NAPIS correlation (green) and correlation based on the 6 references curves (blue) (see text for details). The excursions are highlighted in grey.
[b] Time incertitude: (green) for 22 – 75 ka interval, it corresponds to the ±2σ incertitude from the NAPIS bootstrap calculation. (blue) For the 75 – 115 ka interval, the errors correspond to the standard deviation between the 6 reference curves.
[c] Tie points: C = calcite; N1 – N21 = NAPIS; P1 – P14 = 6 reference cores.

Table 2. Age model tie-point.

Depth 016PC (cm)	Age (cal ka BP)[a]	Error[b]	Tie-Points[c]
0	0.0		C1
16.5	10.0		C2
20	10.7		C3
24	10.8		C4
32	11.0		C5
40	11.4		C6
48	11.9		C7
56	12.0		C8
60	12.2		C9
64	12.8		C10
125	21.4	0.98	N1
157	24	1.19	N2
164	24.5	1.54	N3
174	25	1.74	N4
183	26	1.21	N5
190	27	1.06	N6
198	29	2.15	N7
208	31.5	0.64	N8
223	32.5	2.20	N9
246	34.5	1.27	N10
260	36.5	1.46	N11
275	40.7	1.55	Laschamp
284.5	43	1.10	N12
300	47	1.70	N13
315	49.5	1.46	N14
326	52.5	1.30	N15
346	56	1.00	N16
358	57.5	1.19	N17
367	59	0.83	N18
403	62.5	1.27	N19
422	64.5	1.65	NGS
441	71	1.92	N20
478	74	1.07	N21
492	76.8	1.94	P1
520	80.1	1.24	P2
568	82.7	2.35	P3
584	84.9	2.39	P4
608	90.5	2.81	P5
628	94.7	3.03	P6
641	97.0	3.05	P7
651	99.2	0.96	P8
684	104.0	2.39	P9
688	104.9	2.29	P10
695	107.0	2.00	P11
704	108.9	2.45	P12
715	110.5	2.48	P13
725	112.4	1.56	P14

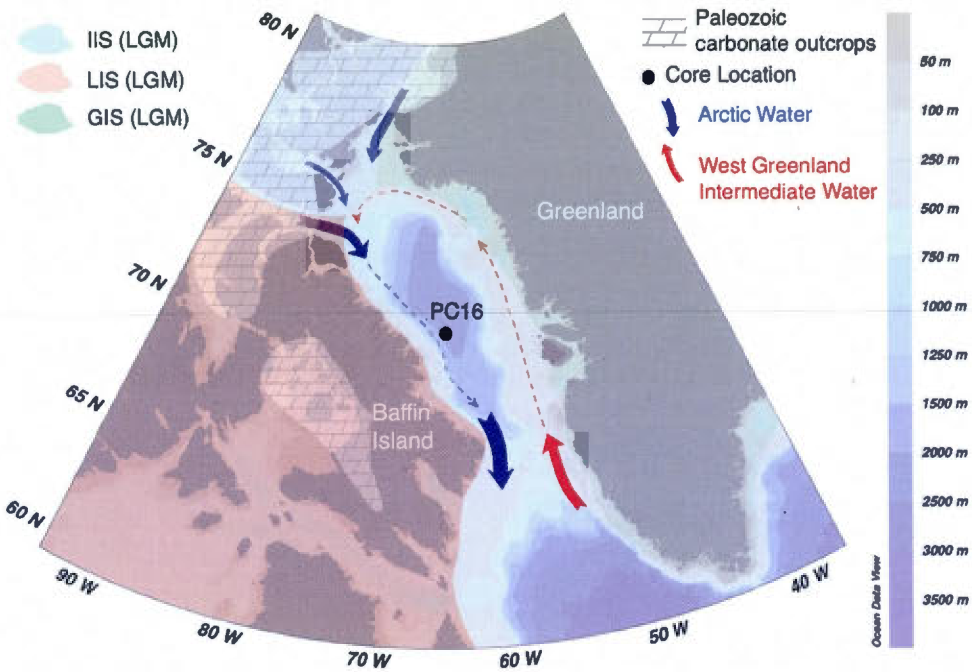

Figure 1. Map of the Baffin Bay area and location of core HU2008-029-016PC sampling site. The general bathymetry, simplified oceanic circulation and a sketch of the Paleozoic outcrops North of Davis Strait [*MacLean*, 1985] are also represented. Red arrows illustrate Atlantic "warm" waters, whereas the blue arrows represent colder Arctic waters. The simplified representation of the regional ice-sheets extent limits during the LGM (colored areas) are adapted from *Funder et al.* [2011], *Dyke* [2004] and *England et al.* [2006]. IIS represents the Innuitian Ice Sheet, LIS represents the Laurentide Ice Sheet, and GIS represents the Greenland Ice Sheet.

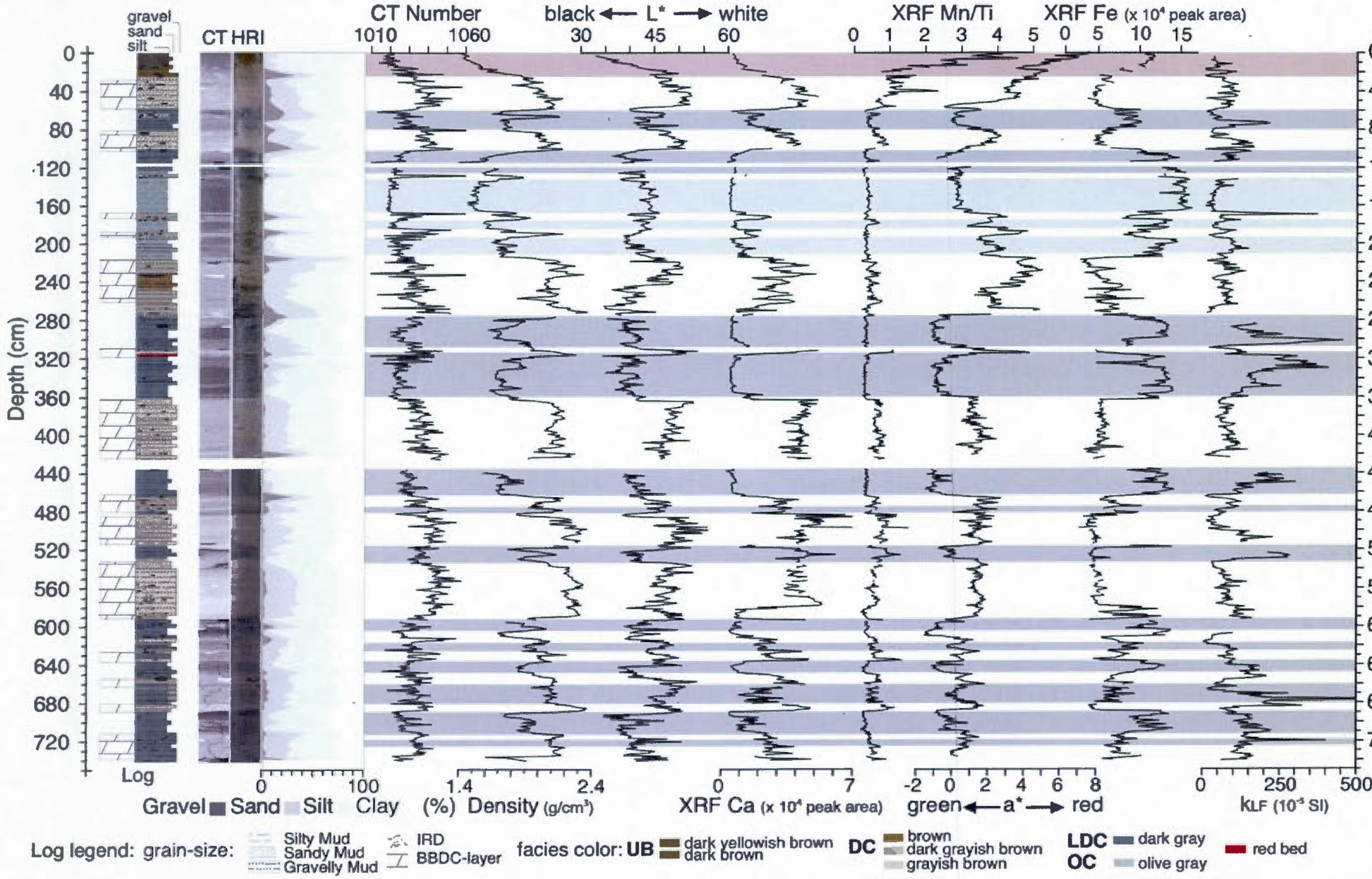
Depth (cm)
gravel
sand
silt
Log
CT HRI
Gravel Sand Silt Clay
(%)
CT Number
1010
1060
Density (g/cm³)
1.4
2.4
black ← L* → white
30
45
60
XRF Ca (x 10⁴ peak area)
XRF Mn/Ti
green ← a* → red
XRF Fe (x 10⁴ peak area)
kLF (10⁻⁵ SI)
Log legend: grain-size:
Silty Mud
Sandy Mud
Gravelly Mud
IRD
BBDC-layer
facies color: UB
dark yellowish brown
dark brown
DC
brown
dark grayish brown
grayish brown
LDC
dark gray
OC
olive gray
red bed

Figure 2. (page 60) High-resolution physical, geochemical and magnetic properties of core PC16. Log: general simplified stratigraphy of the core (see text and legend for details); CT: CAT-Scan image of the core; HRI: high-resolution digital image; CT Number (density proxy); Density: wet bulk density (gamma-ray attenuation); L*: lightness: black to whitė; a*: green to red. µXRF peak areas express the relative element concentration of calcium (Ca) and iron (Fe) measured with the ITRAX™ core scanner; Mn/Ti: µXRF element ratio for manganese and titanium. k_{LF}: low-field volumetric magnetic susceptibility. Grain size (%) for clay, silt, sand and gravel measured at 4 cm intervals. Distinct lithological facies are highlighted with color banding. Red: uppermost brownish gray silty mud unit (Uppermost Brownish, "UB"); light green: olive-black silty to clayey mud unit (Olive Clay, "OC"); white: carbonate-rich yellowish-brown to dark-brown very poorly sorted gravelly sandy mud detrital layers (DC); dark green: olive gray to dark gray poorly sorted silty to sandy mud low carbonate detrital layers (LDC) (see text for details).

Figure 3. (page 62) High-resolution magnetic properties of core PC16. Log: general simplified stratigraphy of the core (see text and legend for details); CT: CAT-Scan images; HRI: high-resolution digital image. Natural (NRM), Anhysteretic (ARM), Isothermal (IRM 0.3T) and Saturated Isothermal (SIRM 0.95T) Remanent Magnetization. k_{ARM}/k_{LF}: magnetic grain size indicators. Pseudo-S ratio $IRM_{0.3T}/SIRM_{0.95T}$ and MDF_{NRM}: magnetic mineralogy and grain size indicators. Distinct lithological facies are highlighted with color banding (see the legend of figure 2 and text for details).

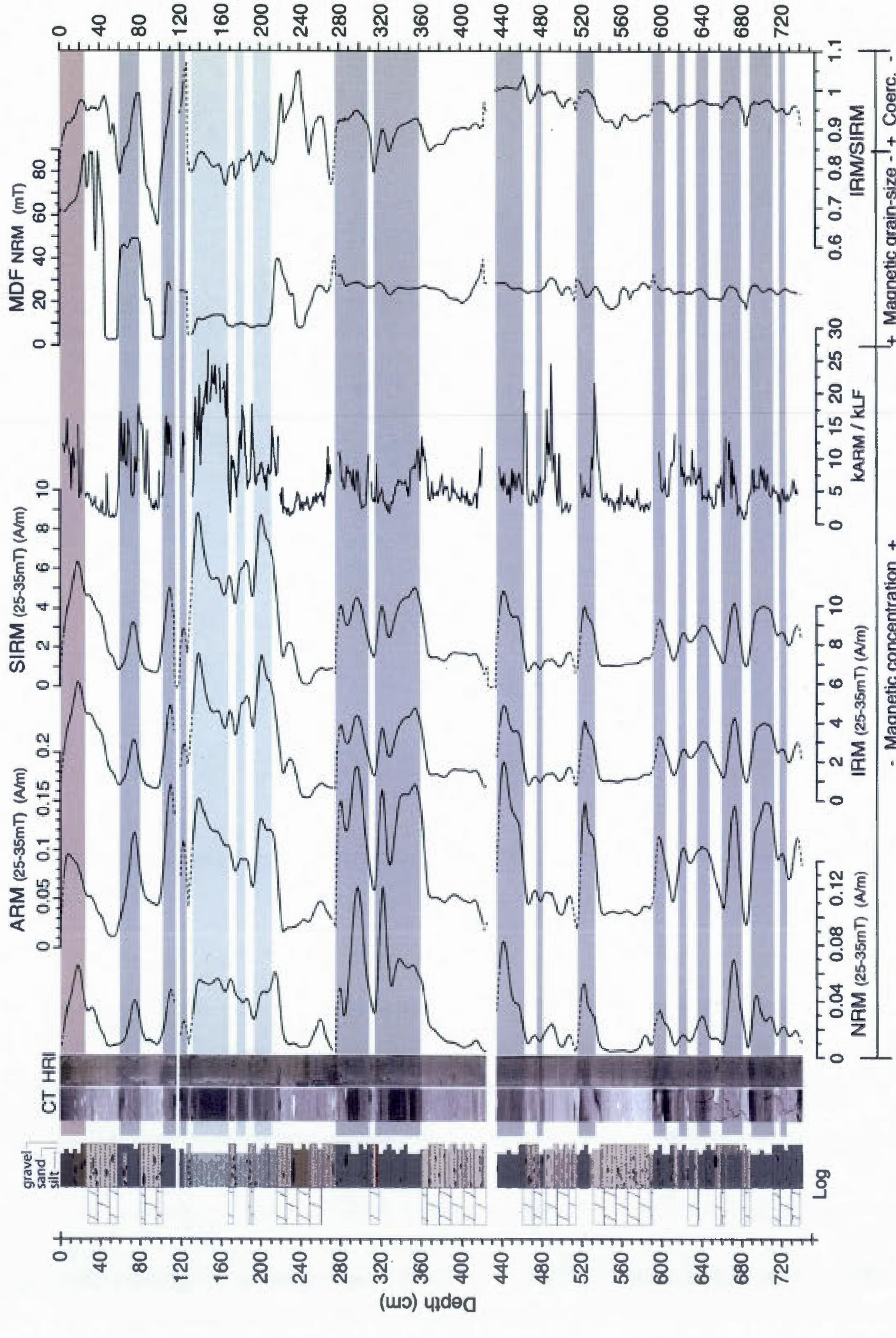
Depth (cm)
Log
gravel
sand
silt
CT HRI
NRM (25-35mT) (A/m)
ARM (25-35mT) (A/m)
IRM (25-35mT) (A/m)
SIRM (25-35mT) (A/m)
kARM / kLF
MDF NRM (mT)
IRM/SIRM
- Magnetic concentration +
+ Magnetic grain-size -
+ Magnetic grain-size - + Coerc. -
- Coerc. +

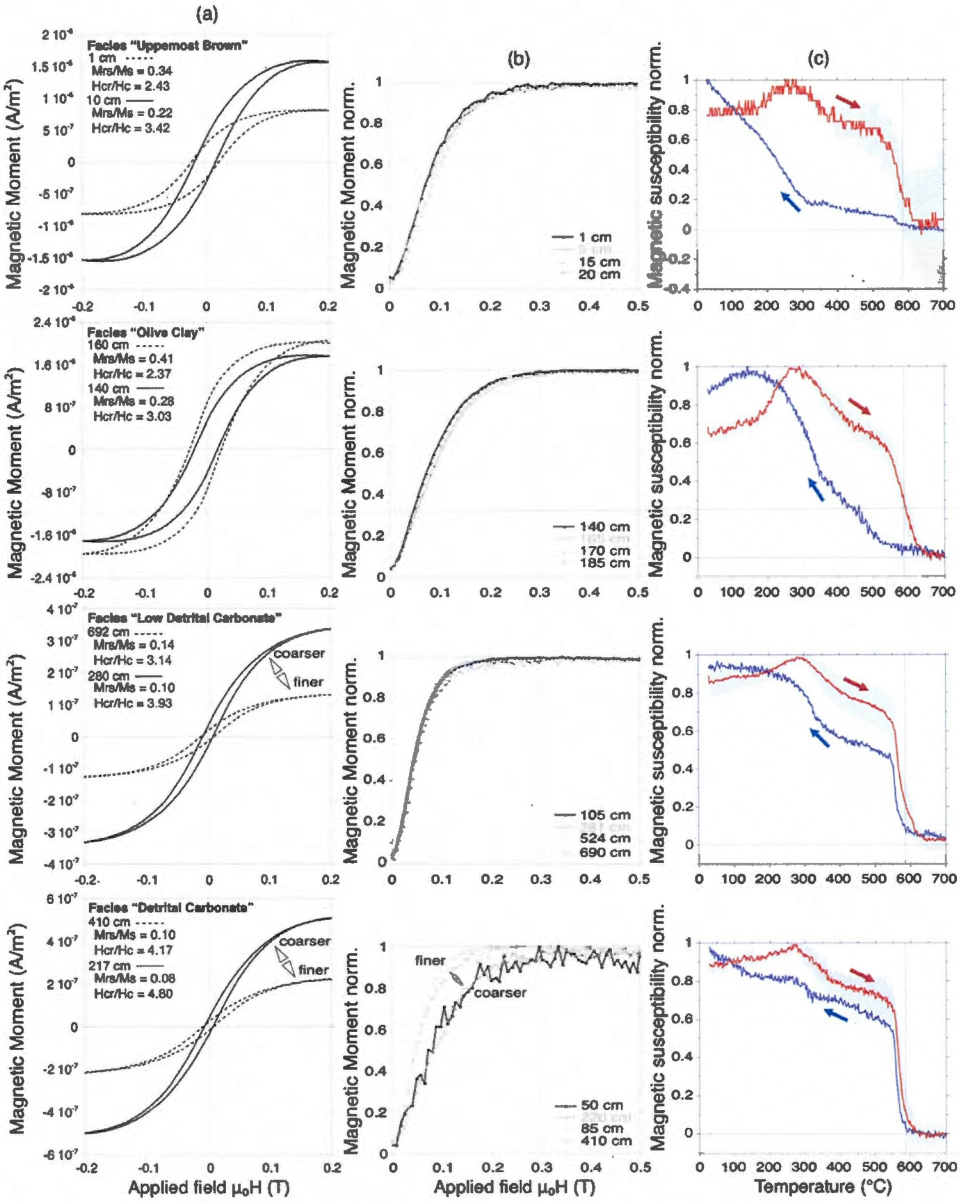

Figure 4. Magnetic mineralogy: (a) Representative hysteresis loops, (b) IRM acquisition curves, and (c) high-temperature dependence of magnetic susceptibility. IRM acquisition and thermal magnetic susceptibility data were normalized. Vertical line at 300 mT is for reference and corresponds to maximal saturation for an assemblage dominated by low coercivity minerals (e.g., magnetite) [*Moskowitz*, 1991]. Vertical line at 580°C corresponds to the Curie temperature of magnetite [*Dunlop and Özdemir*, 1997]. Results are divided in 4 groups according to the 4 facies characterizing the core (see the legend of figure 2 and text for details).

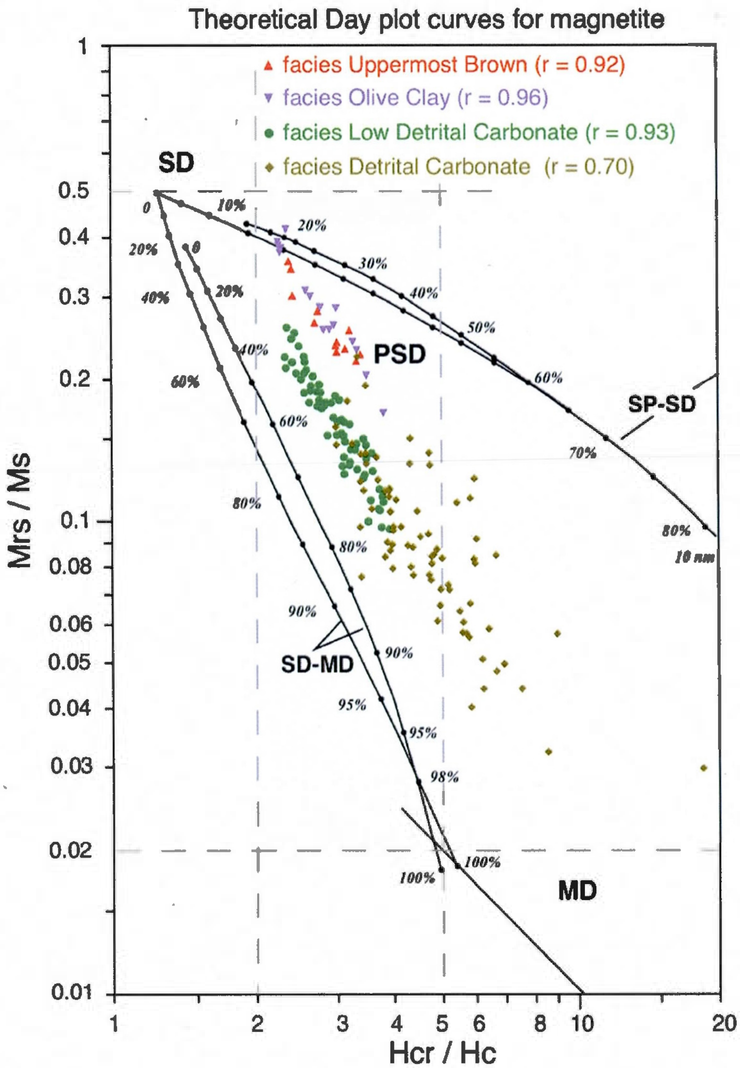

Figure 5. Day plot of selected samples. The horizontal and vertical lines delimitate the theoretical area for single (SD), pseudo-single (PSD) and multi domain (MD) magnetite grains. These lines and the mixing reference curves are from *Dunlop* [2002a, 2002b].

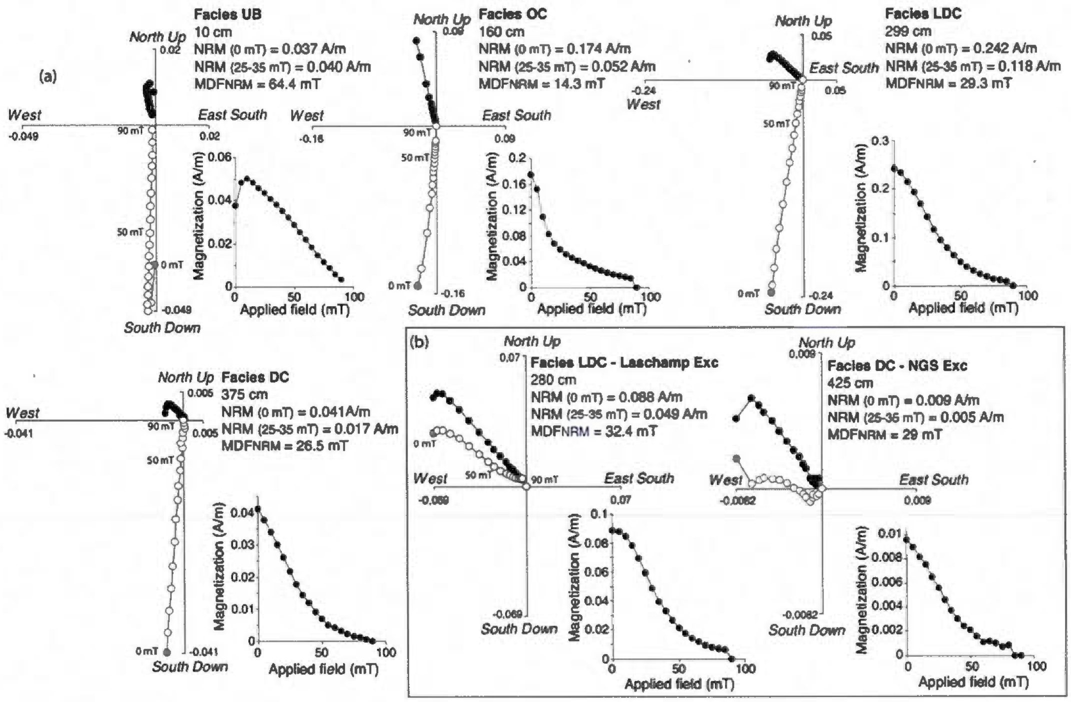

Figure 6. Paleomagnetic vectors. (a) Typical representative vector end-point orthogonal projection diagrams and AF demagnetization diagrams for the 4 facies discussed in the text. Open (closed) circles indicate projections on the vertical (horizontal) plane. (b) Typical vector end-point projection diagrams and AF demagnetization diagrams at the two intervals where geomagnetic excursions were identified (see also Figure 7).

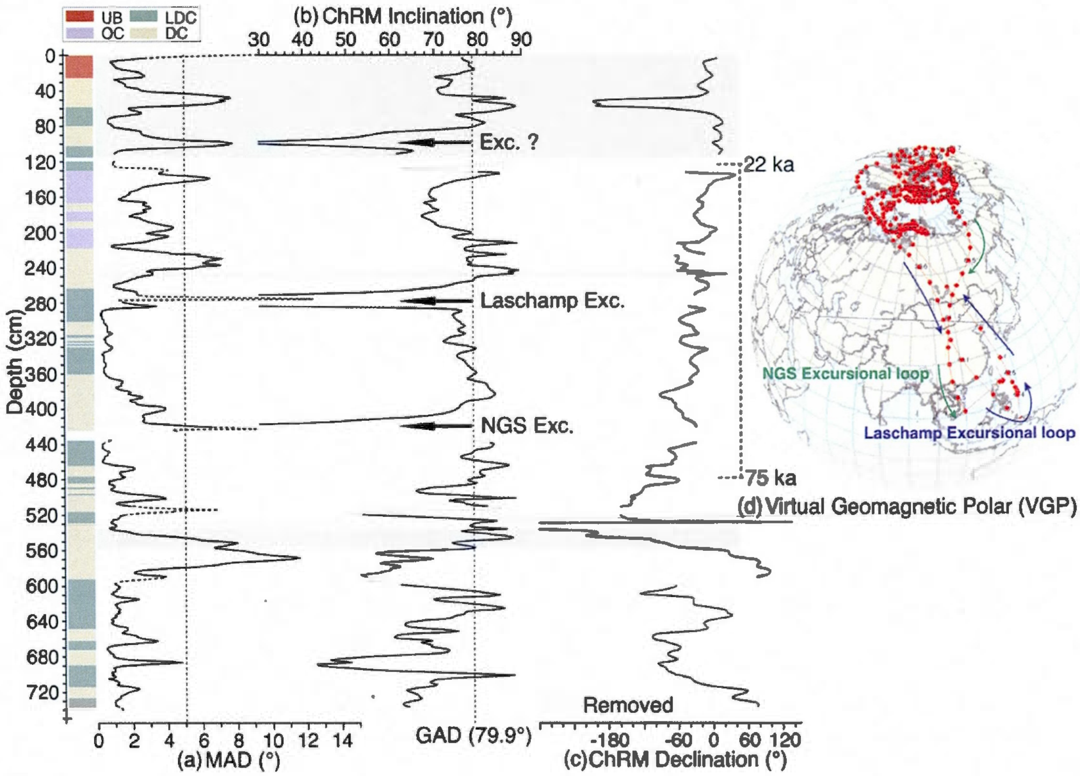

Figure 7. Characteristic remanent magnetization (ChRM). (a) MAD (Maximum Angular Deviation) values, (b) Inclination and (c) Declination. The solid vertical line indicates a MAD value of 5°, whereas the broken vertical line in the ChRM inclination represents the expected inclination for a geocentric axial dipole model (I_{GAD} = 79.9°). Gray shaded areas indicate problematic intervals for paleomagnetic reconstruction (see text for details). Data near core breaks are represented as a dotted line. Two potential geomagnetic excursions have been identified: the Laschamp (41±1 ka) [*Lund et al.*, 2006] and the Norwegian-Greenland Sea (61±2ka) [*Lund et al.*, 2006] excursions. (d) Virtual Geomagnetic Pole (VGP) calculated within the 22 – 75 cal ka BP time interval. The facies are represented on the left side with distinct colors: uppermost brown (red), olive clay (purple), low detrital carbonate layers (green) and detrital carbonate layers (beige) (see text for details).

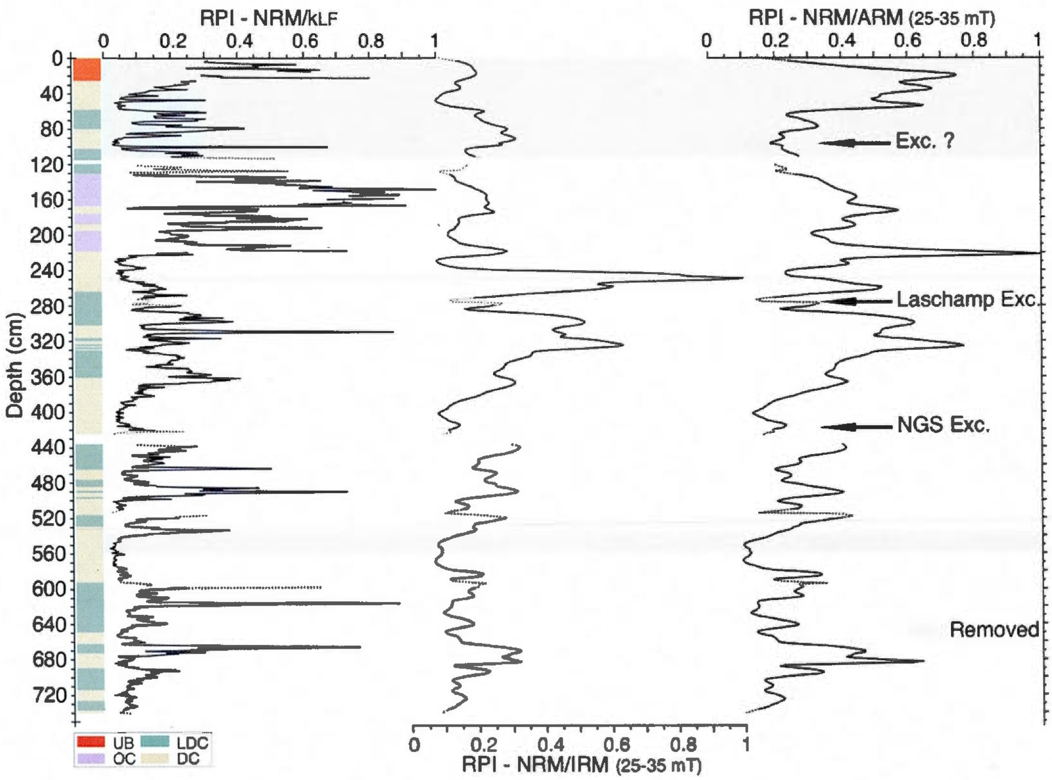

Figure 8. Normalized relative paleointensity. (a) NRM/k_{LF}, (b) NRM/IRM (25-35 mT), (c) NRM/ARM (25-35 mT). Two potential geomagnetic excursions (see also Figure 7) characterized by low intensities are illustrated: the Laschamp (41±1 ka) [*Lund et al.*, 2006] and the Norwegian-Greenland Sea (61±2ka) [*Lund et al.*, 2006] excursions. The facies are represented on the left side with distinct color: uppermost brown (red), olive clay (purple), low detrital carbonate layers (green) and detrital carbonate layers (beige) (see text for details). Data near core breaks are represented as a dotted line.

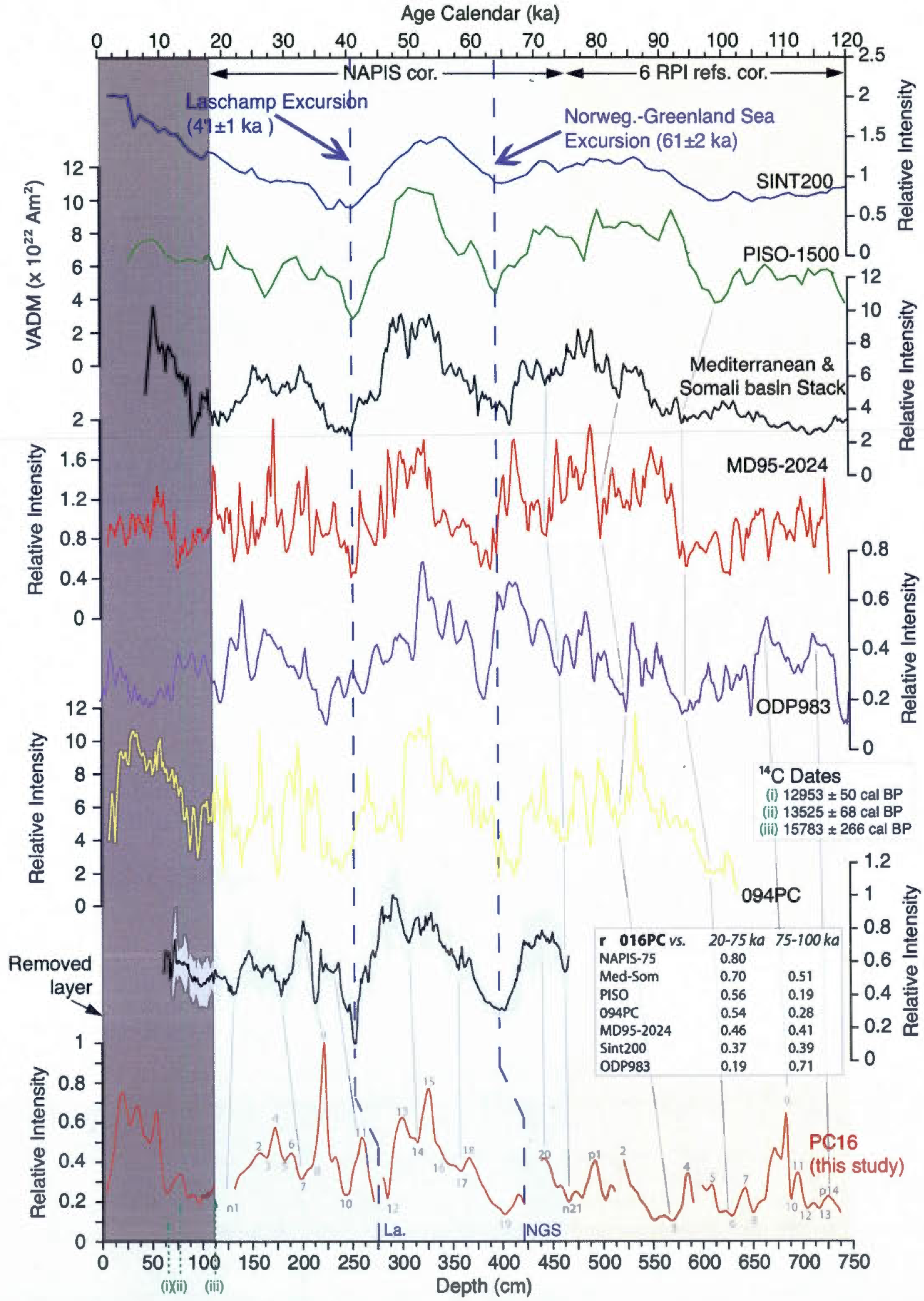

Age Calendar (ka)
NAPIS cor.
6 RPI refs. cor.
Laschamp Excursion (41±1 ka)
Norweg.-Greenland Sea Excursion (61±2 ka)
SINT200
PISO-1500
Mediterranean & Somali basin Stack
MD95-2024
ODP983
094PC
PC16 (this study)
VADM (x 10^22 Am^2)
Relative Intensity
Removed layer
La.
NGS
Depth (cm)
14C Dates
(i) 12953 ± 50 cal BP
(ii) 13525 ± 68 cal BP
(iii) 15783 ± 266 cal BP
r 016PC vs. | 20-75 ka | 75-100 ka
NAPIS-75 | 0.80
Med-Som | 0.70 | 0.51
PISO | 0.56 | 0.19
094PC | 0.54 | 0.28
MD95-2024 | 0.46 | 0.41
Sint200 | 0.37 | 0.39
ODP983 | 0.19 | 0.71

Figure 9. (page 68) RPI correlation. Relative paleointensity inter-comparison between core PC16 (this study) and RPI reference curves from the Labrador Sea: cores MD95-2024 [*Stoner et al.*, 2000] and 094PC [*Stoner et al.*, 1996, 1998]; the North-Atlantic: ODP983 [*Channell et al.*, 1997]; NAPIS-75 (stack of six RPI records from the North Atlantic Ocean) [*Laj et al.*, 2000]; Mediteranean & Somali Stack [Meynadier *et al.*, 1992]; and global stacks: Sint200 [*Guyodo and Valet*, 1996], and PISO-1500 [*Channell et al.*, 2009]. The 22 – 75 ka interval was dated by correlation with the NAPIS-75 stack solely, while the 75 – 115 ka interval was dated using 6 reference curves. The correlation coefficients were calculated between each dataset within the 20 – 75 and 75 – 100 ka intervals in order to provide statistical information where all the records overlap (see text for details).

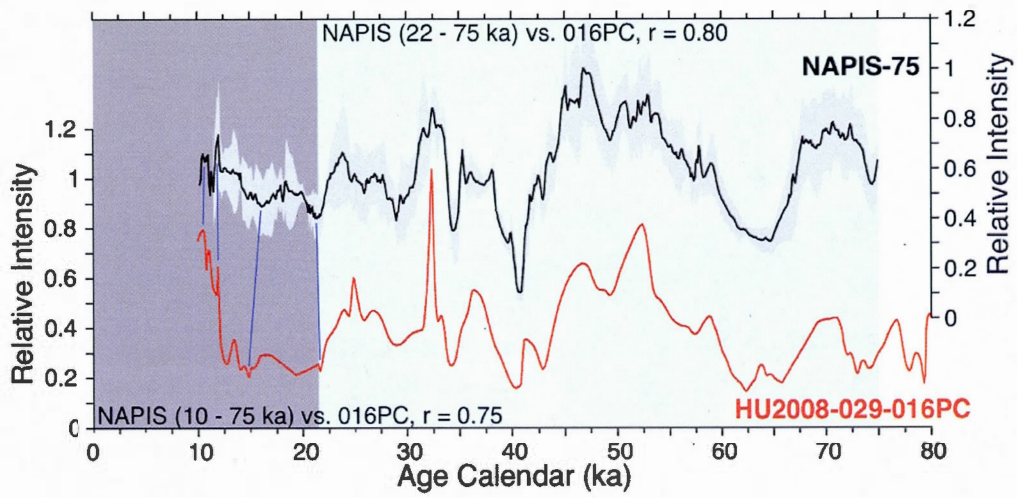

Figure 10. Relative paleointensity correlation between core PC16 and the NAPIS-75 stack (stack of six RPI records from the North Atlantic Ocean) [*Laj et al.*, 2000]. Blue lines represent similar features in both RPI records (not used for the age/depth relationship establishment).

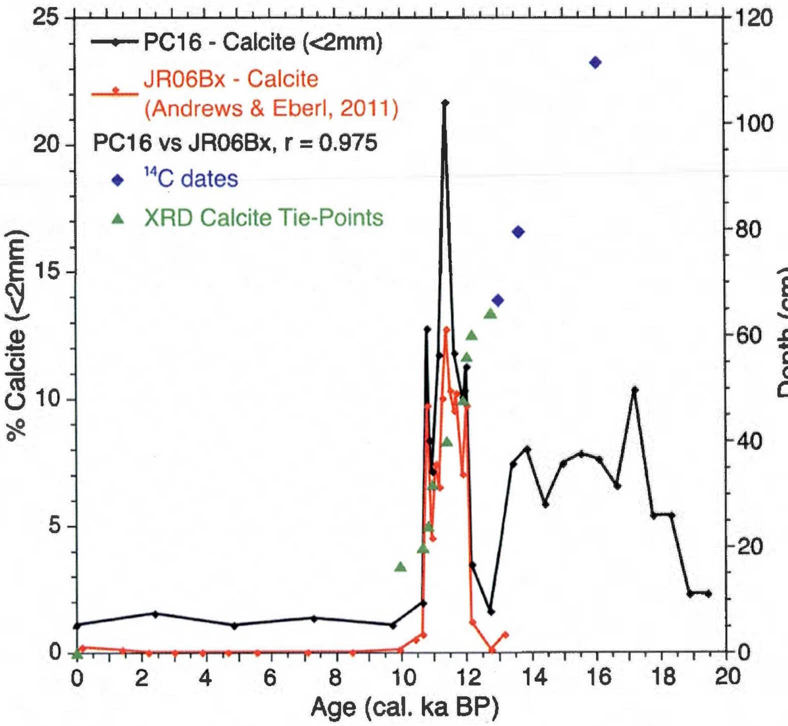

Figure 11. Age/depth relationship for the top of the core. Correlation between calcite percentages between JCR175BC06 box core (wt. %) [*Andrews and Eberl*, 2011] and PC16 (1/2qXRD) (left axis). Calcite-derived tie points (green triangle) and radiocarbon dates (blue diamonds) are plotted against depth (right axis). The correlation (r = 0.975) and radiocarbon dates enable to propose an original age/depth relationship where rock magnetic results are not suitable for paleomagnetic correlation.

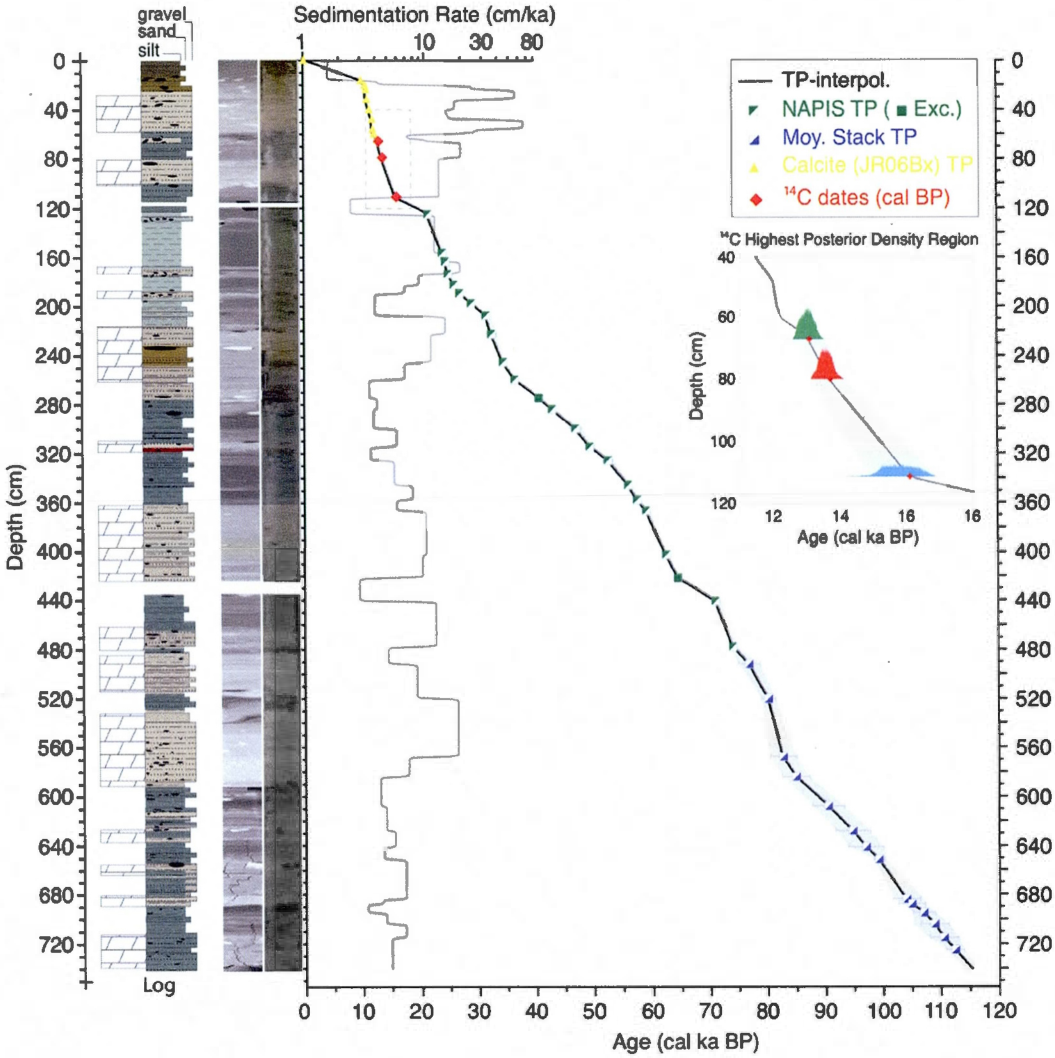

Figure 12. Age/depth relationship and associated sedimentation rates for core PC16. The age model is based on the RPI comparison (Figure 9). NAPIS related tie-points (TP) are represented by green squares. Tie-points derived from the 6 reference curves are illustrated by open blue squares. Three radiocarbon ages (red diamonds) and 2 potential geomagnetic excursions (green filled square) at 41±1 ka and 61±2 ka support the chronology. The radiocarbon ages are presented as the highest posterior density function within the sequence using the Marine09 and a ΔR=200±200 to append the marine reservoir effect. Incertitude in the age model is represented by shaded area. For the 22 – 75 ka interval, it corresponds to the ±2σ incertitude from the NAPIS bootstrap calculation. For the 75 – 115 ka interval, the errors correspond to the standard deviation between the 6 reference curves.

Supplementary material

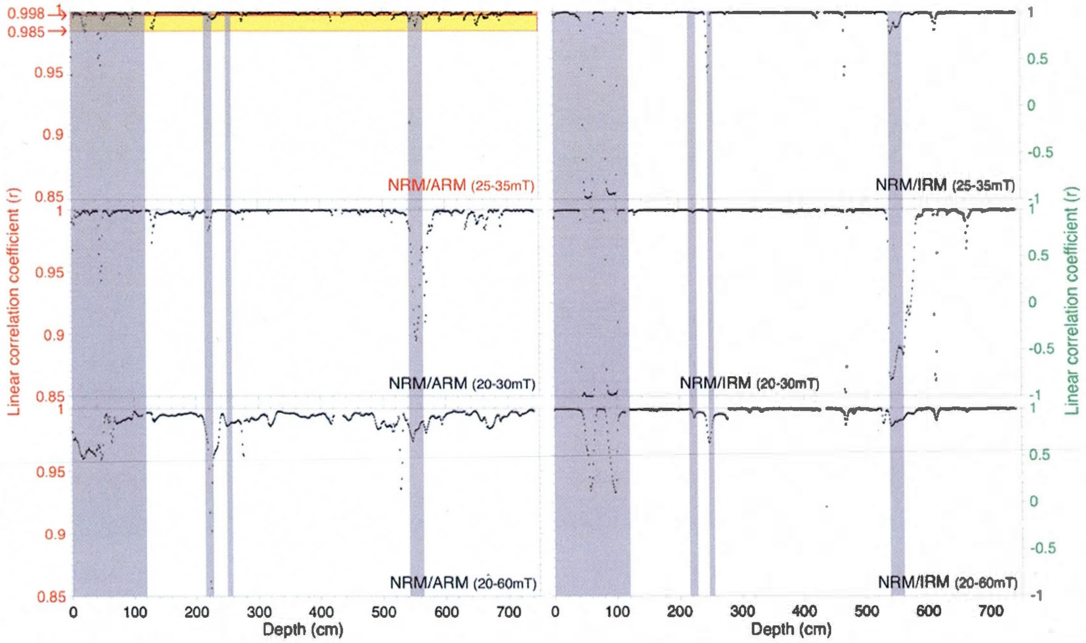

S1. Linear correlation coefficients for slopes of NRM vs. ARM (left) and NRM vs. IRM (right). Problematic intervals are highlighted in grey. The selected RPI (presenting the lowest r coefficient between NRM and its normalizer) is the NRM/ARM within the 25 – 35 mT interval.

S2. (page 73) Coherence of the RPI signal (a) Coherence of the relative paleointensity proxies with their normalizers. We applied a Blackman Tuckey cross-spectral analysis using a Barlett window [Paillard et al., 1996] on NRM/ARM vs ARM (25 – 35 mT) and NRM/IRM vs IRM (25 – 35 mT). The horizontal line represents the 95% confidence level. The r values between the RPI proxies and their normalizers are also presented. (b – c) Coherence of the NRM/IRM (25-35 mT) (b) and the NRM/ARM (25 – 35 mT) (c) with lithological proxies (MDF_{NRM}, k_{ARM}/k_{LF} and IRM/SIRM).

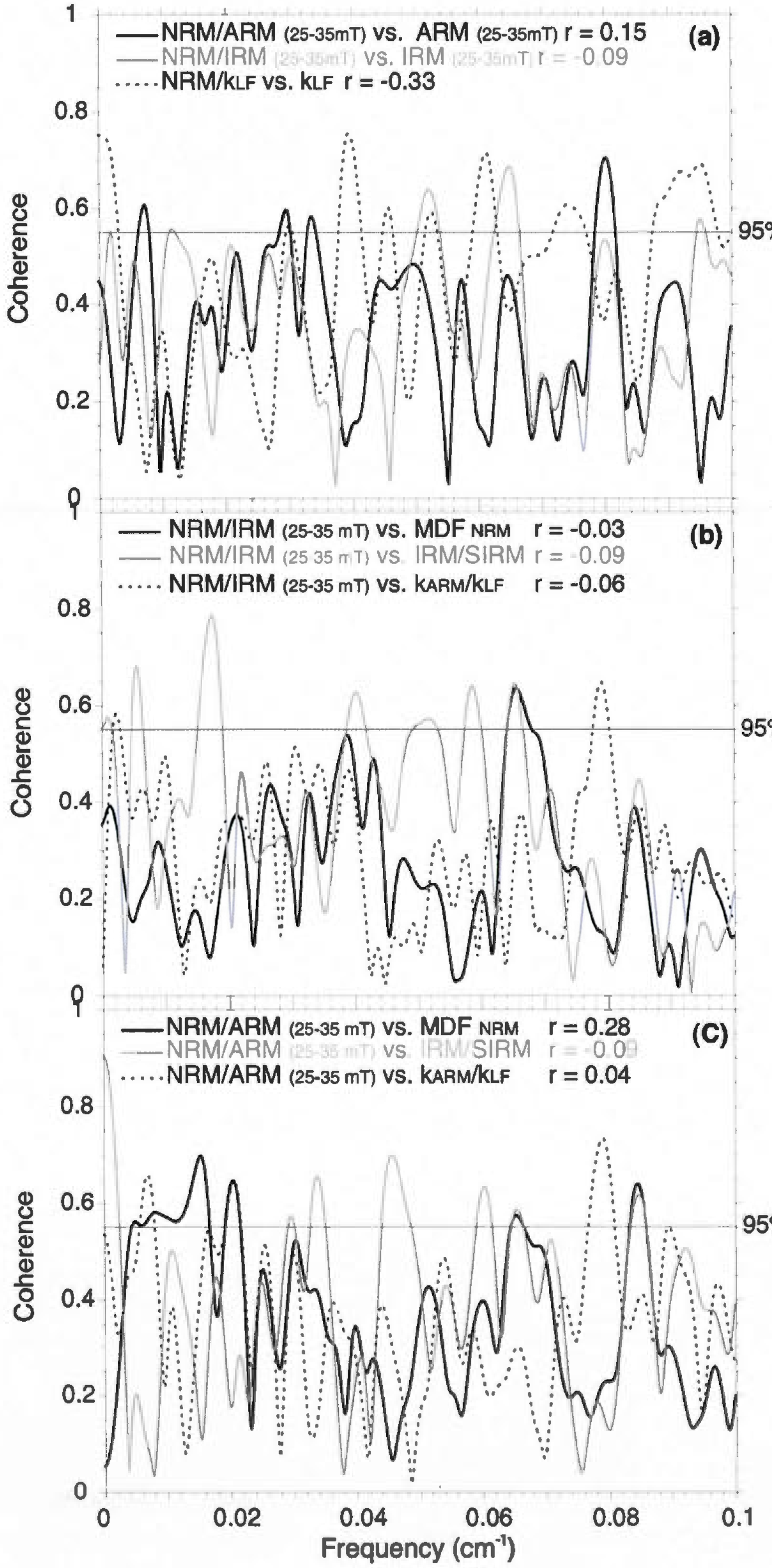
NRM/ARM (25-35mT) vs. ARM (25-35mT) r = 0.15
NRM/IRM (25-35mT) vs. IRM (25-35mT) r = -0.09
NRM/kLF vs. kLF r = -0.33
(a)
NRM/IRM (25-35 mT) vs. MDF NRM r = -0.03
NRM/IRM (25-35 mT) vs. IRM/SIRM r = -0.09
NRM/IRM (25-35 mT) vs. kARM/kLF r = -0.06
(b)
NRM/ARM (25-35 mT) vs. MDF NRM r = 0.28
NRM/ARM (25-35 mT) vs. IRM/SIRM r = -0.09
NRM/ARM (25-35 mT) vs. kARM/kLF r = 0.04
(C)
Coherence
95%
Frequency (cm⁻¹)
0
0.02
0.04
0.06
0.08
0.1
0.2
0.4
0.6
0.8
1

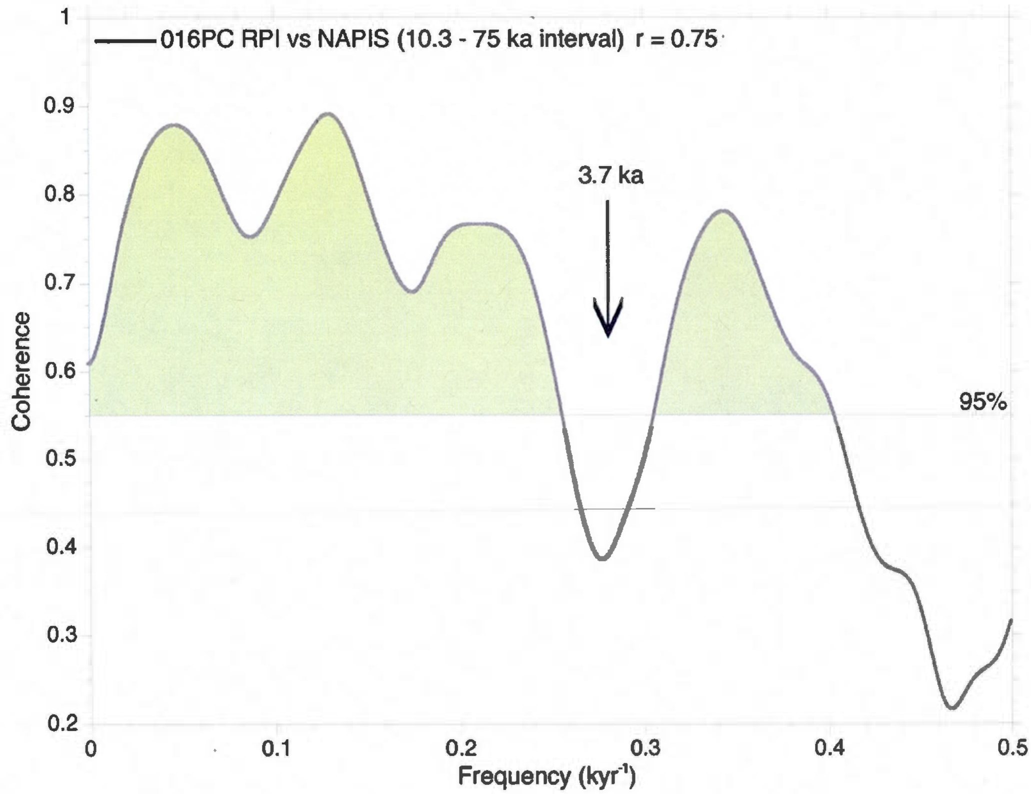

S3. Coherence of the RPI signal. Blackman Tuckey cross-spectral analysis using a Barlett window [Paillard et al., 1996] on NRM/ARM (25 - 35 mT) and the RPI proxy from the NAPIS stack [Laj et al., 2000] calculated between the 10 to 75 ka interval. The horizontal line represents the 95% confidence level.

CHAPITRE II

Detrital carbonate events in Baffin Bay during the last climatic cycle: Their timing vs. the Greenland Dansgaard-Oeschger cycles and North Atlantic Heinrich events

Quentin Simon[1,2], Claude Hillaire-Marcel[1,2], Guillaume St-Onge[1,3]

[1] Geotop Research Centre, Qc, Canada.

[2] Université du Québec à Montréal, Montréal, H3C3P8, Qc, Canada.

[3] Canada Research Chair in Marine Geology & Institut des sciences de la mer de Rimouski (ISMER), Université du Québec à Rimouski, Rimouski, G5L3A1, Qc, Canada.

Keywords:

Baffin Bay, Glaciomarine sediments, Detrital Carbonate layers, Fast-flowing ice stream, Last glacial cycle

Key Points:

Glaciomarine sediments provide evidences of pre-LGM ice-surges in Baffin Bay

Innuitien ice streams were sensitive to high frequency DO oscillations

BBDC are out of phase with H-events and related to Greenland interstadials

Article soumis à Paleoceanography (2012PA002397)

Abstract

A 7.4-m long sediment core (HU2008-029-016PC) from deep Baffin Bay has been analyzed to document Innuitian and Greenland ice margin activities during the last 115 ka. It yielded a high-resolution record of detrital carbonate events (mostly dolomitic) associated with ice streaming episodes from the Devon and Ellesmere islands, in the northern area of Baffin Bay. Earlier studies attributed these Baffin Bay Detrital Carbonate (BBDC) layers to interstadial episodes. A chronology based on magnetic paleointensity data now provides the means to better date these events. Grain-size and mineralogical (XRD) analyses at 4 cm intervals, together with high-resolution environmental magnetism and µXRF scanner proxies were used to link sedimentary features to specific northeastern Laurentide, Innuitian and/or Greenland ice margin events. Principal component analysis indicates the recurrence of two major facies. Fine-grained, Ti-rich sediments imply steady sedimentary supplies from Greenland and/or eastern Baffin Island ice margins. They contrast with the coarser detrital dolomite-rich layers linked to ice-surging episodes from northern Baffin Bay ice streams. Our results indicate that these episodes are out of phase with the North Atlantic Heinrich events, and suggest that these change likely represent a record of local Innuitian ice dynamics, in phase with Dansgaard-Oeschger events. Alternatively, this record may reflect pervasive IRD delivery process related to fast-flowing ice streams during distinct periods of glacial growth.

1. Introduction

Ice sheet dynamics has received a lot of attention during the last decades, namely because it represents a key component of the Earth's climate system, playing an important role in processes affecting freshwater budget, sea-level fluctuations, and ocean circulation [*Alley et al.*, 2010]. However, the detailed relationship between the growth and decay of ice sheets and late Quaternary climate variability, such as Dansgaard-Oeschger cycles (D/O) [*Wolff et al.,* 2010], remains somewhat poorly understood [*Marshall and Koutnik,* 2006]. Because of its proximal location to the margins of major northern hemisphere ice sheets (i.e., the Laurentide, Innuitian and Greenland ice sheets), Baffin Bay glaciomarine sediments have great potential to give an accurate record of ice streaming events and concomitant icebergs calving events along these margins, as well as of changes in the sea ice cover. Yet, paleoceanographic studies in Baffin Bay, and more largely in the Arctic basins, have been proven highly challenging, mainly due to low sedimentation rates in the deeper part of the basin, non-uniform stratigraphies, and poor chronological control [e.g., *Polyak and Jakobsson*, 2011; *Andrews et al.*, 1998; *Simon et al.*, 2012]. The presence of detrital-rich carbonate layers (Baffin Bay Detrital Carbonate - henceforth BBDC) in Baffin Bay sedimentary sequences has been recognized in earlier studies and associated with rapid retreats of large ice streams in the Canadian Arctic Archipelago channels [e.g., *Aksu and Piper*, 1987; *Andrews et al.*, 1998]. However, a clear picture of ice-margin dynamics around Baffin Bay is still missing, in particular due to the lack of a millennial-scale chronology.

Here, based on a new Baffin Bay chronostratigraphic framework [*Simon et al.*, 2012], which allows to accurately constrain sedimentological features such as the BBDC, we intend to reconstruct major ice margin instabilities of the northeastern Laurentide, southern Innuitian, and western Greenland ice sheets, since ca. 115 ka BP. The main objectives of the study concern: (1) the timing and phasing of sedimentary processes revealed by changes in multi-proxy variables, related to individual ice-stream responses to climatic/oceanographic variability, (2) the phasing relationships (synchronicity?) of BBDC-events with Heinrich events and Dansgaard-Oeschger cycles, and (3) providing geological evidence of circum-Baffin Bay ice stream dynamics during the last glacial cycle. We interpret and discuss the timing of deep Baffin Bay sediment deposition for the last glacial cycle with regard to ice streaming events, based on a detailed lithological, environmental magnetism, and geochemical dataset.

2. Regional setting

2.1. Hydrography

Baffin Bay (Figure 1) is an elongated oceanic basin (1300 km long and 450 km wide, ~690 000 km^2), which is flanked by Baffin Island and Greenland (Figure 1). The morphology of the bay consists of a central abyssal plain (2000–2500 m) surrounded by continental shelves. The continental shelf of Baffin Island is 25–50 km wide with an average depth of 200 m, whereas the shelf of Greenland is larger (>250 km), deeper (>300 m), and characterized by large submarine fans at the mouth of cross-shelf troughs, which are absent on the shelf of Baffin Island [*Ó Cofaigh et al.*, 2012]. Steep continental slopes characterize the eastern and western sides of the bay, whereas the northern continental shelf declines gently towards the abyssal plain [*Li et al.*, 2011]. Exchanges between Baffin Bay and the Arctic Ocean occur through shallow channels between the islands of the Canadian Arctic Archipelago, notably through Nares Strait, while Davis Strait (sill depth: 650 m) connects the bay to the North Atlantic. Baffin Bay has a counter-clockwise surface circulation and is bathed by three main water masses [*Tang et al.*, 2004] (Figure 1): (1) the cold and low-saline Arctic Waters (100–300 m), which flow southward along the western coast of Baffin Island, (2) the warmer and more saline West Greenland Intermediate Waters (300–800 m), which flow northward along the Greenland continental shelf, and (3) the cold Deep Baffin Bay Waters (>1200 m). The modern specific oceanographic conditions of the bay result in a very shallow lysocline, characterized by poor preservation of calcareous microfossils [*Aksu*, 1983; *de Vernal et al.*, 1992; *Azetsu-Scott et al.*, 2010].

2.2. Sea ice and icebergs

Extensive sea ice (mainly first year sea ice) covers the bay except in August and September. The influence of Atlantic Waters on the Greenland margin contributes to an asymmetric distribution of the sea-ice cover [*Tang et al.,* 2004]. Nares Strait and the Canadian Arctic channels export about 150–250 km^3 of sea ice to Baffin Bay [*Kwok et al.*, 2010]. Icebergs are formed and maintained mainly by fast-flowing outlets of the Greenland Ice Sheet (GIS), with limited contributions from tidewater glaciers on the Canadian Arctic Archipelago (Figure 1) [*Weidick and Bennike*, 2007; *Andrews and Eberl*, 2011]. *Bigg et al.* [2001] estimated the present-day icebergs flux to be ~141 km^3/yr for Nares Strait and western Greenland, and nearly 84 km^3/yr of the total iceberg production is calved from the Disko Bugt and the Uummannaq ice stream complex [*Weidick and Bennike*, 2007]. *Bigg et al.* [2001] estimated the LGM iceberg flux to be ~98 km^3/yr for Nares Strait, western Greenland and the Lancaster Sound palaeo-ice stream, while *Marshall and Koutnik* [2006] estimated a total iceberg flux of ~16.8 x 10^6 km^3 for Baffin Bay during the last glacial cycle.

2.3 Bedrock geology

The Baffin Bay geology is mostly characterized by a Precambrian crystalline basement overlain by a lower Paleozoic succession dominated by shallow marine platform carbonates. Archean and Paleoproterozoic basement rocks (age ranging from ~3.2 to 1.7 Ga) are by far the largest outcropping units on each side of the bay [e.g., *MacLean et al.,* 1990; *Harrison et al.*, 2011]. The Paleozoic carbonates, principally dolomites of different maturities [Parnell et al., 2007] with minor abundance of limestones and cherts [*Reid et al.*, 2008], outcrop in northwestern Greenland and in the Canadian High Arctic (Figure 1). Tertiary (Paleocene) rifting resulted in the development of a series of large grabens, with basaltic flows observed along Canadian and Greenland Precambrian Shield margins near Cape Dyer and the Disko Island/Uummannaq fjord complex [*Harrison et al.*, 2011].

2.4. Late Quaternary

Almost no geological evidence of Sangamonian (Marine Isotopic Stages - MIS - 5a-e) or early and mid-Wisconsinan (MIS4–3) glaciations have been found regarding the southeastern Innuitian Ice Sheet (IIS) dynamics, likely because they were eroded by earlier ice flow events, i.e., during the last glacial maximum (LGM) and final deglaciation [*England et al.*, 2009]. Based on sedimentary facies analysis of deep Baffin Bay cores, researchers [e.g., *Aksu*, 1985; *Andrews et al.*, 1985; *Vincent and Prest*, 1987] inferred a period of major ice accumulation during the stage 5 to 4 transition, following a smaller one at the transition between substages 5e and 5d. Regarding the Greenland Ice Sheet (GIS), only the Scoresby Sund (East Greenland) and the Thule region (North-West Greenland) yielded detailed paleogeographical records from MIS5d-a to MIS3 [*Funder et al.*, 2011; *Alley et al.*, 2010; *Kelly and Lowell*, 2009]. Nonetheless, a review of the literature indicates that ice advanced during cold periods (i.e., MIS5d, 5b, 4 and 2) and retreated during warm periods (i.e., MIS5c, 5a, 1), although the extents, rates, and time responses of the ice-margin remain unclear [*Alley et al.*, 2010]. Climate modeling simulations suggest that the last glacial cycle might have started with a relatively abrupt lateral expansion of the northeastern Laurentide, Innuitian and Greenland ice sheets immediately following the last interglacial period (i.e., Sangamonian or MIS5e) between 120-115 ka BP [*Wang et al.*, 2005; *Ganopolski et al.*, 2010]. Recent simulations have shown a (1) rapid glacial inception followed by several phases of ice sheet growth and reduction, and (2) a strong asymmetry between the ice sheet growth phase and glacial termination [*Ganopolski et al.*, 2010; Stokes et al., 2012].

During the LGM, the northeastern Laurentide Ice Sheet (LIS), the Innuitian Ice Sheet (IIS) and the western Greenland Ice Sheet (GIS) formed a nearly continuous ice belt surrounding Baffin Bay (Figure 1). The GIS probably extended westward over the inner shelf, and likely as far as the shelf edge off Disko Bugt and the Uummannaq trough [e.g., *Ó Cofaigh et al.,* 2010, 2012; *Funder et al.,* 2011]. The GIS and IIS likely joined across Nares Strait, forming the Smith Sound ice stream, which produced large streamlined bedforms on land and on the sea floor [*England et al.*, 2006], and possibly extended as an ice shelf towards the northern Baffin Bay [*Alley et al.*, 2010]. East of the Boothia Peninsula, several ice streams merged into Lancaster Sound, forming a thick-grounded glacier (at least 1600 m thick) [*Klassen and Fisher*, 1988]. This major ice stream advanced into northern Baffin Bay [*MacLean et al.*, 2010] with a LGM maximum grounding line located 270 km off the mouth of Lancaster Sound (in a water depth of 1300 m) [*Li et al.*, 2011], and potentially expanded laterally to create an ice shelf in the northern part of the bay [*Hulbe et al.*, 2004; *Marcott et al.*, 2011]. The channels between the islands of the Canadian Arctic Archipelago were occupied by warm-based palaeo-ice streams resulting from the enhanced strain heating produced by the coalescent ice flow during the ice sheet growing phase [*England et al.*, 2006]. The LIS extended through Baffin Island, probably as far as the fjord mouths and inlets, and possibly over part of the Baffin Island shelf [*Briner et al.*, 2003, 2006]. Deglaciation began as early as ~16 ka BP [*Briner et al.,* 2006; *Funder et al.,* 2011; *Jennings et al.,* 2011; *Ganopolski et al.*, 2010]. However, Nares Strait was not deglaciated until 8.5 ka BP [*Dyke,* 2004; *Jennings et al.,* 2011]. According to *Kelly and Lowell* [2009], the latest deglacial - GIS retreat occurred in two distinct stages: (1) collapse of the shelf-based ice sheet, and (2) subsequent melting of the land-based ice sheet margin up to the present coastline. The GIS and small Canadian island ice caps retreated behind their present margins at ~6 ka BP but readvanced during the Neoglaciation (~6–3 ka BP) [*Funder et al.,* 2011; *Weidick and Bennike*, 2007].

2.5. Sedimentation pattern in Baffin Bay during the last climatic cycle

The impact of the Sangamonian and Wisconsinan ice-advances on Baffin Bay sediment delivery is poorly documented, especially due to poorly constrained chronostratigraphies [*Vincent and Prest*, 1987; *Andrews*, 2009]. Based on the mineralogy of detrital supplies, sediment textures and limited oxygen isotope results, *Aksu* [1983] interpreted the cycle of turbidites and debris flow deposits interbedded with ice-rafted debris (IRD) and hemipelagic sediments, as being the result of glacial/interglacial control. However, subsequent interpretations based on a revised age model [see *Andrews et al.*, 1998] suggest a much shorter sedimentary record. For instance, the large sporadic detrital coarse-carbonate layers (BBDC) deposited in the bay through the last glacial cycle and originating from the erosion and transport of Paleozoic carbonate debris from northern ice streams by icebergs, sea ice and/or associated meltwater discharges [e.g., *Aksu and Piper*, 1987; *Parnell et al.*, 2007] could be associated to climatic changes and possibly be synchronous with incursions of warm North Atlantic Waters [*Srivastava et al.*, 1987; *Hiscott et al.*, 1989]. Therefore, records of ice margin dynamics during the last glacial cycle exist, but the extent and timing of the related glacial events remain unclear due to a lack of well-dated records [*Alley et al.*, 2010; *Andrews et al.*, 1998].

3. Materials and methods

Core HU2008-029-016PC (PC16 hereinafter) is a 741-cm long piston core raised from central Baffin Bay during the 2008-029 CCGS Hudson cruise (70°46.14 N/-64°65.77 W; water depth 2063 m) [*Campbell and de Vernal*, 2009]. The core location (Figure 1) is within proximity of an ODP site previously drilled in 1985 (ODP 645, leg 105) [*Srivastava et al.,* 1989] and of several cores raised from deep central Baffin Bay during the 1970s and 1980s [e.g., *Aksu*, 1981; *Aksu and Piper*, 1987; *Andrews et al.,* 1998].

3.1. Physical and geochemical properties

Diffuse spectral reflectance data were acquired at 1 cm interval immediately after core-splitting, using a Minolta CM-2600d™ handheld spectrophotometer. The core sections (1.5 m long) were described, then sampled on-board with u-channels (rigid u-shaped plastic liners, 2 x 2 cm cross section) from the centre of the working halves. Low-field volumetric magnetic susceptibility (k_{LF}) was measured on u-channel samples using a Bartington point sensor (MS2E) at 0.5 cm intervals. The archive halves were run through a computerized coaxial tomography scanner (CAT-Scan) at 0.1 cm intervals at INRS-ETE in Québec City to visualize the sedimentary structures and to derive the CT numbers, which mainly reflect changes in bulk density [*St-Onge et al.*, 2007]. Grain-size analyses were performed on sediment samples (1–2 g) at ISMER using a Beckman Coulter™ LS13320 laser diffraction grain size analyzer at 4 cm intervals. Wet sediment was mixed in a solution of 20 gL^{-1} of Calgon electrolytic solution (sodium hexametaphosphate) and water. The samples were rotated for 3 hours and then sieved at 2 mm prior to analysis. Grain size distribution and statistical parameters (mean, standard deviation) were calculated using the Gradistat™ software [*Blott and Pye*, 2001]. The relative content of calcium (Ca), titanium (Ti), iron (Fe), manganese (Mn), strontium (Sr), potassium (K) and silicon (Si), among others, were determined at 0.5 cm intervals by micro X-ray fluorescence (µXRF) spectrometry on the u-channels, and during a 50 s counting time using an ITRAX™ core scanner (Cox Analytical Systems) at the GIRAS laboratory (Geochemistry, Imagery and Radiography of Sediment) at INRS-ETE. The output data represent relative concentrations, which are reported using element ratios to improve the geochemical interpretation as several factors related to the sediment matrix could interfere with the concentration estimation [*Thomson et al.*, 2006; *Francus et al.*, 2009].

3.2. Mineralogy

Bulk and clay mineralogical assemblages were determined by X-ray diffraction (XRD) at UQAM using a Siemens D-5000™ diffractometer (°2Θ, CoKα1,2 radiation and a Si detector). The analyses were performed on sediment fractions sieved at 63 µm and 2 mm with a 4 cm sampling interval. Semi-quantitative estimates ($\pm 1\sigma \sim 5\%$) of the main mineral species were based on the peak height (in counts per second) of the first diffraction peak for each mineral corrected for quartz and normalized to 100% [*Thorez,* 2003]. The clay fraction (<2 µm) was separated by settling (Stokes's Law) and deposited on oriented mounts using the glass-slide method [*Moore and Reynolds*, 1997]. It was then X-ray scanned three times: (1) under natural conditions (i.e., air-dried), (2) after solvation with ethylene-glycol for 24 hours, and (3) after heating at 500°C for 4 hours [*Cook et al.,* 1975; *Thorez*, 2003]. Semi-quantitative estimates (amounting to 100 %) of the main clay minerals (i.e., smectite, illite, kaolinite and chlorite) were obtained using the weighting factors of *Biscaye* [1965]. The clay-mineral assemblage is a useful indicator for identifying the origin and transport pathway of sediments in polar and subpolar regions where physical weathering processes prevail [*Stein*, 2008] and/or where sedimentary bedrocks exist.

3.3. Environmental magnetism

Paleomagnetic and rock magnetism data were measured at the *Laboratoire de paléomagnétisme sédimentaire et géologie marine* at ISMER using a 2G-Enterprises™ u-channel cryogenic magnetometer allowing the continuous measurement, at 1 cm intervals, of the natural, anhysteretic and isothermal remanent magnetizations (respectively NRM, ARM, IRM), and an alternating gradient force magnetometer (AGM) MicroMag™ 2900 from Princeton Measurements Corporation. These measurements allowed the calculation of common environmental magnetic parameters sensitive to magnetic minerals properties such as the concentration (magnetic susceptibility ARM, SIRM), mineralogy (MDF_{NRM} and IRM/SIRM) and grain size (k_{ARM}/k_{LF}, SIRM/k_{LF}, MDF_{NRM}, Mrs/Ms, Hcr/Hc) [*Simon et al.*, 2012;

Stoner and St-Onge, 2007 and references therein for a review of these proxies]. First order reversal curve (FORC) diagrams providing information on the distribution of coercivities and interaction fields among magnetic grains [*Pike et al.*, 1999; *Muxworthy and Roberts*, 2007] were measured using 100 partials FORCs and an averaging time of 200 ms. Representative samples are presented and compared with SIRM/k_{LF} and Day plot (Figures 3 and 4) in order to interpret the FORC diagrams with the magnetic grain size variability. The data were processed using FORCinel™ [*Harrison and Feinberg*, 2008] and IgorPro™ softwares with a smoothing factor of 4.

3.4. Core chronology

Core PC16 age model (Figure 2) is primarily based on the relative paleointensity (RPI) correlation with regional and global RPI reference curves. Three radiocarbon ages and two geomagnetic excursions further support this age model. The age model is consistent with previous regional models but offers a significantly improved temporal resolution [see *Simon et al.*, 2012 for details].

4. Results

Five lithofacies were identified in the core and represent distinct sediment delivery processes. Low detrital carbonate (1) and detrital carbonate (2) facies are found at specific intervals within the entire sequence, while distinct facies are found at given depths and represent: Last Glacial Maximum (3), last deglaciation (4) and Holocene (5) time intervals. These lithofacies are described and interpreted below with some emphasis on their physical and magnetic properties. Additional information on the environmental significance of several magnetic parameters possibly unfamiliar of paleoceanographers, can be found in *Stoner and St-Onge* [2007], and *Muxworthy and Roberts* [2007].

4.1. Lithofacies

4.1.1. Low detrital carbonate layers (LDC)

Low carbonate percentages (<10%, except at the bottom of the core where values up to 15% are found) and high silty-clay fraction (0–63 μm >80–95%, with ~30% clay and 50% fine to very fine silt, Figures 2 and 3) characterize this dark gray to olive-gray unit (Figure 2). In addition, the LDC facies is outlined by low a* (green) and density values, low Ca/Fe, K/Ti ratios (Figure 5), together with Ti-rich sediments, high magnetic susceptibilities (k_{LF}), and illite percentages ranging from 70 to 80% (Figure 6). This facies has been attributed to steady sedimentary supplies from the Greenland and/or Baffin Island ice margins (i.e., lateral inputs). Low sedimentation accumulation rates (SAR) (~6–7 cm/kyr) characterize this hemipelagic sediment unit (Figures 2 and 5). We propose to relate such low SAR to low debris-laden ice streams due to hard subglacial substrate (i.e., not easily erodible) beneath Greenland and Baffin Island glaciers and fast-flowing ice streams [*Smith et al.*, 2012]. The magnetic sediments of this unit are mainly (titano)magnetite (i.e., MDF_{NRM} ~20–30 mT, $IRM_{0.3mT}/SIRM_{0.95mT}$ close to 1, Figure 3) within a magnetite mixing line in the pseudo-single-domain (PSD) range (i.e., Day plot, Figure 4a). Additional magnetic proxies such as (1) IRM acquisition saturated below 300 mT, (2) typical shape of hysteresis loops, and (3) thermomagnetic analyses are in conformity with this interpretation of the magnetic assemblage [see *Simon et al.*, 2012 for a comprehensive rock magnetism description]. The FORC diagram #6 depicts low coercivities and medium interactions within the magnetic grain assemblage (Figure 4b), a feature that illustrates a relatively fine magnetic grain-size range within this magnetic facies [*Carvallo et al.*, 2006; *Xuan et al.*, 2012].

4.1.2. Baffin Bay detrital carbonate layers (BBDC)

Numerous grayish-brown layers assigned to the BBDC facies are associated with gravelly sandy mud (sand + gravel >20–30%, Figures 2 and 5) and XRD carbonate percents comprised between 40 to 60% (with 30–40% dolomite, Figures 2 and 5). The mineralogical signature of BBDC layers is dominated by high percentages of dolomite; and chlorite within the clay fraction (Figures 5, 6 and 7). These provenance characteristics highlight the main source region, i.e., the lower Paleozoic carbonates outcropping in the Canadian Arctic islands [*Andrews and Eberl*, 2011]. Sediments from the carbonate-bearing ice stream in Home Bay could also contribute for a smaller fraction to these BBDC layers as proposed by *Andrews and Eberl* [2011]. At ~10 ka BP however, the wt% dolomite in PC16 is ~35%, which is way higher than the 8% dolomite percentages found at the same period in the HU85-079TWC from outer Home Bay [*Andrews and Eberl*, 2011]. It suggests a major northern provenance with possibly a minor contribution from Home Bay. BBDC layers are also characterized by high Ca/Fe, K/Ti, Mn/Ti ratios, high-density proxy values (GRA and CT number) due to the higher density of carbonate detritus, high a* values (red) (Figures 2, 5 and 6), low Ti contents and low k_{LF} probably due to the carbonate (dolomite) diamagnetic (paramagnetic) properties (Figure 6). In addition, coarse magnetic grain sizes are characteristic of these DC-intervals, i.e., coarse-PSD to multi-domain (MD) grains on the Day plot; these are associated with low k_{ARM}/k_{LF}, SIRM/k_{LF}, Mrs/Ms and high Hcr/Hc values (Figures 3, 4a and 5). The FORC diagrams (FORC#2 and 3, Figure 4b) illustrate coarse PSD to MD grains characterized by lower coercivities and higher interactions within the magnetic grain assemblage. Poorly sorted to very poorly sorted sediments (trimodal to polymodal mode), together with similar variations of the different size fractions >63 μm (Figure 5), as well as with the large amount of dropstones recognizable on the CAT-Scan images (Figures 2), favor an IRD discharge deposition mode rather than a turbiditic process [*Andrews*, 2000]. SAR are highly variable throughout the core but exhibit increases (>10 cm/kyr) for some of these DC layers (Figure 5). Higher SAR are explained by (1) higher IRD fluxes, and (2) substrate/basement geology (i.e., Paleozoic carbonates more easily erodible than Precambrian granites) beneath the fast-flowing ice streams from the northern end of the bay that allow more detritus to be incorporated within the basal zone of icebergs. These grayish brown, gravelly to sandy mud decimetric detrital carbonate layers (~10-60 cm) correspond to the BBDC layers previously reported in other Baffin Bay cores [*Aksu et al.*, 1981; *Aksu and Pipper*, 1987; *Andrews et al.,* 1998].

4.1.3. The Last Glacial Maximum sedimentary unit

Brownish-black to olive-black silty to clayey muds are distinguished between 120 and 215 cm (~16–32 ka BP) and correspond to the Olive Clay facies (OC) of *Simon et al.* [2012]. This homogeneous facies is made up of nearly 100% of clay and silt, clay amounts to 40-60% and silt is mostly fine silt from 2–8 μm (Figure 3), with very low carbonate contents (XRD <10%, low Ca/Fe, Figure 5) and Ti-rich sediments (Figure 6). Environmental magnetism proxies also correspond to very fine grain size material, i.e., very high k_{ARM}/k_{LF}, SIRM/k_{LF}, Mrs/Ms and low Hcr/Hc values (Figures 3 and 5), within a magnetite mixing line in the fine PSD to single-domain (SD) (Figure 4a). The FORC diagrams (FORC#4 and 5, Figure 4b) illustrate SD to small PSD grains (i.e., higher coercivities and reduced interactions). Therefore, these results of very fine grains (magnetic and bulk) impart a specific signature to the LGM layer most probably due to mechanical grinding of rocks (i.e., glacial flour) by extended ice streams developed over Greenland (e.g., Disko Bugt, Uummannaq), and/or eastern Baffin Island shelves. Smectite percents are much higher within this interval comparatively to the rest of the core (Figure 6), which would advocate for a Greenland provenance (i.e., from the Tertiary basalts) [cf. *Satte*, 2010; *Andrews and Eberl*, 2011].

4.1.4. The last deglaciation unit

The 20 to 112 cm interval (10.6–16 ka BP) is largely dominated by carbonate coarse sediments, i.e., gravel percents oscillate between 5% and 20% and large amount of dropstones (Figures 2 and 5). Two sharp peaks of grain size >63 μm and high Hcr/Hc (Figure 5) associated with lows of magnetic grain size proxies (i.e.,

k_{ARM}/k_{LF}, SIRM/k_{LF}, Mrs/Ms, MDF_{NRM} and IRM/SIRM, Figure 3) are dated to the beginning of the Bølling-Allerød and the Youger-Dryas period, respectively. The Day plot and FORC diagrams (FORC#2 and 3, Figure 4b) also illustrate coarse magnetic MD grains characterized by smaller coercivities and higher interactions within the magnetic assemblage. These layers are characterized by very high sedimentation rates, from 10 to 50 cm/kyr (Figures 2 and 5).

4.1.5. The Holocene sediments

The Holocene period (10.6–0 ka BP, Figure 2) is characterized by a brown to dark brown silty-mud (almost 80% silt, Figure 2 and 3), highlighted by increasing a* values (red, Figure 5), relatively high carbonate percentages (~30%), without evidence of biogenic calcite (mostly due to calcite dissolution) [*Azetsu-Scott et al.*, 2010] as well as very low sedimentation rates (<2 cm/kyr). These low SAR values (<2 cm/kyr) are in agreement with previously reported similar data for Baffin Bay Holocene sediments [*Andrews and Eberl*, 2011]. High values of magnetic grain-size parameters such as k_{ARM}/k_{LF}, SIRM/k_{LF} are related to smaller magnetic grain size (Figures 3 and 5), a feature confirmed by the Day plot and FORC diagram (FORC#1, Figure 4b).

4.2. Principal Component Analysis (PCA)

Principal component analysis (PCA) was used to synthesize the large and miscellaneous set of proxies into a few principal components that retain the main features of sedimentological variability [*Davis*, 2002]. The first two principal components account for 51.08% (PC1, 37.15%, and PC2, 13.93%) of the total variance (Figure 7). PC1 has positive loadings with coarse grain-size proxies and with detrital carbonate proxies. Negative loadings correspond with finer sediment such as clay, very fine silt (interpreted as glacial flour, 0–4 μm) and magnetic grain-size proxies. The PC1 variability highlights the sediment transportation and source processes. Positive values are related to coarse-detrital carbonate layers being transported by sea ice/iceberg and meltwater from northern (axial) sources, while negative values are associated to finer sediment originating mostly from lateral sources (i.e., Greenland and/or Baffin Island margins).

5. Discussion

In this section, we will examine deeper the succession of glacial events and their sedimentological imprint in the deep Baffin Bay. Some attention will also be paid to linkages between this relatively well-dated record, with existing times series such as the North Atlantic Heinrich events, the Dansgaard-Oeschger cycles and relevant information about relative sea level (RSL) changes, which could have had some influence on the stability of ice shelves and ice streams.

5.1. The last glacial cycle

Sedimentological evidences of pre-LGM ice-advances have been recognized and discussed primarily based on (1) sedimentation accumulation rate (SAR) increases and (2) lithofacies changes. SAR directly relates to (1) the dynamics of ice sheets (i.e., their advance and retreat, and melting pattern), (2) calving and melting of icebergs, and (3) large meltwater pulses contributing to increase the clay charge [*Sarnthein et al.*, 2003]. Large sporadic increases of SAR up to 15–20 cm/kyr occurred during the last glacial cycle. SAR increased up to 50 cm/kyr at the end of the deglaciation (Figure 5), while it was extremely low (<2 cm/kyr) during the Holocene. This variability clearly illustrates the climatic and/or glaciological control on sedimentation pattern in the bay during the last glacial cycle. Steady supplies (see the Ti-cumulative on Figure 2) of sediments from the Greenland margin and the Baffin Island fjords are notably characterized by Ti-rich sediments, high illite percentages, low K/Ti ratio, small grain size range (bulk and magnetic grain size) defined as “glacial flour” (Figures 3, 6 and 7) and low SAR values (Figure 5). On the other hand, high percentages of carbonates and coarse materials (bulk and magnetic) together with high chlorite percentages, higher densities (Figures 2, 4 and 5) and fairly higher SAR are associated with intensive calving from northern ice streams (see section 4 above, for a comprehensive lithofacies description).

5.1.1. The MIS5d-a interval

At the base of the core, from 115–105 ka BP (late MIS5d), relatively important carbonate (15–30%) and low coarse sediment percentages, together with enhanced glacial flour, provide evidence for the establishment and advance of ice streams in the Innuitian margin and the Greenland and/or Baffin Island shelves (BBDC-9a and 9b, Figures 3, 5 and 6, Table 1). The long BBDC-9b interval (>5 ka) is thought to record an increasing sedimentary flux from ice streams of the newly formed Innuitian Ice Sheet, whose inception occurred during the early MIS5d stage [*Ganopolski et al.*, 2010]. We assign it to an increased calving period coeval to the Greenland Interstadial (IS hereinafter) 25, which is associated with a "rebound-type feature" (i.e., warming interval) [*Capron et al.*, 2010] in response to the slow cooling that followed MIS5e [*Capron et al.*, 2012]. The BBDC-9a layer had a depositional duration of about 1 ka, and thus indicates a limited/minor calving episode (as shown by lower PC1 values, Figure 5) associated with IS 24. During MIS5c (105–92 ka BP), two distinct BBDC layers (8b and 8c) with depositional durations of about 1.5 ka each (Table 1) are assigned to calving episodes during the warmer IS 23, associated with high summer insolation values (Figure 5). The long interval of BBDC-8a (~3.5 ka) is assigned to an important development of northern fast-flowing ice streams during the stadial stage of DO 23 (i.e., the cold interval following warmer IS, which forms DO cycle) [*Wolff et al.*, 2010] coeval with low summer insolation values (Figure 5), and delivering large amounts of icebergs into the bay. During MIS5b (92–84 ka BP), LDC facies sediments (Figures 3 and 6) together with the absence of BBDC layers would favor a fairly constant and large glacial expansion corresponding to a major relative sea level (RSL) drop (~50-60 meters) [*Waelbroeck et al.*, 2002; Cutler et al., 2003] (Figure 8). Such low RSL would favor the large advance of lateral ice streams over shallow continental shelves of Baffin Island and Greenland, contributing to increase the LDC facies sediment deposition in Baffin Bay (increased Ti-rich sediments, Figure 6). During MIS5a (84–72 ka BP), two large BBDC depositional intervals (i.e., 7a=6.5 ka and 7b=4 ka, Table 1) are interpreted as an evidence for some intense and nearly continuous calving stages of the northern Baffin Bay ice streams. They are assigned to the long-duration IS 21, also characterized by high summer insolation values and a RSL rise (Figures 5 and 8). The BBDC-7b layer seems coeval to the onset of IS 21, while the dawn of BBDC-7a layer deposition might have been concomitant with the abrupt warming event described as a "rebound-type feature" by *Capron et al.* [2010] during the cooling phase of IS 21. BBDC-7a then continued over IS 20. To sum up, the MIS5d-a glaciomarine sedimentation regimes in Baffin Bay suggest a high variability of the ice sheets during an overall ice-spreading interval. This variability was due to (1) internal forcing parameters of newly formed ice sheets and glaciers over land and continental shelves, and (2) external forcing parameters such as relative sea level change, higher magnitude precessional cycles and the stronger eccentricities of MIS5 allowing large seasonal insolation fluctuations that would have easily destabilized the smaller MIS5 ice sheets (e.g., BBDC-8c, 8b and 7b during maximum summer insolation values) [*Timmermann et al.*, 2010; *Bintanja et al.*, 2005]. Moreover, as proposed by *Marshall and Clark* [2002], a large fraction of the northeastern LIS and IIS would have been frozen-based, a feature which might have prevented full melting of these small ice sheets during IS, even though these IS summer insolation values were similar to those of the last glacial termination.

5.1.2. MIS4

From ~72 ka BP, and during the early MIS4, the western Greenland and eastern Baffin Island ice streams most likely experienced a massive advance period with increasing glacial flour sediment supplies and decreasing SAR values (following an initial increase, probably due to increased clay load when the ice margins moved over the shallow continental shelves, Figure 5). Unfortunately, 11 cm of sediments corresponding to the 69.2-65.5 ka BP interval were lost on-board (a slice of clayey mud sediments detached after the cutting of the piston core liner), thereby preventing a precise interpretation of the glacial advance within this interval. Nonetheless, the hypothesis of an ice advance over the western Greenland and/or Baffin Island shelves at that time would be in accordance with (1) a lowering RSL (Figure 8, Cutler et al., 2003); (2) very low July insolation values (Figure 5). Some evidence for an ice advance beyond the southwestern Greenland shelf edge has also been reported during MIS4 by *Seidenkrantz et al.* [2010]. The late MIS4 interval includes a BBDC layer that was deposited over a long period (BBDC-6, ~60 cm, 6 ka, Figure 5, Table 1), possibly due to some instability of the newly formed wet-based ice streams in Jones Sound, Lancaster Sound and Nares Strait. BBDC-6 is assigned to the onset of IS 18, marked by increasing summer insolation values, a RSL rise (from about -85 to -50 m, Figure 8) and possibly by the advection of warm Atlantic Waters in the bay [*Seidenkrantz et al.*, 2010; *Andrews et al.,* 1998; *Hiscott et al.*, 1989] (which would be accompanied by a retreat of Greenland ice margin). This instability of the northeastern LIS and IIS was probably linked to a major Laurentide purge during Heinrich event 6 as they appear coeval. According to *Hulbe et al.* [2004], a catastrophic breakup of an ice shelf in northwestern Baffin Bay (i.e., Boothia ice stream) may have contributed to the release of large amounts of IRD, rather than a more progressive retreat along the ice streams. However, as the northeastern LIS and IIS surges continued after the end of Heinrich event 6, a progressive retreat of their ice margin was more likely (see section 5.3).

5.1.3. MIS3

During MIS3, ice margin readvanced steadily until ~41 ka BP. This glacial advance released fine hemipelagic sediments (i.e., LDC facies), with a decreasing SAR and high magnetic susceptibilities (Figures 3, 5 and 6). It was interrupted by short intervals at ~47, ~50 ka BP (BBDC-5, 10 cm, 1.5 ka, Figure 5), ~52 and ~55 ka BP, marked by coarser sediment supplies. The short BBDC-5 event and IS 13 seem coeval. IS 13 succeeded the long cooling period following IS 14. This cooling period witnessed sporadic advection of warmer Atlantic Waters along the western Greenland margin possibly triggering the brief IRD episodes (i.e., 52 and 55 ka BP). The warming of IS 13 probably triggered a larger-scale calving episode from the fully-developed northern ice streams. Similarly to BBDC-9b and 7a, the BBDC-5 could be associated with a "rebound-type feature", which occurred after the long cooling phase subsequent to IS14 (Figure 5). The coarser sediment pulse at ~47 ka BP and IS 12 are thought to be coeval. Contrasting with the BBDC intervals, the absence of carbonates associated with this sediment coarsening event suggests an eastern Baffin Island or a western Greenland origin. Between ~41 and ~32 ka BP, increases in carbonates and coarse grain contents with higher SAR values (Figure 5) are interpreted as a response to higher dynamic from the northeastern LIS and southern IIS ice streams. Higher values of a* and of the Si/Sr ratio (Figure 5) suggest an increased delivery of Proterozoic siliclastic minerals, originating from northern Greenland, Ellesmere Island, and northern Baffin Island [*Hiscott et al.*, 1989]. The massive BBDC-4 layer (~55 cm, 5 ka) dating from the 37–32 ka BP interval, was probably associated with some purge along the northeastern LIS and southern IIS margins, during Heinrich event 4 (at around 38 ka BP). It is not clear however why such a retreat would have happened during a RSL lowering stage (from -60 to -80 m, Figure 8). Still, the high-frequency occurrence of 4 DO events during this interval suggest some external forcing mechanisms promoting higher instability of the northern ice stream. Peaks of Si/Sr, Fe/Ti and Ca/Fe ratios (Figures 5 and 6) match distinct IS during this critical period. They are consistent with the assumption that the BBDC-4 layer was deposited in several pulses rather than through a continuous regime. Moreover, a gravelly layer dated at ~32.5 ka BP (gravel >80%, and MD magnetic grains, Figures 2, 4 and 5) might be assigned to IS 5, and linked to some IRD, and possibly to a turbidity current related to massive calving and melting of Innuitian and/or eastern Baffin Island ice streams during the late MIS3.

5.1.4. An extended LGM

Subsequent to the intense MIS3 calving period, regional ice stream readvances occurred, as far as the late Winsconsinan (LGM) limits of the northeastern LIS and IIS, between 32 ka BP and ~19–24 ka BP [*Dyke et al.*, 2002; *England et al.*, 2006]. This ice advance probably continued on the Greenland margin side until ~21 ka BP [*Funder et al.*, 2011] and possibly until ~16 ka BP [*Ó Cofaigh et al.*, 2012]. In our interpretation and timing of the circum-Baffin Bay ice sheet development, the build-up of shelf-based ice around western Greenland would have initiated slightly before ~30 ka BP. This chronology is consistent with IRD records in the Arctic Ocean [*Larsen et al.*, 2010; *Funder et al.*, 2011], with ice expansion to the edge of the continental shelf off Scoresby Sund (East Greenland) from ~31–19 ka BP [*Andrews et al.*, 1997], and with a RSL drop from -80 to -120 m during the interval (Figure 8) [*Waelbrock et al.*, 2002]. Within this glacial growth period, two short BBDC (2 and 3) layers are present and dated at ~25 and ~27.7 ka BP (Table 1). They suggest brief calving episodes (with durations of 0.3 and 1.3 ka respectively, Figure 5). According to *Funder et al.* [2011], sea ice along the Baffin Bay coast was in sufficient motion during the LGM to allow the dispersal of calving ice from ice streams. This would explain the presence of the BBDC-2 and 3 layers within a homogeneous glacial flour sediment unit. Moreover, a gravelly-sandy layer dated at ~21.5 ka BP (Figures 2 and 5) indicates some turbidity currents from ice-proximal settings, associated with the production of large volumes of sediment-laden meltwater plumes from subglacial outlets [*Ó Cofaigh and Dowdeswell*, 2001; *Syvitski*, 1991; *Hesse et al.*, 1997, 2004]. This probably marked the maximum extent of the Greenland and/or Baffin Island ice-margins over their respective shelf edges. During this last glacial extended stadial interval, SAR shows three major steps (Figure 5): (1) Low SAR values (~5 cm/kyr) from ~32 to ~27 ka BP illustrate the early, relatively steady ice margin expansion (Figure 5). (2) Higher SAR values (~15 cm/kyr) immediately following the first coarse carbonate layer, marked the ~27 to ~21 ka BP interval; they correspond to the main glacial advance and thickening of ice streams on continental shelves. Increased clay loads (Figure 3), due to the formation of sea ice and related dense brines [*Levitan and Stein*, 2008], and a rapid RSL drop (Figure 8) constitute complementary features of the interval. (3) Extremely low SAR values follow (<2 cm/kyr) between ~21 and ~16 ka BP. They match (i) minimum RSL values (~-120 m), (ii) maximum ice limits on the Greenland continental shelf [*Ó Cofaigh et al.*, 2012], and (iii) a fully glaciated bay. Unfortunately the sediments from 17 to 19 ka BP (112–120 cm) were lost onboard, preventing any further interpretation of the late LGM. However, a low SAR is still calculated above the sedimentary gap and the lost sediment rough description (i.e., olive-black clayey-mud), suggest that such intense glacial conditions might have prevailed possibly until ~16 ka BP. The OC lithofacies of this extended LGM unit implies a Greenland ice stream advance over to the shelf edge, i.e., near the core study site.

5.1.5. The last deglaciation

Deglaciation started at ~16 ka BP and continued until ~10.6 ka BP with large SAR increases, coarser grain size, high carbonate percentages and significant amounts of dropstones (Figures 2, 4 and 5). They indicate major retreat of the northeastern LIS, southern IIS and western GIS. Deglaciation was achieved more effectively though calving rather than melting, which provided large amounts of IRD within the bay (Figures 2 and 5) [*Ó Cofaigh et al.*, 2012; *Hogan et al.*, 2012]. This timing of the ice retreat in the circum-Baffin Bay is consistent with previous regional studies [*Darby et al.*, 2002; *England et al.*, 2006; *Jennings et al.*, 2011; *Funder et al.*, 2011; *Larsen et al.*, 2010]. Within this deglacial period, two BBDC layers (BBDC -1 and -0) have been recognized and dated at 15-13.7 and 12-10.5 ka BP, respectively (Table 1). These BBDC intervals are concomitant with the Bølling-Allerød (IS 1) and the pre-Boreal periods, respectively. The final stage of the IIS deglaciation (i.e., BBDC-0) matches the highest July insolation values for the site latitude. It is marked by maximum SAR values (up to 50 cm/kyr, Figure 5), and seems to be also recorded in the Arctic Ocean by a peak of Innuitian IRD at ~10 ka BP [*Darby et al.*, 2002].

5.2. The Holocene

Increasing a* values (red) and Mn/Ti ratio (Figure 5) in post-glacial sediments indicate changes in redox conditions of deep Baffin Bay sediments [*Croudace et al.*, 2006]. Such redox changes are also highlighted by higher Mn-inputs and likely relate to relatively enhanced organic carbon fluxes under the low sedimentation rate of the interval. Similar features have been recognized in sediments of the Arctic Ocean during warm climatic intervals [*Polyak and Jakobsson*, 2011; *März et al.*, 2011]. These interglacial-type sedimentary features are not seen below in the core (Figure 5). This confirms the absence of the last interglacial period (i.e., MIS5e) in the cored sequence. Small peaks of coarse grain during the Holocene correspond mainly to IRD from Greenland tidewater glaciers (Figures 1 and 5) and to a lesser extent from Canadian Arctic glaciers [*Marshall and Koutnik*, 2006].

5.3. The BBDC vs. Heinrich events

In earlier studies, the BBDC layers were associated with rapid retreat phases of northern Baffin Bay ice streams (see section 2.5). However, the long depositional duration of some of these BBDC layers in PC16 (i.e., BBDC-7a, -7b, -8a and -9b, Table 1) as well as in other cores [see *Andrews et al.*, 1998] is difficult to explain by an abrupt and massive ice-surge scenario (or the breakup of an ice shelf). Based on the new chronological frame [*Simon et al.*, 2012], we tentatively assign these long depositional-duration BBDC layers to intervals of very active fast-flowing ice stream systems in the source area, during glacial intervals [see *Dowdeswell and Elverhøi*, 2002], whereas the BBDC-4 and -6 are better explained by sequential retreats of well-developed northern ice streams. Such layers are thus less an indication of a "H-event type" process (i.e., internal ice dynamical instability) [*Hemming*, 2004], than that of some climatically-controlled pervasive ice dynamics processes. The shorter depositional-duration BBDC layers (-0, -1, -2, -3, -5, -8b, -8c and -9a, Table 1) show some similarity with Heinrich events from a duration perspective. This raises the question of a potential connection between the triggering of the short depositional-duration BBDC layers and that of the Heinrich layers. According to the above data and interpretations, intensive iceberg calving events in Baffin Bay were not in phase with Heinrich events, but rather matched warm interstadial periods (Figures 5 and 8). Nonetheless, BBDC are not unequivocally related to major interstadials, as assumed by *Andrews et al.* [1998], but more likely to specific interstadials that followed relatively long periods of ice growth (i.e., IS -1, -8, -13, -18, -21, -23). In this scenario, warming periods associated with (1) maximum temperatures in Greenland ice cores (Figures 3, 5, 6 and 8) and (2) the large advection of Atlantic Waters in the bay, related to an enhancement of the AMOC [as proposed by *Hiscott et al.*, 1989 and *Andrews et al.*, 1998], would have favored the destabilization of the large northern Baffin Bay ice streams, leading to extensive IRD. These results demonstrate that ice margins in the Baffin Bay area were affected by Dansgaard-Oeschger cycles, which was not anticipated based on simulations from *Marshall and Koutnik* [2006]. This shortcoming could be explained by underestimations of (1) the sensitivity of regional ice streams and outlet fjords by the models [*Marshall and Koutnik*, 2006], (2) regional ice volumes [*Ganopolski et al.*, 2010], (3) the ice margin extents [*Li et al.*, 2011] and (4) the sporadic advection of warm Atlantic Waters into the bay during the last glacial cycle [*Srivastava et al.*, 1987; *Hiscott et al.*, 1989].

From a broader point of view, the time lags between the BBDC deposition, LIS instabilities in the Hudson Strait area leading to major North Atlantic H-events, and non-Laurentide components (i.e., Icelandic, European sources) of detrital layers in the North Atlantic [*Bond and Lotti*, 1995; *Bond et al.*, 1999; *Grousset et al.*, 2000] would validate a scenario with at least partly independent pan-Atlantic ice sheet discharges, during the last glacial cycle (see Figure 8). Still, this assumption remains questionable due to (1) age model uncertainties, (2) the DC- fingerprinting issues raised by *Farmer* *et al.* [2003] and (3) distinct sedimentary processes that create a time delay between proximal and distal records [see *Rashid et al.*, 2012].

6. Conclusions

We presented sedimentological evidences for Greenland and/or Baffin Island ice stream advances characterized by hemipelagic glacial flour, interbedded with IRD layers (i.e., BBDC) linked to calving of ice streams along the northeastern Laurentide and southern Innuitian ice sheet margins during the last glacial cycle. Regional ice sheets started to advance immediately following MIS5e and experienced several growth phases during cooling intervals, especially during MIS4 (from ~72–64 ka BP) and MIS2 (from ~32–16 ka BP). Based on an improved chronological framework [*Simon et al.*, 2012], we demonstrate that intensive iceberg calving periods and Heinrich Stadials are not coeval and that calving in Baffin Bay mostly occurred during interstadial warming intervals. We documented the fact that Baffin Bay Detrital Carbonate (BBDC) layers result from two distinct processes: (1) pervasive and continuous iceberg delivery during periods of fast-flowing ice streams and/or gradual retreats (long depositional-duration BBDC layers), and (2) abrupt calving periods associated with interstadial warming (short depositional-duration BBDC layers). This shows that Heinrich and BBDC events responded to distinct glaciological processes. Our data also suggest that the last glacial northeastern Laurentide, southern Innuitian, and western Greenland ice sheets, were sensitive to high frequency climate reorganization such as the Dansgaard-Oeschger cycles. Questions remain concerning the precise location of lateral sediment provenance.

Acknowledgements

We thank Jacques Labrie (ISMER) for his technical support during paleomagnetic measurements, Pierre Francus (INRS) and Arnaud de Coninck (INRS) for their help forthe ITRAX™ core scanning, Michel Preda (UQAM) for assistance with XRD measurements and Joseph Ortiz (Kent State University) for diffuse spectral measurements. We are in debt to Sandrine Solignac for review and constructive comments that significantly improved this manuscript. This study is part of the Canadian contribution to the Past4Future project. Support from MDEIE (Ministère du Développement Economique, de l'Innovation et de l'Exportation), NSERC (Natural Sciences and Engineering Research Council of Canada), FQRNT (Fonds Québécois de la Recherche sur la Nature et les Technologies) and the CFI (Canadian Foundation for Innovation) is acknowledged.

References

Aksu, A. E. (1981), Late Quaternary stratigraphy, paleoenvironmentology, and sedimentation history of Baffin Bay and Davis Strait, Ph.D. Thesis, Dalhousie University, Halifax, NS.

Aksu, A. E. (1983), Holocene and Pleistocene dissolution cycles in deep-sea cores of Baffin Bay and Davis Strait: paleoceanographic implications, *Marine Geology* 53, 331-348.

Aksu, A. E. (1985), Climatic and oceanographic changes over the past 400,000 years: evidence from deep sea cores on Baffin Bay and Davis Strait, in *Quaternary environments: Eastern Canadian Arctic, Baffin Bay and western Greenland*, edited by J. T. Andrews, Allen & Unwin, Boston, 181-209.

Aksu, A. E., and D. J. W. Piper (1987), Late Quaternary sedimentation in Baffin Bay, *Canadian Journal of Earth Sciences* 24, 1833-1846.

Alley, R. B., J. T. Andrews, J. Brigham-Grette, G. K. C. Clarke, K. M. Cuffey, J. J. Fitzpatrick, S. Funder, S. J. Marshall, G. H. Miller, J. X. Mitrovica, D. R. Muhs, B. L. Otto-Bliesner, L. Polyak, and J. W. C. White (2010), History of the Greenland Ice Sheet: paleoclimatic insights, *Quaternary Science Reviews* 29, 1728-1756, doi: 10.1016/j.quascirev.2010.02.007.

Andrews, J. T., A. E. Aksu, M. Kelly, R. Klassen, G. H. Miller, W. N. Mode, and P. Mudie (1985), Land/ocean correlations during the last interglacial/glacial transition, Baffin Bay, northwestern North Atlantic: A review, *Quaternary Science Reviews* 4(4), 333-355.

Andrews, J. T., K. Tedesco, W. M. Briggs, and L. W. Evans (1994), Sediments, sedimentation rates, and environments, southeast Baffin Shelf and northwest Labrador Sea, 8 – 26 ka, *Canadian Journal of Earth Sciences* 31, 90–103.

Andrews, J. T., M. Kirby, A. E. Aksu, D. G. Barber, and D. Meese, (1998), Late Quaternary Detrital Carbonate (DC-) layers in Baffin Bay marine sediments (67°-74° N): correlation with Heinrich events in the North Atlantic? *Quaternary Science Reviews* 17, 1125-1137.

Andrews, J. T. (2000), Icebergs and iceberg rafted detritus (IRD) in the North Atlantic: facts and assumptions, *Oceanography* 13(3),100-108.

Andrews, J. T. (2009), Wisconsinan (Weichselian, Würm) glaciation, in *Encyclopedia of Paleoclimatology and Ancient Environments Part 22*, edited by V. Gornitz, Springer, Dordrecht, The Netherlands, 986–992, doi:10.1007/978-1-4020-4411-3_229.

Andrews, J. T. and D. D. Eberl (2011), Surface (sea floor) and near-surface (box cores) sediment mineralogy in Baffin Bay as a key to sediment provenance and ice sheet variations. *Canadian Journal of Earth Sciences* 48, 1307-1328, doi:10.1139/e11-021.

Azetsu-Scott, K., A. Clarke, and K. Falkner (2010), Calcium carbonate saturation states in the waters of the Canadian Arctic Archipelago and the Labrador Sea, *Journal of Geophysical Research* 115, C11021, doi:10.1029/2009JC005917.

Blott, S. J., K. Pye (2001), GRADISTAT: a grain size distribution and statistics package for the analysis of unconsolidated sediments, *Earth Surface Processes and Landforms* 26, 1237-1248.

Bigg, G. R. (1999), An estimate of the flux of iceberg calving from Greenland, *Arctic, Antarctic, and Alpine Research* 31(2), 174– 178, doi:10.2307/1552605.

Bigg, G. R., and M. R. Wadley (2001), The origin and flux of icebergs released into the Last Glacial Maximum Northern Hemisphere oceans: the impact of ice-sheet topography, *Journal of Quaternary Science* 16(6), 565-573, doi:10.1002/jqs.628.

Bintanja, R., R. S. W. van de Wal, and J. Oerlemans (2005), Modelled atmospheric temperatures and global sea levels over the past million years, *Nature* 437, 125–128.

Biscaye, P. E. (1965), Mineralogy and sedimentation of recent deep-sea clay in the Atlantic Ocean and adjacent seas and oceans, *Geological Society of America Bulletin* 76, 803-832.

Bond, G. C., and R. Lotti (1995), Iceberg Discharges into the North Atlantic on Millennial Time Scales During the Last Glaciation, *Science* 267(5200), 1005-1010, doi:10.1126/science.267.5200.1005.

Bond, G. C., W. Showers, M. Elliot, M. Evans, R. Lotti, I. Hajdas, G. Bonani, and S. Johnson (1999), The North Atlantic's 1–2 kyr climate rhythm: relation to Heinrich Events, Dansgaard/Oeschger cycle and the Little Ice Age, in *Mechanisms of Global Climate Change at Millennial Time Scales,* edited by P. Clark, R. Webb, and L. Keigwin, Geophysical Monograph Series 112, American Geophysical Union, Washington, DC, 35–58.

Briner, J. P., G. H. Miller, P. T. Davis, P. Bierman, and M. Caffee (2003), Last Glacial Maximum ice sheet dynamics in Arctic Canada inferred from young erratics perched on ancient tors, *Quaternary Science Reviews* 22, 437-444.

Briner, J. P., G. H. Miller, P. T. Davis, and R. Finkel (2006), Cosmogenic radionuclides from fiord landscapes support differential erosion by overriding ice sheets, *Geological Society of America Bulletin* 118, 406-420.

Campbell, D. C., and A. de Vernal (2009), CCGS Hudson Expedition 2008029: Marine geology and paleoceanography of Baffin Bay and adjacent areas, Nain, NL to Halifax, NS, August 28- September 23; *Geological Survey of Canada*, Open File 5989, 1 DVD.

Capron, E., A. Landais, J. Chappellaz, A. Schilt, D. Buiron, D. Dahl-Jensen, S. J. Johnsen, J. Jouzel, B. Lemieux-Dudon, L. Loulergue, M. Leuenberger, V. Masson-Delmotte, H. Meyer, H. Oerter, and B. Stenni (2010), Millennial and sub-millennial scale climatic variations recorded in polar ice cores over the last glacial period, *Climate of the Past* 6, 345-365, doi:10.5194/cp-6-345-2010.

Capron, E., A. Landais, J. Chappellaz, D. Buiron, H. Fischer, S.J. Johnsen, J. Jouzel, M. Leuenberger, V. Masson-Delmotte, and T. F. Stocker (2012), A global picture of the first abrupt climatic event occurring during the last glacial inception, *Geophysical Research Letters* 39, L15703, doi:10.1029/2012GL052656.

Channell, J. E. T., D. A. Hodell, O. Romero, C. Hillaire-Marcel, A. de Vernal, J. S. Stoner, A. Mazaud, and U. Röhl (2012), A 750-kyr detrital-layer stratigraphy for the North Atlantic (IODP Sites U1302–U1303, Orphan Knoll, Labrador Sea), *Earth and Planetary Science Letters* 317-318, 218–230, doi:10.1016/j.epsl.2011.11.029.

Cook, H. E., P. D. Johnson, J. C. Matti, and I. Zemmels (1975), Methods of sample preparation and X-ray diffraction data analysis, X-ray mineralogy Laboratory, *Deep See Drilling Project Deep Sea Drilling Project Inital Reports* 28, 999-1007.

Croudace, I., A. Rindby, and R. Rothwell (2006), ITRAX: description and evaluation of a new multi-function X-ray core scanner, *New techniques in sediment core analysis* 267, 51–63.

Cutler, K.B., R.L. Edwards, F.W. Taylor, H. Cheng, J. Adkins, C.D. Gallup, P.M. Culter, G.S. Burr, A.L. Bloom (2003), Rapid sea-level fall and deep-ocean temperature change since the last interglacial period, *Earth and Planetary Science Letters* 206, 253-271, doi:10.1016/S0012-821X(02)01107-X.

Darby, D. A., J. Bischof, R. Spielhagen, S. Marshall, and S. Herman (2002), Arctic ice export events and their potential impact on global climate during the late Pleistocene, P*aleoceanography* 17, 15.1–15.17.

Davis, J. C. (2002), Statistics and Data Analysis in Geology, 3rd Edition, John Wiley and Sons, New York, 656 pp.

de Vernal, A., G. Bilodeau, C. Hillaire-Marcel, and N. Kassou (1992), Quantitative assessment of carbonate dissolution in marine sediments from foraminifer linings vs. shell ratios: Davis Strait, northwest North Atlantic, *Geology* 20, 527-530.

Dowdeswell, J. A., and A. Elverhøi (2002), The timing of initiation of fast-flowing ice streams during a glacial cycle inferred from glacimarine sedimentation, *Marine Geology* 188, 3–14.

Dunlop, D. (2002), Theory and application of the Day plot (Mrs/Ms versus Hcr/Hc) 1. Theoretical curves and tests using titanomagnetite data, *Journal of Geophysical Research* 107 (B3), 2056, doi:10.1029/2001JB000486.

Dyke, A. S., J. T. Andrews, P. U. Clark, J. H. England, G. H. Miller, J. Shaw, and J. J. Veillette, (2002), The Laurentide and Innuitian Ice Sheets during the Last Glacial Maximum, *Quaternary Science Reviews* 21, 9–31.

Dyke, A. S. (2004), An outline of North American deglaciation with emphasis on central and northern Canada, *Developments in Quaternary Science* 2, 373-424.

England, J. H., N. Atkinson, J. Bednarski, A. S. Dyke, D. A. Hodgson, and C. Ó Cofaigh (2006), The Innuitian Ice Sheet: configuration, dynamics and chronology, *Quaternary Science Reviews* 25, 689-703.

England, J. H., M. F. A. Furze, and J. P. Doupé (2009), Revision of the NW Laurentide Ice Sheet: implications for paleoclimate, the northeast extremity of Beringia, and Arctic Ocean sedimentation, *Quaternary Science Reviews* 28 (17-18), 1573–1596, doi:10.1016/j.quascirev.2009.04.006.

Farmer, G., D. G. Barber, and J. T. Andrews (2003), Provenance of Late Quaternary ice-proximal sediments in the North Atlantic: Nd, Sr and Pb isotopic evidence, *Earth and Planetary Science Letters* 209, 227-243.

Funder, S., K. K. Kjeldsen, K. H. Kjær, and C. Ó Cofaigh (2011), The Greenland Ice Sheet During the Past 300,000 Years: A Review, in: *Developments in Quaternary Sciences*, *Quaternary Glaciations, Extent and Chronology*, Part IV, A Closer Look, vol. 15, edited by J. Ehlers, P. L. Gibbard and P. D. Hughes, Elsevier, Amsterdam, The Netherlands, 699-713, 10.1016/B978-0-444-53447-7.00050-7.

Francus, P., H. Kamb, T. Nakagawa, M. Marshall, E Brown, and Suigetsu 2006 Project members (2009), The potential of high-resolution X-ray fluorescence core scanning: applications in paleolimnology, *PAGES News* 17, 93–96.

Ganopolski, A., R. Calov, and M. Clausen (2010), Simulation of the last glacial cycle with a coupled climate ice-sheet model of intermediate complexity, *Climate of the Past* 6, 229-244.

Grousset, F. E., C. Pujol, L. Labeyrie, G. Auffret, and A. Boelaert (2000), Were the North Atlantic Heinrich events triggered by the behavior of the European ice sheets? *Geology* 28, 123–126.

Harrison, R. J., and J. M. Feinberg (2008), FORCinel: An improved algorithm for calculating first-order reversal curve distributions using locally weighted regression smoothing, *Geochemistry Geophysics Geosystems* 9, Q05016, doi:10.1029/2008GC001987.

Harrison, J. C., M. R. St-Onge, O. Petrov, S. I. Strelnikov, B. G. Lopatin, F. H. Wilson, S. Tella, D. Paul, T. Lynds, S. P. Shokalsky, C. K. Hults, S. Bergman, H. F. Jepsen, and A. Solli (2011), Geological map of the Arctic, *Geological Survey of Canada*, Map 2159A, scale 1:5000000.

Hemming, S. R. (2004), Heinrich events: Massive late Pleistocene detritus layers of the North Atlantic and their global climate imprint, *Reviews of Geophysics* 42(1), RG1005, doi:10.1029/2003RG000128.

Hesse, R., S. Khodabakhsh, I. Klaucke, and W. B. F. Ryan (1997), Asymmetrical turbid surface-plume deposition near ice-outlets of the Pleistocene Laurentide ice sheet in the Labrador Sea, *Geo-Marine Letters* 17, 179-187.

Hesse, R., H. Rashid, and S. Khobabakhsh (2004), Fine-grained sediment lofting from meltwater-generated turbidity currents during Heinrich events, *Geology* 32, 449-452.

Hiscott, R. N., A. E. Aksu, and O. B. Nielsen (1989), Provenance and dispersal patterns, Pliocene-Pleistocene section at site 645, Baffin Bay, in *Proceedings of the Ocean Drilling Program, Scientific Results leg 105*, edited by S. P Srivastava, M. Arthur, and B. Clement, College Station, TX (Ocean Drilling Program), 31-52.

Hiscott, R. N., A. E. Aksu, P. J. Mudie, and D. F. Parsons (2001), A 340,000 year record of ice rafting, palaeoclimatic fluctuations, and shelf-crossing glacial advances in the southwestern Labrador Sea, *Global and Planetary Change* 28(1–4), 227-240, doi:10.1016/S0921-8181(00)00075-8.

Hodell, D. A., and J. H. Curtis (2008), Oxygen and carbon isotopes of detrital carbonate in North Atlantic Heinrich Events, *Marine Geology* 256(1–4), 30-35, doi:10.1016/j.margeo.2008.09.010.

Hogan, K. A., J. A. Dowdeswell, and C. Ó Cofaigh (2012), Glacimarine sedimentary processes and depositional environments in an embayment fed by West Greenland ice streams, *Marine Geology* 311–314, 1-16, doi:10.1016/j.margeo.2012.04.006.

Hulbe, C. L., D. R. MacAyeal, G. H. Denton, J. Kleman, and T. V. Lowell (2004), Catastrophic ice shelf breakup as the source of Heinrich event icebergs, *Paleoceanography* 19, PA1004, doi:10.1029/2003PA000890.

Jennings, A. E., C. Sheldon, T. M . Cronin, P., Francus, J. S. Stoner, and J. T. Andrews (2011), The Holocene history of Nares Strait: Transition from glacial bay to Arctic-Atlantic throughflow, *Oceanography* 24 (3), 26–41.

Kelly, M. A., and T. V. Lowell (2009), Fluctuations of local glaciers in Greenland during latest Pleistocene and Holocene time, *Quaternary Science Reviews* 28, 2088-2106.

Klassen, R. A., and D. A. Fisher (1988), Basal-flow conditions at the northeastern margin of the Laurentide Ice Sheet, Lancaster Sound, *Canadian Journal of Earth Sciences* 25, 1740-1750.

Kwok, R., L. T. Pedersen, P. Gudmandsen, and S. S. Pang (2010), Large sea ice outflow into the Nares Strait in 2007, *Geophysical Research Letters* 37(3), L03502, doi:10.1029/2009GL041872.

Larsen, N. K., K. H. Kjær, S. Funder, P. Möller, J. J. M. van der Meer, A. Schomacker, H. Linge, and D. A. Darby (2010), Late Quaternary glaciation history of northernmost Greenland – Evidence of shelf-based ice, *Quaternary Science Reviews* 29, 3399-3414.

Laskar, J., P. Robutel, F. Joutel, M. Gastineau, A. C. M. Correia, and B. Levrard (2004), A long term numerical solution for the insolation quantities of the Earth, *Astronomy & Astrophysics* 428, 261-285, doi:10.1051/0004-6361:20041335.

Levitan, M. A., and R. Stein (2008), History of sedimentation rates in the sea-ice sedimentation zone during the last 130 ka, *Lithology and Mineral Ressources* 43(1), 65-75.

Li, G., D. J. W. Piper, and D. C. Campbell (2011), The Quaternary Lancaster Sound trough-mouth fan, NW Baffin Bay, *Journal of Quaternary Science* 26, 511-522.

Lisiecki, L. E., and M. E. Raymo (2005), A Pliocene-Pleistocene stack of 57 globally distributed benthic $\delta^{18}O$ records, *Paleoceanography* 20, PA1003. doi:10.1029/2004PA001071.

MacLean, B. (1985), Geology of the Baffin Island Shelf, in *Quaternary Environments : Eastern Canadian Arctic, Baffin Bay and Western Greenland,* edited by J. T. Andrews, Allent and Unwin, Boston, 154-177.

MacLean, B., G. L. Williams, and S. P. Srivasatava (1990), Geology of the Labrador Shelf, Baffin Bay, and Davis Strait, Part 2, Geology of Baffin Bay and Davis Strait, in *Geology of the continental margin of eastern Canada, Geology of Canada 2,* edited by M. J. Keen, and G. L. Williams, Canadian Government Publishing Center, Ottawa, Ontario, 293–348.

MacLean B., S. Blasco, R. Bennett, J. H. England, W. Rainey, W. Hughes-Clarke, and J. Beaudoin (2010), Ice keel seabed features in marine channels of the central Canadian Arctic Archipelago: evidence for former ice streams and iceberg scouring, *Quaternary Science Reviews* 29, 2280–2301.

Marcott, S. A., P. U. Clark, L. Padman, G. P. Klinkhammer, S. R. Springer, Z. Liu, B. L. Otto-Bliesner, A. E. Carlson, A. Ungerer, J. Padman, F. He, J. Cheng, and A. Schmittner (2011), Ice-shelf collapse from subsurface warming as a trigger for Heinrich events, *Proceedings of the National Academy of Sciences* 108 (33), 13415-13419, doi:10.1073/pnas.1104772108.

Marshall, S. J., and P. U. Clark (2002), Basal temperature evolution of North American ice sheets and implications for the 100-kyr cycle, *Geophysical Research Letters* 29(24), 2214, doi:10.1029/2002GL015192.

Marshall, S. J., and M. R. Koutnik (2006), Ice sheet action versus reaction: Distinguishing between Heinrich events and Dansgaard-Oeschger cycles in the North Atlantic, *Paleoceanography* 21, PA2021, doi:10.1029/2005PA001247.

März, C., A. Stratmann, J. Matthiessen, A. K. Meinhardt, S. Eckert, B. Schnetger, C. Vogt, R. Stein, and H. J. Brumsack (2011), Manganese-rich brown layers in Arctic Ocean sediments: Composition, formation mechanisms, and diagenetic overprint, *Geochimica et Cosmochimica Acta* 75, 7668-7687, doi:10.1016/j.gca.2011.09.046.

Moore, D. and R. C. Reynolds (1997), X-Ray Diffraction and the Identification and Analysis of Clay Minerals, 2nd ed.: Oxford University Press, New York.

Muxworthy, A. R., and A. P. Roberts (2007), First-order reversal curve (FORC) diagrams, in: *Encyclopedia of Geomagnetism and Paleomagnetism*, edited by D. Gubbins and E. Herrero-Bervera, Springer, 266-272.

Ó Cofaigh, C., and J. A. Dowdeswell (2001), Laminated sediments in glacimarine environments: diagnostic criteria for their interpretation, *Quaternary Science Reviews* 20, 1411-1436.

Ó Cofaigh, C., J. A. Dowdeswell, A. A. Kilfeather, K. Hogan, A. E. Jennings, D. McCarthy, J. M. Lloyd, and JR175 Shipboard scientific party (2010), West Greenalnd Ice Streams on the continental shelf of Baffin Bay during the Last Glacial Cycle: geomorphology, flow trajectories and chronology, presented at 40st Arctic Workshop, Winter Park, Colorado.

Ó Cofaigh, C., J. T. Andrews, A. E. Jennings, J. A. Dowdeswell, K. Hogan, A. A. Kilfeather, and C. Sheldon (2012), Glacimarine lithofacies, provenance and depositionnal processes on a West Greenland trough-mouth fan, *Journal of Quaternary Science*, doi:10.1002/jqs.2569.

Parnell, J., S. Bowden, J. T. Andrews, and C. Taylor (2007), Biomarker determination as a provenance tool for detrital carbonate events (Heinrich events?): Fingerprinting Quaternary glacial sources into Baffin Bay, *Earth and Planetary Science Letters* 257, 71-82.

Pike, C. R., A. P. Roberts, and K. L. Verosub (1999), Characterizing interactions in fine magnetic particle systems using first order reversal curves, *Journal Of Applied Physics* 85, 6660–6667, doi:10.1063/1.370176.

Polyak, L., and M. Jakobsson (2011), Quaternary sedimentation in the Arctic Ocean: Recent advances and further challenges, *Oceanography* 24(3), 52–64, http://dx.doi.org/10.5670/oceanog.2011.55.

Rashid, H., F. Saint-Ange, D. C. Barber, M. E. Smith, and N. Devalia (2012), Fine scale sediment structure and geochemical signature between eastern and western North Atlantic during Heinrich events 1 and 2, *Quaternary Science Reviews* 46, 136-150, doi:10.1016/j.quascirev.2012.04.026.

Rasmusssen, T. L, D. W. Oppo, E. Thompson, and S. J. Lehman (2003), Deep sea records from the southeast Labrador Sea: Ocean circulation changes and ice-rafting events during the last 160,000 years, *Paleoceanography* 18(1), doi:10.1029/2001PA000736.

Reid, C. M., N. P. James, T. K. Kyser, and B. Beauchamp (2008), Diagenetic cycling of nutrients in seafloor sediments and the carbonate–silica balance in a Paleozoic cool-water carbonate system, Sverdrup Basin, Canadian Arctic Archipelago, *Journal of Sedimentary Petrology* 78(8), 562–578, doi:10.2110/jsr.2008.057.

Sarnthein, M., S. van Kreveld, H. Erlenkeuser, P. M. Grootes, M. Kucera, U. Pflaumann, and M. Schulz (2003), Centennial-to-millennial-scale periodicities of Holocene climate and sediment injections off the western Barents shelf, 75°N, *Boreas* 32, 447–461.

Satte, Y. (2010) Assemblages minéralogiques argileux et circulation thermohaline en Atlantique Nord pendant les stades isotopiques 27 à 31, M.Sc. thesis, Dep. des sciences de la Terre, Université du Québec à Montréal, Montréal, Qc, Canada.

Seidenkrantz, M. S., A. Kuijpers, S. Aagaard-Sørensen, S. Andersson, H. Lindgreen, J. Ploug, P. Przybyło, I. Snowball, and M. Ivanov (2010), Glacial ocean circulation and shelf edge glaciation offshore SW Greenland during the past 75,000 years, *Geophysical Research Abstract* 12, EGU2010-4721.

Smith, A. M., C. R. Bentley, R. G. Bingham, and T. A. Jordan (2012), Rapid subglacial erosion beneath Pine Island Glacier, West Antarctica, *Geophysical Research Letters* 39, L12501, doi:10.1029/2012GL051651.

Simon, Q., G. St-Onge, C. Hillaire-Marcel (2012), Late Quaternary chronostratigraphic framework of deep Baffin Bay glaciomarine sediments from high-resolution paleomagnetic data, *Geochemistry, Geophysics, Geosystems*, 13, Q0AO03, doi:10.1029/2012GC004272.

Srivastava, S. P., M. Arthur, and B. Clement (1987), Introduction, in *Proceedings of the Ocean Drilling Program, Scientific Results leg 105*, edited by S. P

Srivastava, M. Arthur, and B. Clement, College Station, TX (Ocean Drilling Program), 5-20.

Srivastava, S. P. (1989), Proceedings of the Ocean Drilling Program, Scientific Results. Baffin Bay and Labrador Sea, Leg 105, Sites 645-647. 1-17.

St-Onge, G., T. Mulder, P. Francus, and B. Long (2007), Continuous physical properties of cored marine sediments, in: Developments in *Marine Geology, Proxies in late Cenozoic paleoceanography*, vol. 1, edited by C. Hillaire-Marcel and A. de Vernal, Elsevier, Amstrerdam, The Netherlands, 63-98.

Stein R. (2008), Arctic Ocean sediments: processes, proxies, and paleoenvironment, Developments in *Marine Geology, Proxies in late Cenozoic paleoceanography,* vol. 2, Oxford, Elsevier.

Stokes, C. R., L. Tarasov, and A. S. Dyke (2012), Dynamics of the North American Ice Sheet Complex during its inception and build-up to the Last Glacial Maximum, *Quaternary Science Reviews* 50, 86-104, doi:10.1016/j.quascirev.2012.07.009.

Stoner, J. S., J. E. T. Channell, C. Hillaire-Marcel (1998), A 200 ka geomagnetic chronostratigraphy for the Labrador Sea: Indirect correlation of the sediment record to SPECMAP, *Earth and Planetary Science Letters* 159, 165-181.

Stoner, J. S., J. E. T. Channell, C. Hillaire-Marcel, and C. Kissel (2000), Geomagnetic paleointensity and environmental record from Labrador Sea core MD95-2024: global marine sediment and ice core chronostratigraphy for the last 110 kyr, *Earth and Planetary Science Letters* 183, 161-177.

Stoner, J. S., and G. St-Onge (2007), Magnetic stratigraphy in paleoceanography: reversals, excursions, paleointensity and secular variation, in *Developments in Marine Geology. Proxies in late Cenozoic paleoceanography*, vol. 1, edited by C. Hillaire-Marcel and A. de Vernal, Elsevier, Amstrerdam, The Netherlands, 99-137.

Syvitski, J. P. M., and F. J. Hein (1991), Sedimentology of an arctic basin: Itirbilung Fiord, Baffin Island, Canada, *Geological Survey of Canada Professional Paper* 91-11, 67 pp

Tang, C., C. Ross, T. Yao, B. Petrie, B. DeTracey, and E. Dunlap (2004), The circulation, water masses and sea-ice of Baffin Bay, *Progress in Oceanography* 63, 183-228.

Timmermann, A., J. Knies, O. E. Timm, A. Abe-Ouchi, and T. Friedrich (2010), Promotion of glacial ice sheet buildup 60–115 kyr B.P. by precessionally paced Northern Hemispheric meltwater pulses, *Paleoceanography* 25, PA4208, doi:10.1029/2010PA001933.

Thomson, J., I. W. Croudace, and R. G. Rothwell (2006), A geochemical application of the ITRAX scanner to a sediment core containing eastern Mediterranean sapropel units, in *New Techniques in Sediment Core Analysis*, edited by R. G. Rothwell, Geological Society, London, Special Publications 267, 65–77.

Thorez, J. (2003), L'argile, minéral pluriel. Bulletin de la Société Royale des Sciences de Liège 72(1), 19-70.

Vincent, J., and V. Prest (1987), The early Wisconsinan history of the Laurentide ice sheet, *Géographie physique et Quaternaire* 41, 199–213.

Waelbroeck, C., L. Labeyrie, E. Michel, J. C. Duplessy, J. F. McManus, K. Lambeck, E. Balbon, and M. Labracherie (2002), Sea-level and deep water temperature changes derived from benthic foraminifera isotopic records, *Quaternary Science Reviews* 21(1–3), 295-305, doi:10.1016/S0277-3791(01)00101-9.

Wang, Z., A. S. B. Cochelin, L. A. Mysak, and Y. Wang (2005), Simulation of the last glacial inception with the green McGill Paleoclimate Model, *Geophysical Research Letters* 32, L12705, doi:10.1029/2005GL023047.

Weidick, A. and O. Bennike (2007), Quaternary glaciation history and glaciology of Jakobshavn Isbræ and the Disko Bugt region, West Greenland: a review, *Geological Survey of Denmark and Greenland Bulletin* 14, 78 pp.

Wolff, E. W., J. Chappellaz, T. Blunier, S. O. Rasmussen, and A. Svensson (2010), Millennial-scale variability during the last glacial: The ice core record, *Quaternary Science Review*, 29, 2828-2838, doi:10.1016/j.quascirev.2009.10.013.

Xuan, C., J. E. T. Channell, L. Polyak, and D. A. Darby (2012), Paleomagnetism of Quaternary sediments from Lomonosov Ridge and Yermak Plateau: implications for age models in the Arctic Ocean, *Quaternary Science Reviews* 32, 48-63, doi:10.1016/j.quascirev.2011.11.015.

Table 1. Detrital carbonate (DC-) Layers

DC- Heinrich- Events	H0	H1	H2	H3	H4	H5	H5a	H6	H7a	H7b	H8	H9	H10
Hemming (review paper, 2004)		16.8	24	31	38	45		60					
MD95-2025 (Hiscott et al., 2001)	11 - 12	18 - 22		28 - 29	39 - 42		50 - 53	59 - 61	69		92 - 108		
EW9302-1JPC -2JPC (Rasmussen et al., 2003)	12	16	24.5	29	36	46.5		61	70	74	87	90 - 96	
MD95-2024 (Orphan Knoll) (Stoner et al., 2000)		15.5	24	30	39.5	46	52.5	59.5					
Site U1302/03 (Orphan Knoll) (Channell et al., 2012)	12.7 (12.3)	17.1 (15.8)	26.7 (24.3)	33.7 (30.5)	40.7 (38.8)	48 (48)	55.7 (55.5)	63.5 (60.1)					
Site U1308 (Central NA - 'Rudiman') (Hodell et al., 2008)		17.5	24.5		39.4	48.6		63.5					
HU91-045-94P (Orphan Knoll) (Stoner et al., 1998)	12	16.5	23	29	35.5	48	59	67	85		92		
nortwest Labrador Sea (Andrews et al., 1998)		13 - 14.5	19.5 - 21	34?									

BBDC- Events (This study)	0	1	2	3	4	5	6	7a	7b	8a	8b	8c	9a	9b
BBDC timing interval (cal ka BP)	10.5 - 12	13.7 - 15	24.7 - 25	26.4 - 27.7	31.9 - 37	48.5 - 50	58 - 64	73 - 79.5	80.5 - 84.5	91.5 - 95	99 - 100.5	103 - 104.5	107.5 - 108.5	110 - 115?
BBDC duration (ka)	1.5	1.3	0.3	1.3	5.1	1.5	6	6.5	4	3.5	1.5	1.5	1	>5?
Interstadial link	pre-Boreal	1	?	3	5-6-7-8	13	18'	20-21 reb.[a]	21	?	23	23	24	25 reb.[a]

[a] Rebound-type features, see Capron et al., 2010.

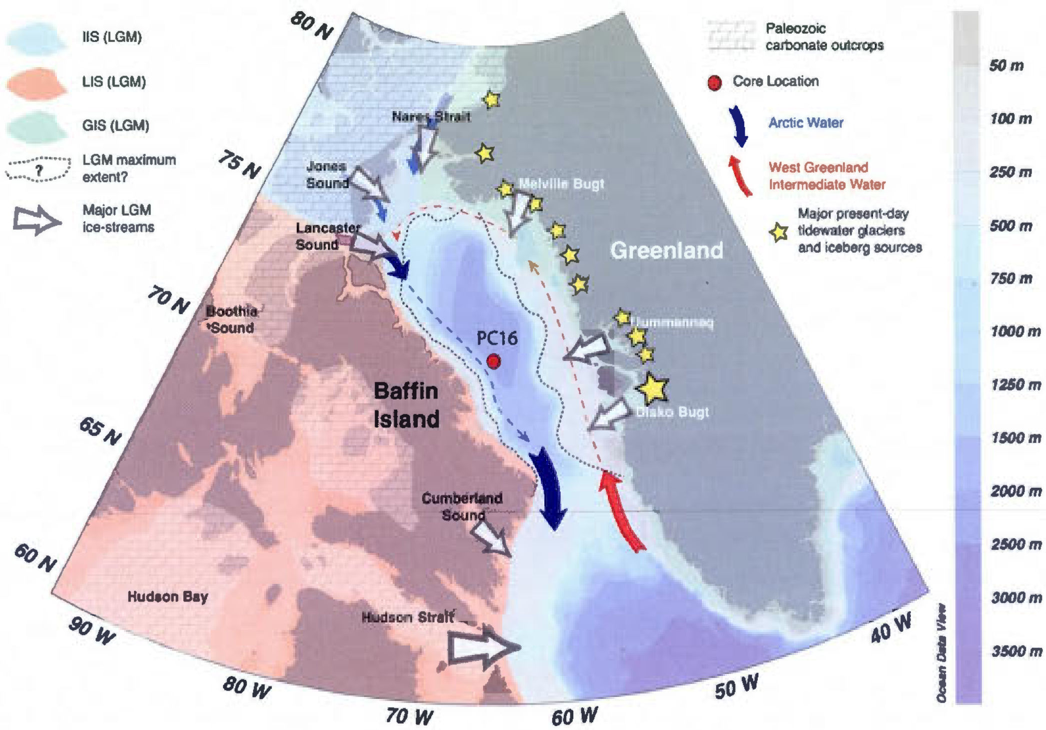

Figure 1. Map of the Baffin Bay area and location of core HU2008-029-016PC sampling site. The general bathymetry, simplified oceanic circulation, sketch of the Paleozoic outcrops [*MacLean*, 1985] and LGM paleogeography (including LGM unknown maximum ice margin extents) are also represented. Red arrows illustrate Atlantic "warm" waters, whereas the blue arrows represent colder Arctic waters. Major present-day tidewater glaciers locations (yellow star) are from *Bigg* [1999]. The simplified representations of the Greenland (green), Innuitian (blue) and Laurentide ice sheet (red) limits and major ice stream locations during the LGM (colored areas) are adapted from *Funder et al.* [2011], *Dyke* [2004], *Hulbe et al.* [2004] and *England et al.* [2006].

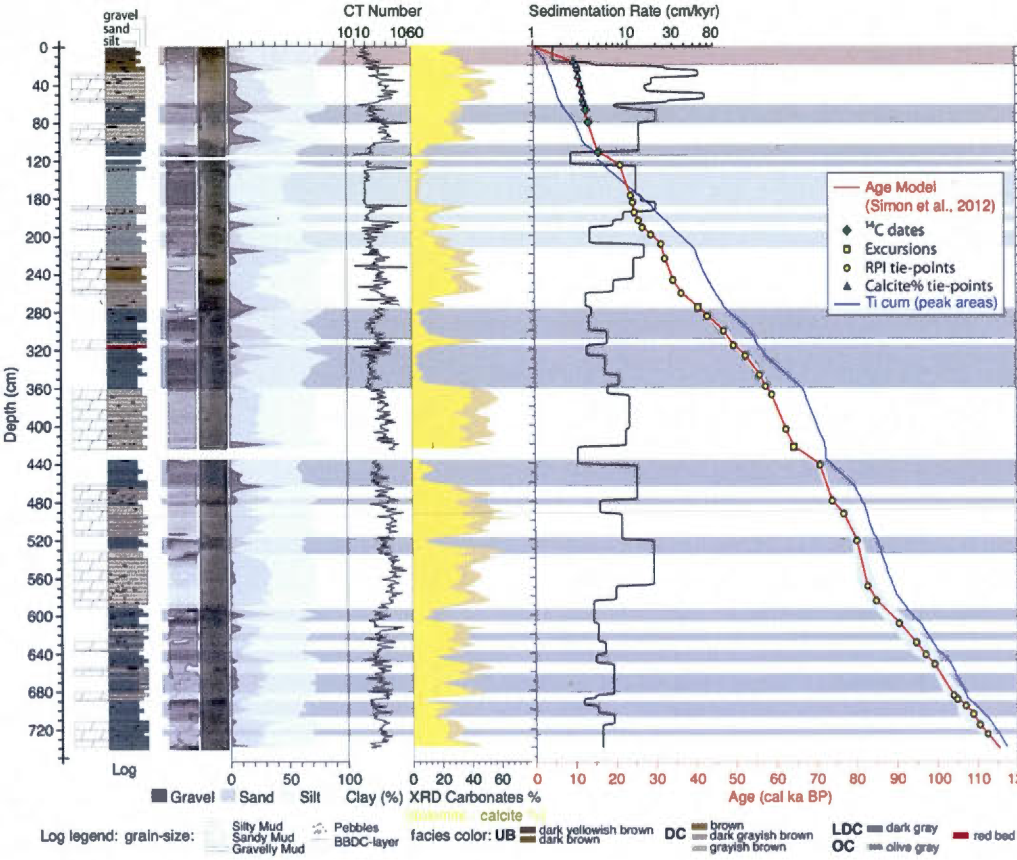

Figure 2. Core lithostratigraphy and age model. Log: general simplified lithofacies log (see text and legend for details); CT: CAT-Scan image (X-ray); HRI: high-resolution digital image; CT Number: density proxy; Grain size (%) for clay, silt, sand and gravel. XRD relative percentage of carbonates (dolomite (yellow) + calcite (chamois)). PC16 age model with tie-points used for its establishment [see *Simon et al.*, 2012 for details], and associated sedimentation rate. The Ti cumulative curve is calculated using the cumulative addition (with depth) of Ti peak areas measured with the µXRF ITRAX™ core scanner. It gives independent information about sedimentation rates. Distinct lithological facies are highlighted with color banding. Red: uppermost brownish gray silty mud unit; light green: olive-black silty to clayey mud unit; white: carbonate-rich yellowish-brown to dark-brown very poorly sorted gravelly sandy mud detrital layers; dark green: olive gray to dark gray poorly sorted silty to sandy mud low carbonate detrital layers.

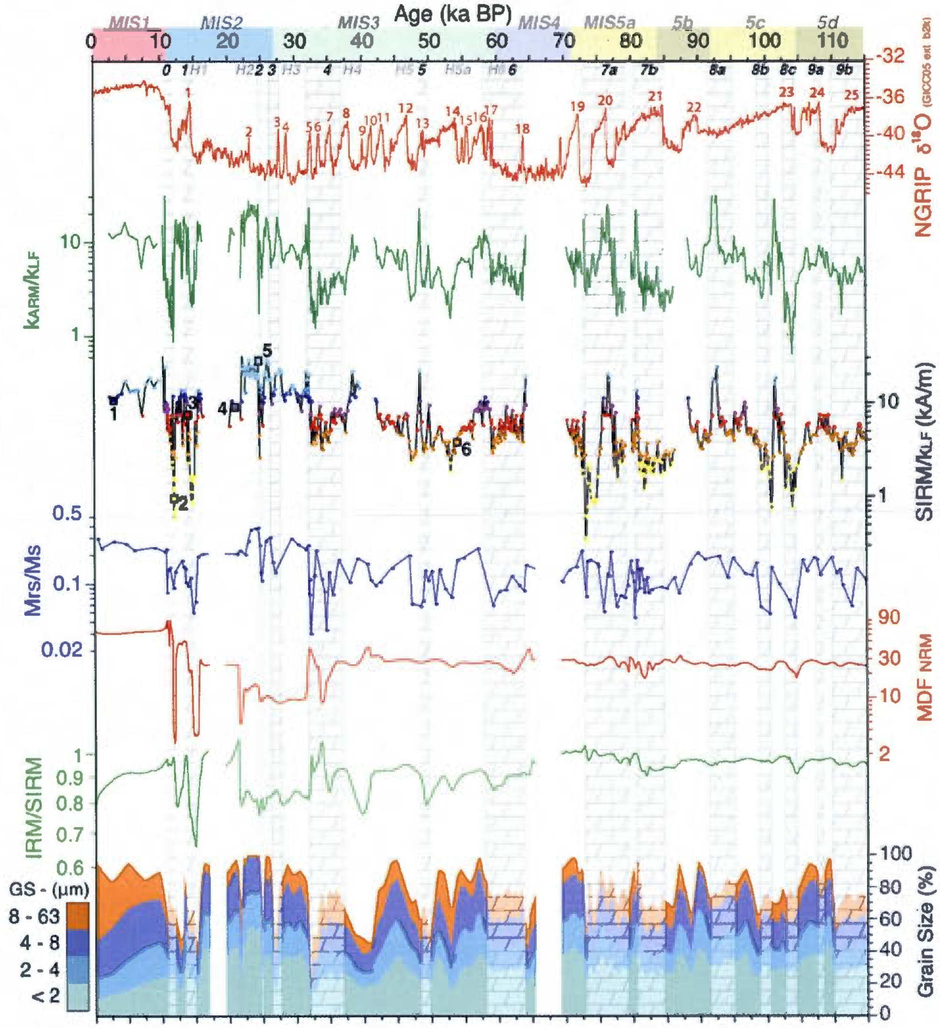

Figure 3. Bulk and magnetic grain-size. k_{ARM}/k_{LF}, $SIRM/k_{LF}$ and Mrs/Ms are grain-size sensitive with high (low) values corresponding with finer (coarser) magnetic grain while Pseudo-S ratio ($IRM_{0.3T}/SIRM_{0.95T}$) and MDF_{NRM} are also influenced by magnetic mineralogy (see text for interpretation). The grain-size results (laser diffraction) display large variability within the fine fraction. The clay and silt percentages are divided between clay (0-2 µm), very fine silt (2-4 µm), fine silt (4-8 µm) and pseudo sortable silt (8-63 µm) in order to interpret their source and transport mode. The 0 to 4 µm is considered as "glacial flour" while pseudo sortable silt is driven by current and sea ice. NGRIP $\delta^{18}O$ and Greenland interstadials (1 to 24) are from www.icecores.dk and Wolff et al. (2010). Marine isotope stages from 1 to 5d are represented with color boxes. Baffin Bay Detrital Carbonate layers (BBDC) are represented by vertical white carbonate pattern bars and numbered according to our arrangement. The North Atlantic Heinrich events [Hemming, 2004] (Table 1) are indicated for comparison.

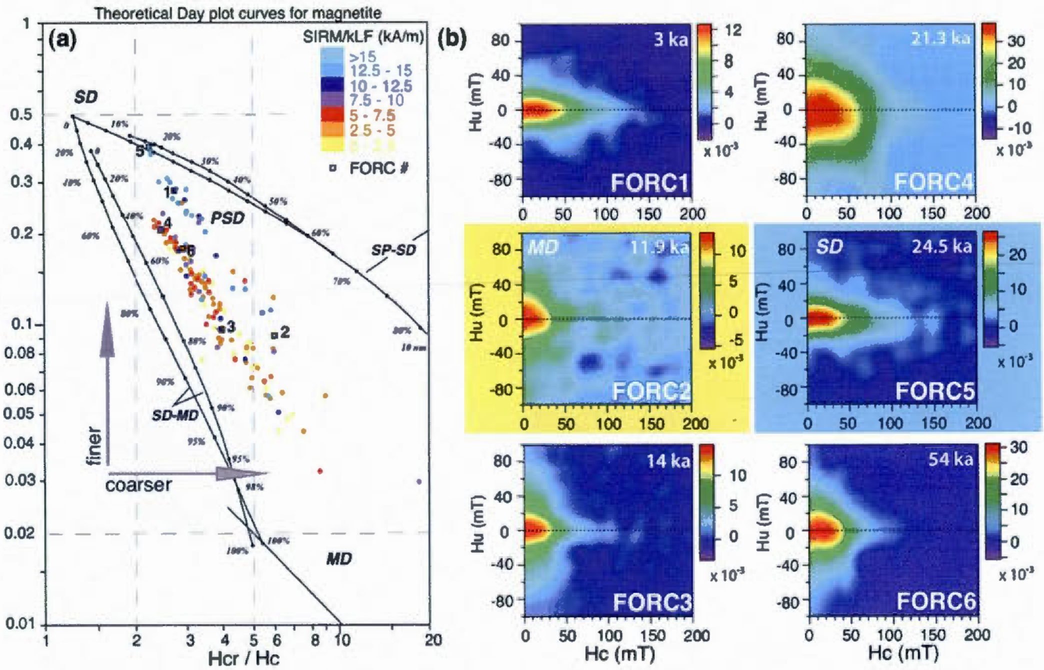

Figure 4. (a) Day plot. Samples are represented with color dots according to their corresponding SIRM/k_{LF} values (see Figure 4 for sample position). The horizontal and vertical lines delimitate the theoretical area for single (SD), pseudo-single (PSD) and multi domain (MD) magnetite grains. These lines and the mixing reference curves are from *Dunlop* [2002]. (b) First Order Reversal Curves (FORC) diagram of representative samples (open squares in Figure 4 and Figure 5(a)) processed using the FORCinel™ software [*Harrison and Feinberg*, 2008] with IgorPro™ software and a smoothing factor (SF) of 4. FORC diagrams show coercivities (x axis) and interactions (y axis) between magnetic grains within a sample. FORC diagrams 2 and 5 are highlighted as they correspond to SD and MD magnetic grains.

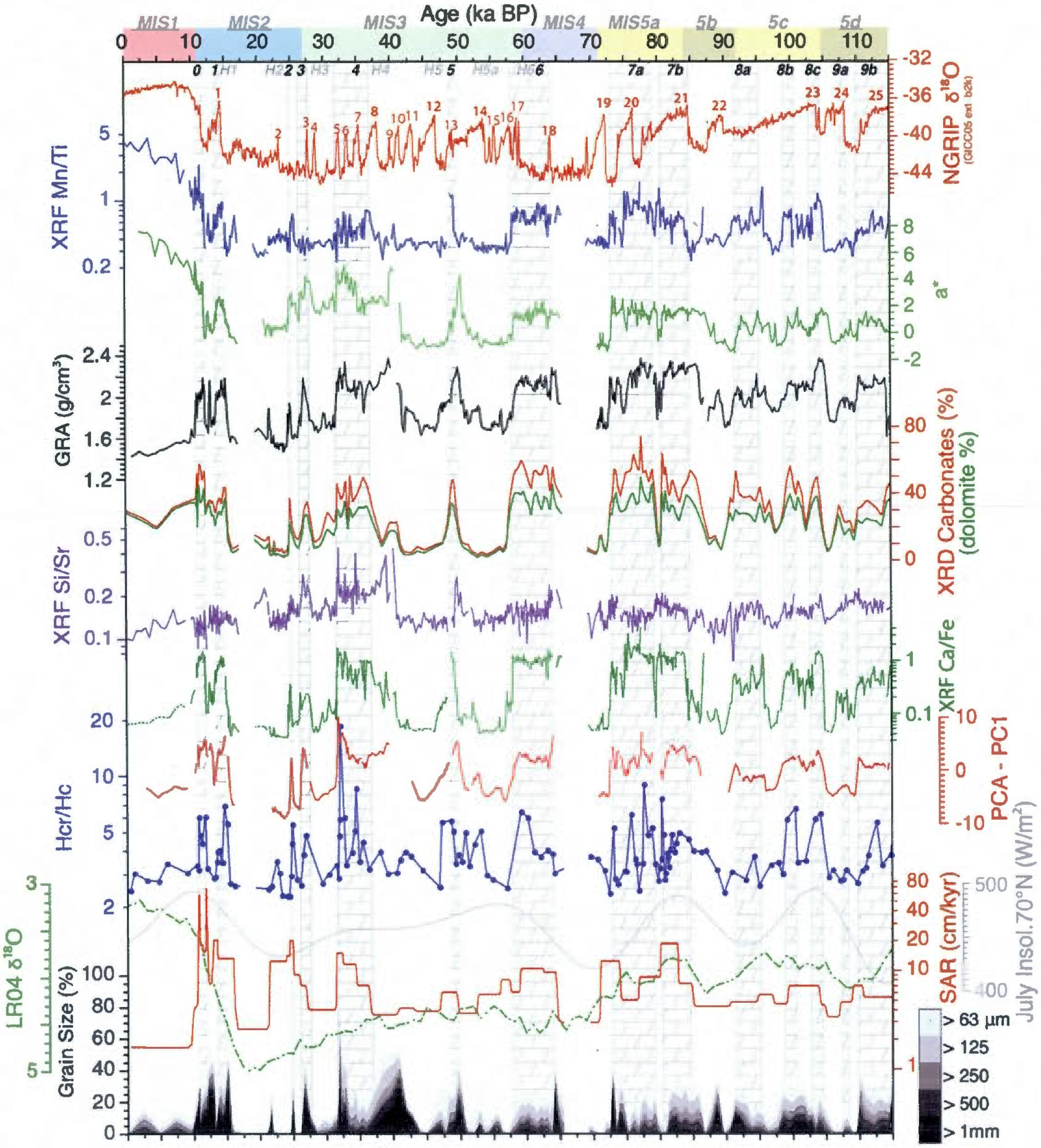

Age (ka BP)
MIS1
MIS2
MIS3
MIS4
MIS5a
5b
5c
5d
NGRIP δ18O (GICC05 ext b2k)
XRF Mn/Ti
a*
GRA (g/cm3)
XRD Carbonates (%)
(dolomite %)
XRF Si/Sr
XRF Ca/Fe
PCA - PC1
Hcr/Hc
SAR (cm/kyr)
July Insol.70°N (W/m2)
LR04 δ18O
Grain Size (%)
> 63 µm
> 125
> 250
> 500
> 1mm

Figure 5. (page 115) Coarse-carbonate sediment layers. µXRF Mn/Ti ratio illustrates a sharp change in redox conditions associated with the Holocene period. a*: green (low) to red (high) within the Commission Internationale de l'Eclairage (CIE) color space. XRD carbonates (calcite + dolomite, red line) and dolomite (green line) represent relative percentages calculated on X-ray diffraction height peaks for selected minerals. High µXRF Ca/Fe ratio values and increased density measured by Gamma Ray Attenuation (GRA) illustrate higher density layers corresponding with DC-layers. High µXRF Si/Sr is a proxy for IRD rich in silicate minerals. Hcr/Hc ratio values indicate coarser magnetic grains within DC-layers. The cumulative percentages of coarser grain sizes (> 63, 125, 250, 500 µm and > 1 mm) are presented. PC1 has been calculated using the whole dataset and enable to pinpoint BBDC layers. The sediment accumulation rate (SAR) curve is derived from the age model. LR04 $\delta^{18}O$ is the globally distributed benthic $\delta^{18}O$ isotope stack from *Lisiecki and Raymo* [2005] that constitutes a broad approximation of global ice volume and deep ocean temperature. The July insolation is calculated at 70°N [from *Laskar et al.*, 2004].

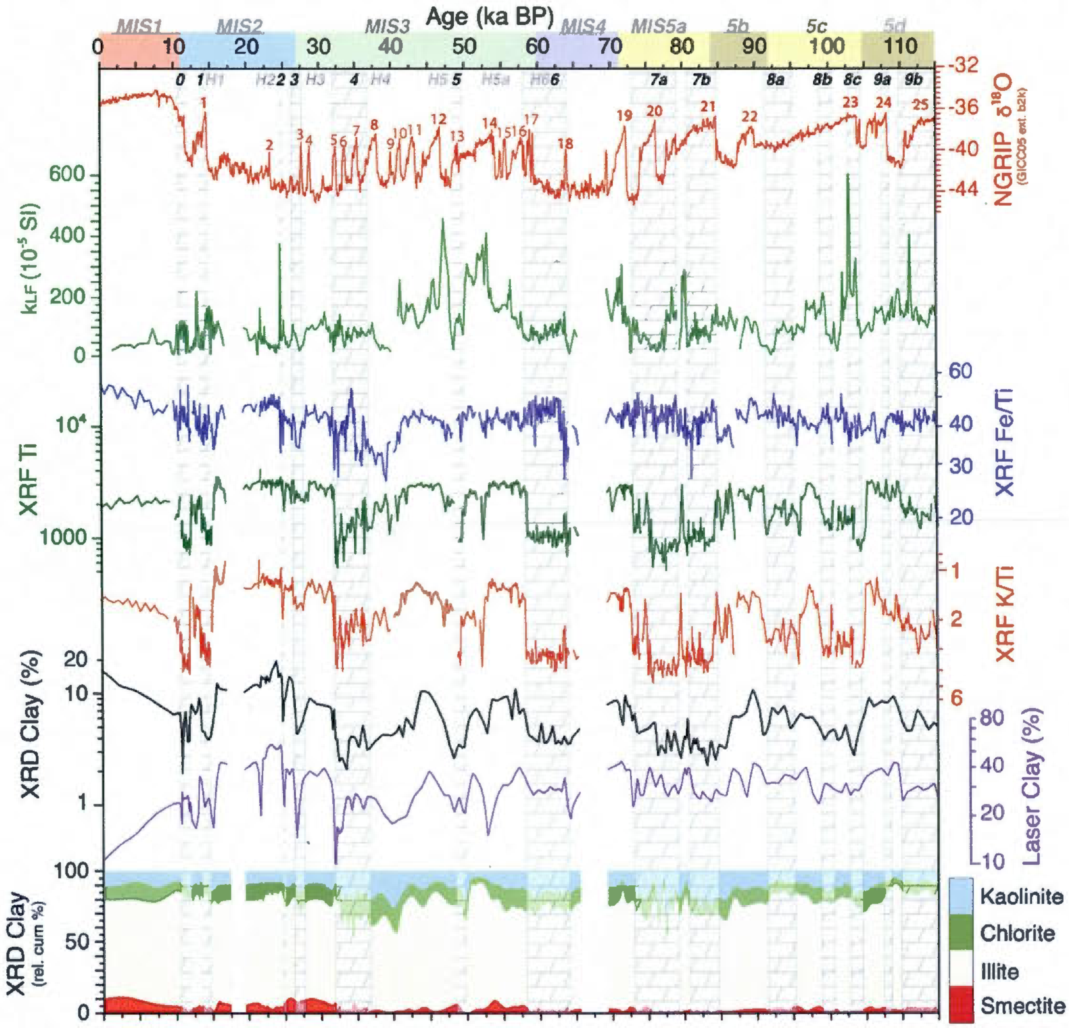

Figure 6. Physical, μXRF and XRD clay properties. k_{LF} is the low-field volumetric magnetic susceptibility and expresses primarily the ferromagnetic concentration. XRD and laser-calculated clay percentage values are represented. The relative percentages of the 4 main clay species (summed to 100 %) have been calculated using Biscaye's weighting factors. μXRF K/Ti (inverse axis) and Fe/Ti ratios are illustrated for comparison with the clay percentages. μXRF Ti peak areas express the relative element concentration of titanium.

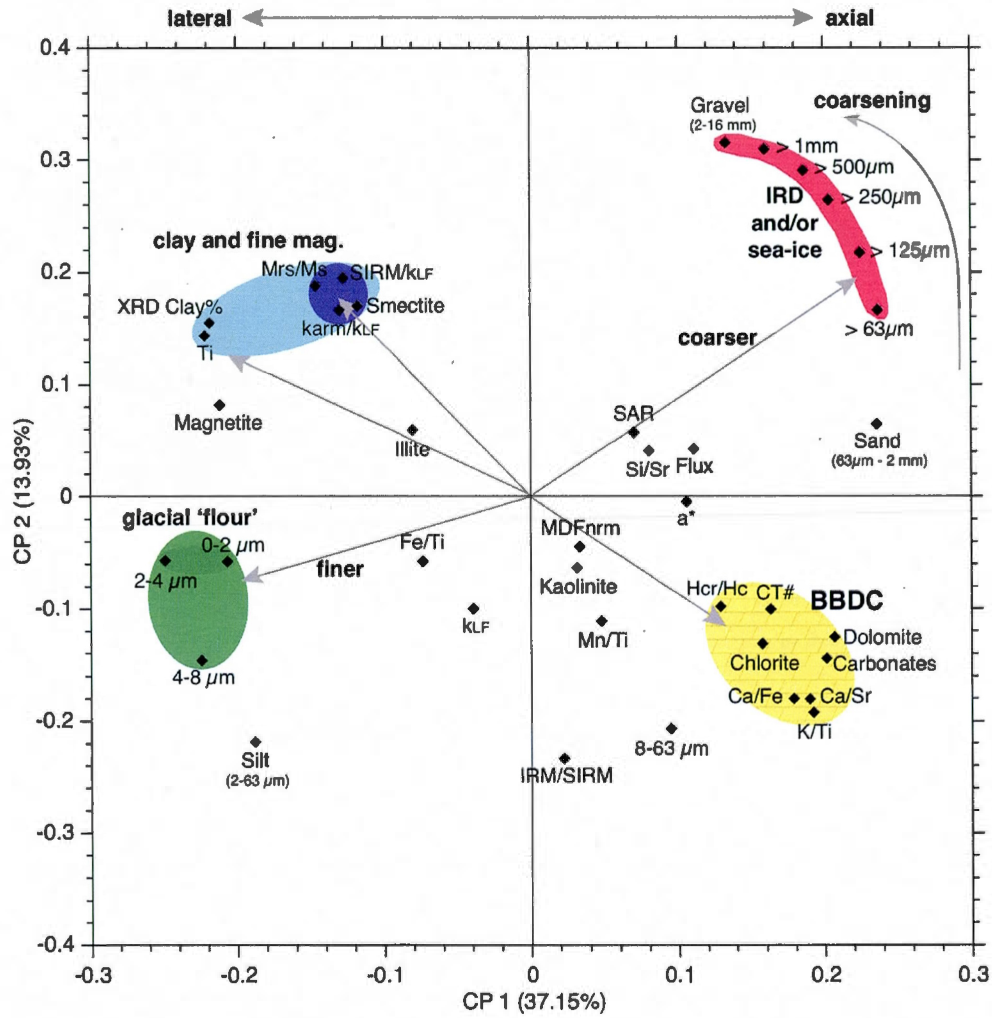

Figure 7. Principal component analysis (PCA) of studied proxies. Variable loading scores for PC1 vs. PC2 explain respectively 35.3 % and 14.4 % of the total variance.

Figure 8. (page 119). DC-layers timing comparison between Baffin Bay and the North Atlantic. Yellow boxes are for dolomite DC-layers while chamois color patterns are for calcite DC-layers. Timing and numbering of DC-layers are from their respective age model and description. The numbering of BBDC-dated events is proposed from our study in order to establish correspondences between regionally distinct DC-layers. DC-layers are from (1) this study; (2) *Andrews et al.* [1998]; (3) *Andrews et al* [1994]; (4) *Stoner et al.* [1998]; (5) *Channell et al.* [2012]; (6) *Stoner et al.* [2000]; (7) *Rasmussen et al.* [2003]; (8) *Hiscott et al.* [2001]; (9) *Hemming* [2004]. The Relative Sea Level (RSL, blue line) reconstruction is from *Waelbrock et al.* [2002]. Marine isotope stages 1 to 5d are represented with colors on the time axis on the left.

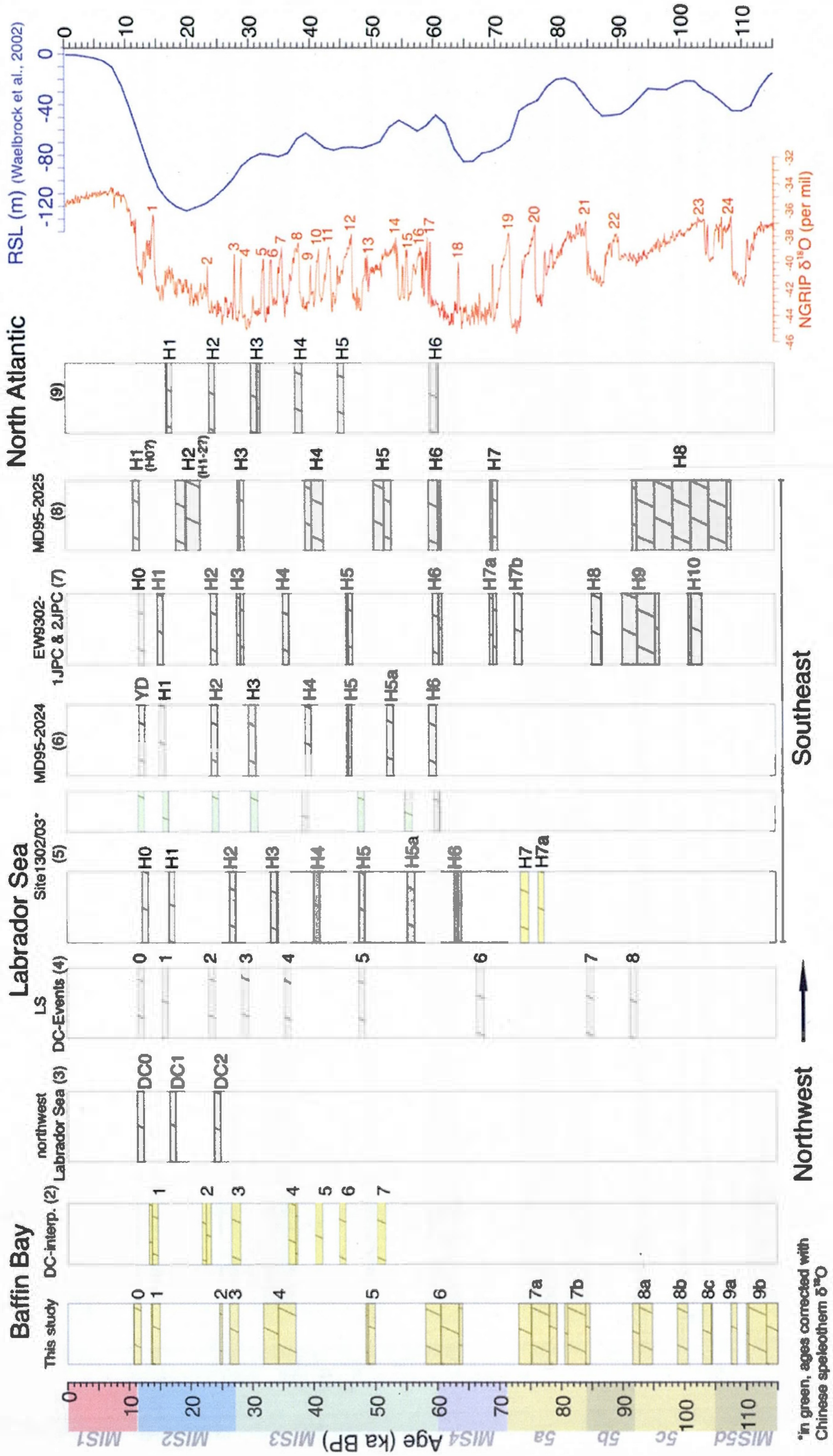
Baffin Bay
This study
DC-interp. (2)
northwest Labrador Sea (3)
Labrador Sea
LS DC-Events (4)
Site1302/03* (5)
MD95-2024 (6)
EW9302-1JPC & 2JPC (7)
MD95-2025 (8)
North Atlantic
(9)
RSL (m) (Waelbrock et al., 2002)
NGRIP δ18O (per mil)
Age (ka BP)
MIS1
MIS2
MIS3
MIS4
5a
5b
5c
MIS5d
Northwest
Southeast
*in green, ages corrected with Chinese speleothem δ18O

CHAPITRE III

Northeastern Laurentide, western Greenland and southern Innuitian ice stream dynamics during the last glacial cycle

Quentin Simon[1,2], Guillaume St-Onge[1,3], Claude Hillaire-Marcel[1,2], John T. Andrews[4]

[1] Geotop Research Centre, Qc, Canada.

[2] Université du Québec à Montréal, Montréal, H3C3P8, Qc, Canada.

[3] Canada Research Chair in Marine Geology & Institut des sciences de la mer de Rimouski (ISMER), Université du Québec à Rimouski, Rimouski, G5L3A1, Qc, Canada.

[4] INSTAAR & University of Colorado, Boulder, CO, USA.

Keywords:

Sediment provenance, X-ray diffraction, Ice stream, Last glacial cycle, Baffin Bay

Key Points:

Lithofacies and mineralogical analyses were used to determine sediment provenance

Uummannaq signature provides evidence of pre-LGM Greenland ice margin extents

Eastern Baffin Island ice streams were sensitive to high frequency DO oscillations

Article accepté à Journal of Quaternary Sciences (doi:10.1002/jqs.2648)

Abstract

Precise relationships between high-frequency ice sheet dynamics and late Quaternary climate variability are still poorly understood, notably with regard to their relative timing and causal mechanisms. Baffin Bay is of particular interest in this regard due to the influence of ice streaming activities from the northeastern Laurentide, southern Innuitian and western Greenland ice margins on its sedimentary regimes during glacial times. In this paper, we document such ice margin dynamics by means of a sedimentological analysis performed on a piston core from central Baffin Bay and spanning the last 115 ka. Lithofacies analysis and mineralogical assemblages are used to reconstruct sediment sources (using the SedUnMix program) and depositional mechanisms. Coarse detrital carbonate (dolomite-rich) layers are attributed either to northeastern Laurentide and Innuitian ice streaming pulses or to pervasive ice rafted debris (IRD) delivery processes at distinct periods. Out-of-phase fine-grained glaciomarine sediments with a mineralogical signature from western Greenland, linked to Uummannaq ice streaming activity, are interbedded with the coarse DC layers. The new results suggest that during the last glacial cycle, the northeastern Laurentide and southern Innuitian ice streams were sensitive to high frequency climate fluctuations such as the Dansgaard-Oeschger events, while the western Greenland margins were more sensitive to large-scale climatic/oceanic reorganizations such as relative sea level changes and likely to advection of warmer Atlantic waters into the bay.

1. Introduction

Over the last few decades, ice sheet and glacier dynamics have received a lot of attention, notably due to the acceleration of the Greenland Ice Sheet (GIS) melting and major outlet retreats (e.g., Weidick and Bennike, 2007; Holland *et al.*, 2008; Alley *et al.*, 2010; Rignot and Mouginot, 2012). Numerous studies and publications have also focused on past ice sheet dynamics, especially with regard to the linkages between Laurentide Ice Sheet (LIS) dynamics and Quaternary climatic changes (e.g., MacAyeal, 1993; Bond *et al.*, 1995, 1999; Dowdeswell *et al.*, 1995, 1997, 1999; Andrews *et al.*, 2000, 2003, 2012; Hemming, 2004; Hulbe *et al.*, 2004). The growth and decay of ice sheets are controlled by (1) mass balance parameters (e.g., accumulation of snow and ice, calving at marine-based margins, basal melting) relating to atmospheric and oceanic changes (Marshal and Koutnik, 2006), and (2) intrinsic ice sheet instabilities (e.g., Heinrich events). The mass balance and stability of ice sheets is associated to rapidly flowing ice streams and outlet glaciers along their margins (Stokes and Clark, 2001). The modeling of the ice sheet responses to past and present climatic changes is a prerequisite to understanding their past behavior and is important for the interpretation of the ongoing ice stream retreats along the Greenland ice margin. However, building such simulations requires knowledge of rates and timing of the rapid and/or long-term ice streaming processes (Stokes and Tarasov, 2010). Yet, the triggering and driving mechanisms behind such processes and their timing are still poorly documented. As a consequence, recent changes in Greenland ice margin dynamics could be attributed to either climate/ocean warming (through mass balance changes) or to longer-term changes in the GIS budget responses to Holocene climate changes (i.e., a mix of mass balance and internal dynamics; Stokes *et al.*, 2012).

In this respect, and because it was surrounded by some of the largest Late Quaternary ice sheets, Baffin Bay holds great interest for the identification of ice margin dynamics (i.e., the western Greenland, northeastern (NE) Laurentide and southern Innuitian Ice Sheets) from its sedimentary records. To achieve this, the recognition of sedimentary features in terrigenous layers that are characteristic of their origin, transport and depositional mechanisms is required. In addition, the temporal relationship between such layers and high-frequency ice sheet and/or climate variability is also critical. Until now, the interpretations of sedimentary sequences from Baffin Bay have been proven challenging due to the lack of well-dated records (Simon *et al.*, 2012). Moreover, very few marine geophysical and geological data of ice stream advances and retreats predating the Last Glacial Maximum (LGM) are available, largely due to ice erosion during the LGM itself and the last deglaciation (Andrews *et al.*, 1998; Alley *et al.*, 2010), thus hampering any direct reconstruction of the longer (pre-LGM) history of paleo-ice streams and their dynamics during glacial times.

In this paper, we use sedimentological and mineralogical properties of a piston core (HU2008-029-016PC, Fig. 1) raised from central Baffin Bay and spanning the last 115 ka (Simon *et al.*, 2012) to document surrounding ice margin dynamics. Lithofacies analysis and mineralogical assemblages are used to unravel and discuss sediment provenance and depositional mechanisms. The main objectives of this paper are to (1) reconstruct sediment provenances based on mineralogical assemblages (using the SedUnMix program developed by Andrews and Eberl, 2012a), (2) compare provenance signatures and transport/depositional processes, (3) document the advance and retreat of western Greenland and eastern Baffin Island ice margins, and their timing with regard to climatic/oceanic variability (e.g., Dansgaard-Oeschger cycles) during the last glacial cycle, and (4) compare these reconstructions to recent model experiments (e.g., Ganopolski *et al.*, 2010; Stokes *et al.*, 2012).

2. Regional setting

Baffin Bay (Fig. 1) is a narrow oceanic basin (1300 km long and 450 km wide, ~690 000 km^2) resulting from the extension of the North Atlantic-Labrador Sea rift system (MacLean *et al.*, 1990). The bedrock geology of the circum-Baffin Bay region is largely characterized by a Precambrian crystalline basement overlain by a Lower Paleozoic succession dominated by shallow marine platform carbonates at the northern end of the bay (Hiscott *et al.*, 1989). Paleocene rifting resulted in basaltic flows observed on the Greenland Precambrian Shield margins near the Disko Island and Uummannaq fjord regions (see Fig. 1 for a geology overview, and Harrison *et al.*, 2011, for a detailed geological map of the area). Baffin Bay is bounded to the north by Nares Strait, a probable transform fault, and to the south by the Ungava transform fault system underlying Davis Strait (Ehrhardt *et al.*, 2008). Thick sedimentary strata are found along the narrow east Baffin Island shelf (25–50 km) and the opposing and much broader west Greenland shelf (>250 km), which is also characterized by large submarine fans at the mouth of cross-shelf troughs. The central abyssal plain (2000–2500 m) is surrounded by steep continental slopes on both sides, while the northern slope dips slightly toward the abyssal plain (Li *et al.*, 2011). Surface current circulation is counter-clockwise in the bay (Tang *et al.*, 2004; Fig. 1). Extensive sea ice (mainly first-year sea ice) covers the bay except in August and September. The influence of Atlantic waters on the Greenland margin contributes to an asymmetric distribution of the sea ice cover (Tang *et al.*, 2004). The present-day fast-flowing outlets of the GIS are estimated to have a total iceberg flux of ~141 km^3/yr (Fig. 1) (Bigg et al., 2001), while the contribution from tidewater glaciers on the Canadian Arctic Archipelago are found to be minor (Weidick and Bennike, 2007). Marshall and Koutnik (2006) have estimated the total iceberg flux originating from ice sheets that surrounded Baffin Bay during the last glacial cycle to be ~16.8 x 10^6 km^3.

During the LGM, the NE LIS, the Innuitian Ice Sheet (IIS) and the western GIS constituted an almost continuous ice belt surrounding Baffin Bay (Fig. 1). The buildup of the IIS as late as ~19k cal a BP is out of phase with the buildup of the LIS (Dyke *et al.*, 2002; England *et al.*, 2006, 2009), which had attained its maximum extent between 24 and 20k cal a BP, while the GIS may have been extending as late as ~14k cal a BP (Funder *et al.*, 2011; Ó Cofaigh *et al.*, 2013). This phasing and the continued fall of global eustatic sea level until ~18k cal a BP indicate that the growth of the LIS, GIS and IIS probably responded to different forcings (Dyke *et al.*, 2002; England *et al.*, 2006; Clark and Mix, 2002). Northeastern LIS and southern IIS ice streams (in Lancaster Sound, Jones Sound and Smith Sound – Nares Strait) advanced into northern Baffin Bay (MacLean *et al.*, 2010) with a LGM grounding line situated 270 km off the mouth of Lancaster Sound (in a water depth of 1300 m; Li *et al.*, 2011) and potentially expanded laterally to create an ice shelf in the northern part of the bay (Hulbe *et al.*, 2004; Marcott *et al.*, 2011). The LIS outlets extended through Baffin Island, probably as far as the fjord mouths and inlets, and possibly over part of the Baffin Island shelf (Briner *et al.*, 2003, 2006, 2007; Young *et al.*, 2012), while the GIS outlets expanded westward onto the Greenland inner shelf, and as far as the shelf edge off Disko Bugt and the Uummannaq Trough at the LGM (Ó Cofaigh *et al.*, 2012, 2013; Funder *et al.*, 2011). Although pre-LGM glaciations are poorly documented around Baffin Bay, recent simulations suggest a (1) rapid glacial inception of the NE LIS, IIS and GIS after the last Interglacial, followed by several phases of ice sheet growth and reduction, and (2) a strong asymmetry between the ice sheet growth phases and glacial termination (Ganopolski *et al.*, 2010; Stokes *et al.*, 2012). The deglaciation of the northern hemispheric ice sheets began after 20k cal a BP and accelerated significantly after 16k cal a BP (Jennings *et al.*, 2011; Ganopoloski *et al.*, 2010).

3. Materials and methods

The HU2008-029-016PC piston core, referred to as PC16 hereinafter, is a 741-cm long piston core raised from central Baffin Bay during the 2008-029 CCGS Hudson expedition (70°46.14 N/-64°65.77 W; water depth: 2063 m; Campbell and de Vernal, 2009). The core location (Fig. 1) is near an Ocean Drilling Program (ODP) site that was drilled in 1985 (ODP 645, leg 105; Srivastava *et al.*, 1989) and of several cores retrieved from the deep central Baffin Bay during the 1970s and 1980s (e.g., Aksu, 1981; Aksu and Piper, 1987; Hillaire-Marcel *et al.*, 1989; Andrews *et al.*, 1998).

3.1. Physical and geochemical properties

The core sections (1.5 m long) were described and sampled with u-channels (rigid u-shaped plastic liners, 2 x 2 cm cross section) from the centre of the working halves. To allow visualizing the sedimentary structures, the archive halves were run through a computerized coaxial tomography scanner (CAT Scan) at 1 mm intervals at INRS-ETE in Quebec City (Fig. 2). The results of this scan mainly reflect changes in bulk density (quantified through the CT numbers; e.g., St-Onge *et al.*, 2007). High-resolution micro X-ray fluorescence (μXRF) spectrometry measurements were performed at 0.5 cm intervals and during a 50-s counting time using an ITRAX™ core scanner (Cox Analytical Systems) at the GIRAS (Geochemistry, Imagery and Radiography of Sediment) laboratory of INRS-ETE. The output data represent relative concentrations, which have been reported here as cumulative concentrations (relative to depth) to provide independent information about sedimentation deposition variability (Fig. 2). Grain size analyses were performed on sediment samples (1–2 g) at the *Institut des sciences de la mer de Rimouski* (ISMER) using a Beckman Coulter™ LS13320 laser diffraction grain size analyzer at 4 cm intervals. Wet sediment was mixed in a solution of 20 gL^{-1} of Calgon electrolytic solution (sodium hexametaphosphate) and water. The samples were rotated for 3 h and then sieved at 2 mm prior to analysis. Grain size distribution and statistical parameters (mean, standard deviation) were calculated using the Gradistat software (Blott and Pye, 2001).

3.2. Mineralogy

Bulk mineralogical assemblages were determined by X-ray diffraction (XRD) at UQAM using a Siemens D-5000™ diffractometer (°2Θ, CoKα1,2 radiation and an Si detector). Semi-quantitative estimates ($\pm 1\sigma \sim 5\%$) of the main mineral species were based on the peak height (in counts per second) of the first diffraction peak for each mineral corrected for quartz and normalized to 100% (Thorez, 2003). The analyses were performed on sediment fractions sieved at 63 μm and 2 mm with a 4-cm sample interval and then merged in order to compare our mineralogical assemblages with the source signatures (Andrews and Eberl, 2011). We used weighting factors (ratio between the weight of individual fractions) on both fractions (i.e., 63 μm; 63 μm - 2 mm) to respect grain-size proportion. High correlation coefficients between the weight percentage and laser grain size analysis ($r=0.88$ for silt and $r=0.91$ for sand) confirmed the reliability of the merging process.

To unravel sediment provenance based on the mineralogical composition, we applied the sediment unmixing model (SedUnMix) proposed by Andrews and Eberl (2012a). The model calculates the contribution of different source areas of mixed sediments. SedUnMix seeks an iterative solution (we used 20 iterations in this study) to optimize a non-linear solution for the respective percentages of source regions and sample compositions. This iteration process optimizes (i.e., reduces) the average absolute difference between the observed and the calculated mineralogy (see Andrews and Eberl, 2012a for details about the method).

3.3. Chronology

The age model of core PC16 (Fig. 2) is primarily based on the correlation of its relative paleointensity (RPI) profile with regional and global RPI reference curves (Simon *et al.*, 2012). Three radiocarbon ages and two geomagnetic excursions further support the established age model. The derived age model is consistent with previous regional age models (Andrews *et al.*, 1998) but offers a much more precise and accurate temporal resolution (see Simon *et al.*, 2012 for details).

4. Results

Five lithofacies were identified in the core and represent distinctive sediment delivery processes (Fig. 2a). Fine-grained sediments with low detrital carbonate percentages (LDC) and coarse detrital carbonate sediments (i.e., Baffin Bay Detrital Carbonate, BBDC) are found at specific intervals within the entire sequence, whereas the LGM, last deglaciation and Holocene units are found only at specific depths (see Simon *et al.*, subm. for a comprehensive facies and unit description). Following this lithofacies interpretation, the XRD relative mineralogical composition demonstrates a significant down-core variability (Fig. 2d). Two principal modes are distinguished: (1) carbonate-rich layers with about 30–40% of dolomite and 10–15% of calcite; and (2) feldspar-rich layers (i.e., K-feldspar and plagioclase minerals) with values between 30% and 50% associated with increases of clay minerals (Figs. 2d and 3). This pattern is consistent with the identification and interpretation of BBDC layers related to the glacial erosion of basement rocks at the northern end of Baffin Bay, where major ice streams of the NE LIS and northwestern GIS merged (Aksu and Piper, 1987; Andrews *et al.*, 1998; Parnel *et al.*, 2007), while the feldspar-rich layers are associated with lateral sources (from Greenland and Baffin Island; Simon *et al.*, subm.).

In order to test the reliability of our semi-quantitative estimate with the quantitative XRD (qXRD) method used by Andrews and Eberl (2011) for source identification, we measured 10 samples with the qXRD method described in Eberl (2003, 2004). The results present nearly identical relative distribution and similar percentage values (within the statistical uncertainty, supplementary materials, S1). Nevertheless, a large deviation of the quartz weight percentage in one sample, associated with the overall ubiquity of quartz in the sources composition (12.7±7.2 wt%), raised the question of its impact on the provenance calculation. We therefore ran SedUnMix analyses (10 iterations) by including/excluding the quartz. The results without the quartz have lower degrees-of-fit (DOF) and smaller average deviation values (a measure of the level of agreement between the observed and expected mineralogy, see Andrews and Eberl, 2012a), thereby expressing a better fit between sources and core samples. Accordingly, we removed the quartz from the mineralogical assemblage to obtain statistically more robust results. Besides, the dissolution of carbonates in deep-basin surface sediments (due to corrosive waters, see Azetsu-Scott *et al.*, 2010) introduces an important "no analog" problem, as the mineralogical assemblage failed to accurately represent the respective sources with respect to the carbonate contents (i.e., calcite is almost totally absent and dolomite wt% are significantly lower in surface samples) as previously demonstrated by Andrews and Eberl (2011). Consequently, the carbonate minerals have also been removed from the mineralogical assemblage. An important consequence of the removal of the carbonates implies that the northern Baffin Bay contribution is significantly reduced from the provenance calculation results. Thus, the weight percentages attributed to the sources represent essentially lateral source contributions, while the BBDC signal is significantly reduced. This is of particular interest for reconstructing the lateral source changes and their precise timing, as the strong BBDC signal may prevent the recognition of these changes.

The removal of dolomite, calcite and quartz from the mineralogical assemblage allows a more statistically robust provenance calculation using our semi-quantitative estimates (based on the partial composition using the nine mineralogical species selected, which have been summed to 100%) and the SedUnMix program. In particular, it allows to clearly differentiate between lateral sediments (i.e., eastern Baffin Island versus western Greenland), which is the main objective of our study. This implies that the weight percentages calculated between the sources are relative and not absolute due to the artificial reduction of the northern Baffin Bay sources. Consequently, we interpret our results in terms of relative change in any given source activity (ice stream dynamics) in time rather than providing a precise estimate of sediment provenance.

Given the distinct lithofacies already described and the mineralogical composition variability, we expect to find variations in sediment provenance within the core. This is well illustrated by comparing the composition of the surface samples (i.e., the top two samples) with the down-core assemblages using a SedUnMix calculation. Large deviations from 100% occur within several layers, indicating major changes in primary sediment sources throughout the core (up to 40 wt%, Fig. 2g). To unravel these sediment provenance changes from the surrounding ice streams, we ran SedUnMix using data from our new mineralogical semi-quantitative estimates from PC16 and from the different possible sources previously determined by Andrews and Eberl (2011) based on box cores and surface sediments. These possible end-members represent sediment signatures from the Jakobshavn Trough, Uummannaq Trough, eastern Baffin Island and northern Baffin Bay (see Table 4 in Andrews and Eberl, 2011). We decided to exclude the Jakobshavn source in our calculations because the core location lies too far north of the Jakobshavn Trough outlet to allow for the presence of Jakobshavn sediments at the study site, as demonstrated by Andrews and Eberl (2011) with analysis of a nearby box core (JCR175-BC06) analysis. Moreover, as our semi-quantitative XRD approach does not yield a detailed record of the Feldspar mineral suite, in comparison to the qXRD approach used by Andrews and Eberl (2011), it precludes a strong distinction between eastern Baffin Island and Jakobshavn signatures, which could induce biases in the provenance calculation.

According to our analysis, the largest non-carbonate and non-quartz contribution is attributed to Uummannaq (average 53.7wt%) and eastern Baffin Island (38.5wt%) sources, while the northern Baffin Bay source is nearly absent from the calculation (0.5wt%) (Fig. 2). The fraction of source not resolved by the program is relatively low (7.3wt%). These values confirm the removal of the BBDC signal (i.e., northern Baffin Bay sources) from the calculation.

Finally, we tested the results of SedUnMix runs on 10 samples measured with the semi-quantitative and qXRD methods. For the last glacial period, the results yield comparable source contributions, with high correlation coefficients for Uummannaq (r=0.90) and eastern Baffin Island (r=0.85) respectively (Supplementary materials, S2), which validate the use of semi-quantitative estimates for the provenance calculation using SedUnMix.

Principal component analysis (PCA) was used to simplify the dataset to only a few primary clusters that retain the main features of the mineralogical and grain-size variability (Davis, 2002). The first two principal components accounted for 52% (PC1 40.7% and PC2 11.3%) of the total variance (Fig. 3). PC1 has positive loadings for finer sediments such as clay and very fine silts (i.e., "glacial flour"; Table 1). Moreover, the positive loadings with the Uummannaq source confirmed the Simon *et al.* (subm.) interpretation of fine-grained sediments originating from Greenland ice streams (Fig. 4g). On the other hand, PC1 has negative loadings with proxies of coarse detrital carbonate layers such as XRD dolomite and calcite, chlorite, CT number (density) and sand (Table 1). Therefore, positive loadings on PC1 likely represent western Greenland ice margin advance stages, while negative loadings on PC1 are associated with coarser sediments originating from either eastern Baffin Island or the northern end of the Baffin Bay. Given this association between mineralogy and grain size, the mineralogical variability is probably a combination of changes in sediment delivery processes at the ice margin and sediment transport (i.e., shown by grain size variability), as well as of sediment provenance.

5. Discussion

5.1. Axial origin (BBDC)

Previous recognition and interpretation of large BBDC layers (i.e., coarse dolomite-rich IRD) in deep Baffin Bay cores (Aksu and Piper, 1987; Andrews *et al.*, 1998; Parnel *et al.*, 2007) and their precise timing in core PC16 (Simon *et al.*, subm.; Figs. 2 and 4) confirmed recent numerical simulations (Ganopolski *et al.*, 2010; Stokes *et al.*, 2012) of a rapid NE LIS and IIS inception and extension. The identification of coarse glaciomarine sediments in the BBDC-9b layer (Fig. 4; Simon *et al.*, subm.), attributed to northern ice streaming episodes as early as 115 ka (at the bottom of the core), is consistent with a substantial ice accumulation and extent over the central and eastern Canadian Arctic Archipelago from 118 ka, as recently modeled by Stokes *et al.* (2012). Simon *et al.* (subm.) suggested two causal processes to explain the deposition of BBDC layers: (1) initiation of fast-flow ice streams with increasing iceberg flux over a long period, and/or (2) rapid collapse of the marine-based ice sheet margin, which delivers numerous icebergs over short periods of time. These causal processes were likely related to external forcing such as the Dansgaard-Oeschger cycles (i.e., mass balance factors), rather to internal ice sheet instabilities (i.e., ice sheet dynamics processes and associated surges) (see Simon *et al.*, subm.).

5.2. Lateral sources

In contrast to the above IRD releases from northern ice streams, fine-grained Ti-rich sediments in the LDC facies have been related to a "lateral" mode characterized by sediment supplies from the advances and/or retreats of western Greenland and eastern Baffin Island ice streams (Aksu and Piper, 1987). However, to date no common provenance proxies (e.g., mineralogy, radiogenic isotopes) have confirmed such a "lateral" source provenance or provided a means to distinguish and quantify between sediment originating from eastern Baffin Island or western Greenland. In this study, the removal of carbonates (dolomite and calcite) from the mineralogical composition allows us to eliminate the strong BBDC imprint, thereby highlighting the variability of sediments from the "lateral" sources (Figs. 2 and 4) and reducing the intermingling impact of Greenland- and Laurentide-supplies. These new results illustrate a clear distinction between western Greenland vs eastern Baffin Island sediment supplies, confirming the usefulness of the mineralogical approach (Fig. 2e). The new data also reveal distinct deposition patterns, with sharp peaks of eastern Baffin Island coarse sediments (Fig. 4a-c) that are interbedded with more steady supplies of Uummannaq fine-grained sediment (Fig. 4h-i). These observations raised two questions: (1) Were the lateral ice streams from western Greenland and

Baffin Island in phase and/or did they relate to distinct processes? And (2), were these lateral ice stream advance/retreat phases driven by climatic and/or oceanic reorganization processes (i.e., mass balance) similar to northern ice streaming or rather related to ice sheet dynamics (i.e., ice sheet surges)?

5.3. Greenland and Baffin Island ice-margin dynamics

The identification and recent interpretation of a series of major submarine fans located at the mouths of western Greenland cross-shelf troughs (e.g., Uummannaq fan at the mouth of the Uummannaq Trough), and marine geophysical and geological data provide clear evidence for a former extension of fast-flowing grounded ice stream across the West Greenland continental shelf during glacial advances (e.g., LGM; Ó Cofaigh *et al.*, 2012, 2013). Such major fan structures are either absent or very limited on the narrower eastern Baffin Island shelf. Ó Cofaigh *et al.* (2012) suggested that these geomorphological discrepancies may be explained by the wider Greenland shelf together with larger ice sheet outlets, as these allow for a large ice stream flow path on the Greenland side, while the shorter continental shelf and smaller fjord outlets from Baffin Island do not favor the development of large ice streams. Furthermore, the repeated occupation of major cross-shelf troughs by successive grounded ice streams during glacial maxima has probably increased the erosion and recycling of Greenland shelf sediments and their delivery offshore into Baffin Bay. As a result, the large fast-flowing ice streams over the large Greenland cross-shelf troughs have probably contributed to increase Greenland sediment erosion and sediment delivery rates into Baffin Bay, while smaller ice stream systems from Baffin Island did not permit high sediment loads to be deposited at the core location during glacial maxima. This would explain the relative dominance of the Uummannaq sediment percentages relative to eastern Baffin Island sediments in the PC16 site (Figs. 2 and 3) despite the greater distance from the western Greenland margin (Fig. 1).

5.3.1. Eastern Baffin Island

The larger eastern Baffin Island sediment pulses (wt% >50%) correspond typically to short intervals (<1 ka) within the BBDC layers (Fig. 4), pointing to similar activating mechanism and deposition processes. The timing of these sharp peaks of eastern Baffin Island sediments corresponds to Dansgaard-Oeschger events (Greenland Interstadial recorded by higher $\delta^{18}O$ values in the NGRIP ice core, Fig. 4b-c), except for a large peak at the end of MIS5a (associated with a fast-flowing northern Baffin Bay ice stream episode, explaining the deposition of the BBDC-7a layer, see Simon *et al.*, subm.). Therefore, the eastern Baffin Island ice margin dynamics was likely driven by external parameters such as Dansgaard-Oeschger cycles rather than internal ice sheet processes.

Hence, we suggest that the contribution of eastern Baffin Island sediments to the central Baffin Bay sedimentary budget (at least at the core location, Fig. 1) would correspond to the release of IRD from the calving and melting of the marine-based glacier outlets and/or grounded ice streams that advanced onto the outer fjords area and possibly onto the outer shelf of Baffin Island (possibly associated with turbidity currents). During interval of glacial retreat and/or fast flowing ice-streams, an IRD sedimentary setting would resume in Baffin Bay with the deposition of BBDC layers, linked to northern sources as indicated by the presence of large amounts of dolomite-rich carbonates (Fig. 4d; Simon *et al.*, subm.) as well as to pulses of coarse sediments from the eastern Baffin Island margin (Figs. 4a-c and 5a). Yet, BBDC layers might also suggest a contribution of carbonate-bearing ice streams from Home Bay, as proposed by Andrews and Eberl (2011). However, at ~10k cal a BP the weight percentage of dolomite in PC16 is ~35%, which is much higher than the 8% dolomite percentages found at the same period in core HU85-079TWC from outer Home Bay (Andrews and Eberl, 2011). From this discrepancy, we hypothesize only minor inputs of Home Bay carbonate sediments during the deposition of BBDC layers. A “distal” sedimentary mode (relative to central Baffin Bay) might explain these coarse IRD horizons during time intervals when ice margins retreated behind their maximum extent, thereby increasing the Baffin Bay surface and most probably oceanic circulation in the bay (Fig. 5a). During such episodes, western Greenland sediments would have been mostly deposited over the Greenland shelf rather than being transported further away towards the centre of the bay (Fig. 5a).

5.3.2. Western Greenland (Uummannaq)

Interbedded with the rapidly deposited coarse sediments from northern and western Baffin Bay origin, the large increases in Uummannaq source, fine-grained sediments are interpreted as indicating a stable and relatively long-duration (>5 ka) Greenland ice sheet expansion and development, notably over the Greenland shelf along Uummannaq Trough. Large increases in Uummannaq sediment delivery (i.e., with wt% >60%) occurred within the 110–105, 91–85, 72–63 and 32–16 ka intervals, while two additional smaller Uummannaq weight percentage peaks are found between 58–55 ka and around 44 ka (Fig. 4h). From these results, we suggest that the Uummannaq Trough ice stream expanded over the Greenland shelf immediately after the onset of the northern glacial inception (as early as 110 ka) and was followed by subsequent advances during colder episodes. Two of these advances are characterized by wt% values of nearly 100%. They occurred during an "extended MIS2" interval (32–16 ka) and during MIS4 (72–63 ka). The smaller ones (i.e., 80 wt%) correspond to MIS5b (91–85 ka) and late MIS5d (110–105 ka) intervals, respectively (Fig. 4h).

The recording of nearly 100% of Uummannaq sediments during the LGM confirms the development of a grounded, fast-flowing ice stream in the Uummannaq Trough as far as the shelf edge that delivered glaciomarine sediments to the Uummannaq fan and into deep central Baffin Bay, as recently proposed by Ó Cofaigh *et al.* (2012, 2013). The observed mineralogical signatures indicate large Uummannaq ice stream extent and/or activity from ~32 to nearly 12 ka (Fig. 4h), which provide evidence for an extensive grounded fast-flowing ice stream on the Uummannaq

Trough. Therefore, from our study, we propose that the last massive growth of the GIS (reaching a maximum extent during the LGM, stricto sensu) started from ~32 ka, while substantial ice stream retreat from the Greenland shelf did not begin prior to ~16k cal a BP.

The other Uummannaq sediment pulses (e.g., MIS5d and 5b, MIS4) most probably corresponded to somewhat reduced advances and thickenings of the GIS outlet glaciers on the Greenland shelf. However, very high percentages of Uummannaq sediments (almost 100%) and a fine grain size signature (large peak of glacial flour) within the MIS4 interval (Fig. 4i) could be attributed to advances of the western Greenland ice margin comparable to those of MIS2 in scale. Unfortunately, 11 cm of sediments corresponding broadly to the 69–65.5 ka interval are missing, therefore preventing a precise interpretation of the glacial advance within that interval. Nonetheless, the hypothesis of a large advance of the ice margin on the western Greenland shelf at that time is in accordance with the lower relative sea-level (RSL; Fig. 4f), low July insolation values (Laskar et al., 2004) and complementary evidence for the expansion of an ice shelf offshore southwestern Greenland during MIS4 (Seidenkrantz *et al.*, 2010). From our study, we cannot ascertain an advance of the Uummannaq ice stream to the shelf edge during MIS4. However, lower PC1 values during MIS4, -5d/b compared to MIS2, together with facies dissimilarities such as the amount of clay (Fig. 4i) or typical single domain magnetic grains (Simon *et al.*, subm.), suggest a somewhat smaller ice stream expansion during MIS4, -5d/b, as well as a unique maximum extent to the shelf edge (i.e., MIS2) during the last glacial cycle. In this scenario of glacial margin advances, the central Baffin Bay sedimentary regime would have been in an "ice proximal" mode (Fig. 5b) during MIS2 and to a lesser extent MIS4, -5d/b (and additional short intervals; Fig. 4h) in contrast to periods when ice margins occupied an inner position over continental shelves. During these colder episodes, extensive shelf-edge terminating ice streams together with perennial sea ice cover contribute to reduce the marine surface area of

Baffin Bay modifying oceanic circulation and sediment delivery into the bay (Fig. 5b).

5.4. Comparison with numerical simulation and sea-level records

The LGM and pre-LGM Greenland ice stream dynamics reconstructed above is of particular importance with regard to ice sheet modeling experiments, suggesting that the maximum extent of the ice sheets in the circum-North Atlantic was comparable during both MIS5d/b and 2 (at least in surface extent, Ganopolski *et al.*, 2010). Our data point to major advances of the Greenland ice margin during MIS5d/b and MIS4. However it is unlikely that they reached the MIS2 ice-limits. Our findings are consistent with numerical simulations of ice sheet growth during the last glacial cycle (Stokes *et al.*, 2012; Ganopolski *et al.*, 2010; Marshall and Koutnik, 2006) associated with permanent ice-covered sea surface and a reduced oceanic circulation in Baffin Bay (Fig. 5b; Hiscott *et al.*, 1989). On the other hand, according to simulations, periods of Greenland ice stream retreat are associated with warmer temperatures (shown by higher NGRIP $\delta^{18}O$ values, Fig. 4b) and the probable advection of warm Atlantic waters into the bay (Hiscott *et al.*, 1989; Jennings *et al.*, 2011) contributing to reduce the sea ice cover (Srivastava *et al.*, 1987). During these "warm" intervals, an increased cyclonic activity in Baffin Bay (Fig. 5a) would boost the winter snowfall on the Innuitian region (Stokes *et al.*, 2012; Ganopolski *et al.*, 2010; Marshall and Koutnik, 2006) contributing in turn to initiate northern fast-flowing ice streams (Simon *et al.*, subm.). Such intervals correspond here to the "long-duration" BBDC layers in core PC16, when intense ice streaming occurred in northern Baffin Bay and, to as lesser extent, along the eastern Baffin Island (Fig. 4c-d; Simon *et al.*, subm.). Therefore, Greenland ice stream systems would have preferentially retreated during periods of increased advection of Atlantic water masses into Baffin Bay, thereby contributing to more unstable ice margin activities during the last glacial cycle. However, while our dataset exhibits considerable coherence with such a scenario, it cannot be said to strongly support the scenario either. Proxies for the advections of Atlantic water masses (e.g., Atlantic fauna, foraminifera assemblage, sea surface temperature, sea ice cover) into Baffin Bay need to be tested to confirm this hypothesis. Such an incursion of Atlantic waters (via the West Greenland Current) has been recently documented during the last deglaciation by characteristic benthic foraminifera assemblages in cores from the Greenland shelf (Sheldon, 2012).

Advances of the Uummannaq ice stream and sea level variations (Waelbroeck *et al.*, 2002) were apparently in phase during the last glacial cycle, which strongly support our interpretations (Fig. 4f, h). Indeed, during the SL-lowerings, fast-flowing grounded ice streams advanced rapidly towards the (shallower) Greenland outer shelf, providing more Uummannaq sediments to central Baffin Bay. Meanwhile eastern Baffin Island and northern ice stream systems probably exhibited relatively slower and reduced ice stream developments and low calving rates, together with decrease icebergs circulation in the bay due to perennial sea ice cover, reducing their inputs to the total Baffin Bay sedimentary budget.

6. Conclusions

The lithofacies and mineralogical properties of central Baffin Bay sediments spanning the last glacial cycle (i.e., 115 ka) are fairly consistent with recent ice-sheet numerical simulations (given respective time resolution and uncertainty) for a rapid glacial inception and subsequent glacial growth and decay of the NE Laurentide, southern Innuitian and western Greenland Ice Sheets following the last interglacial. Development of the ice sheets and associated ice streams occurred as early as the MIS5d and MIS5b sub-stages. Maximum ice-extent occurred during the early part of MIS4 (72-63 ka) and during an extended-MIS2 (32-16 ka). Sediment signatures during MIS2 illustrate maximum extension of the Uummannaq ice stream to the shelf edge, whereas that of MIS4 sediments suggests a reduced Uummannaq ice stream expansion. The contribution of the eastern Baffin Island glaciers to the central Baffin

Bay sedimentary budget is depicted by short-lived episodes of IRD and turbidity current activity in phase with NE Laurentide and southern Innuitian ice streaming episodes (i.e., BBDC events). Such coarse IRD intervals are seen as an "ice distal" pattern when the ice margins retreated behind their maximum extents, increasing the Baffin Bay marine surface area. On the other hand, large increases of Uummannaq fine-grained sediments are interpreted as stable and continuous expansions of the Greenland Ice Sheet during much colder episodes. These episodes are represented with an "ice proximal" pattern wherein ice margins had advanced as far as the shelf edge, narrowing the Baffin Bay marine realm. We also propose that short-lived IRD events in Baffin Bay were mostly related to northern and eastern ice stream dynamics (i.e., NE Laurentide/Innuitian Ice Sheets and Baffin Island glaciers) due to climate forcings, while western Greenland sediments corresponded more to the extension and thickening of Greenland ice streams onto the outer shelf during glacial maxima. We suggest that these timing differences are explained by distinct dynamic of the smaller Baffin Island glaciers and NE Laurentide/Innuitian ice streams, compared to that of the larger Greenland ice streams.

Acknowledgements

We thank Michel Preda (UQAM) for assistance with XRD measurements, Pierre Francus and Arnaud de Coninck (INRS-ETE) for their help during the ITRAX™ core scanning. We are grateful to the captain, officers, crew and scientists on board the CCGS Hudson during the HU2008-029 expedition. This study is part of the Canadian contribution to the Past4Future project. Support from MDEIE (Ministère du Développement Économique, de l'Innovation et de l'Exportation), NSERC (Natural Sciences and Engineering Research Council of Canada) through ship time and discovery grants to G.S. and C.H.M., FQRNT (Fonds Québécois de la Recherche sur la Nature et les Technologies) and the CFI (Canadian Foundation for Innovation) is acknowledged.

References

Aksu AE. 1981. Late Quaternary stratigraphy, paleoenvironmentology, and sedimentation history of Baffin Bafy and Davis Strait. PhD. Thesis, Dalhousie University, Halifax, NS.

Aksu AE. 1983. Holocene and Pleistocene dissolution cycles in deep-sea cores of Baffin Bay and Davis Strait: paleoceanographic implications. Marine Geology **53**: 331-348.

Aksu AE. 1985. Climatic and oceanographic changes over the past 400,000 years: evidence from deep sea cores on Baffin Bay and Davis Strait. In Quaternary environments: Eastern Canadian Árctic, Baffin Bay and western Greenland. Edited by J.T. Andrews. Allen & Unwin, Boston, pp. 181-209.

Aksu AE, Piper DJW. 1987. Late Quaternary sedimentation in Baffin Bay. Canadian Journal of Earth Sciences **24**: 1833-1846.

Alley RB, Andrews JT, Brigham-Grette J, et al. 2010. History of the Greenland Ice Sheet: paleoclimatic insights. Quaternary Science Reviews **29**: 1728-1756.

Andrews JT, Kirby M, Aksu AE, et al. 1998. Late Quaternary Detrital Carbonate (DC-) layers in Baffin Bay marine sediments (67°-74° N): correlation with Heinrich events in the North Atlantic? Quaternary Science Reviews **17**: 1125-1137.

Andrews JT. 2000. Icebergs and iceberg rafted detritus (IRD) in the North Atlantic: facts and assumptions. Oceanography **13**:100-108.

Andrews JT, MacLean B. 2003. Hudson Strait ice streams: a review of stratigraphy, chronology and links with North Atlantic Heinrich events. Boreas **32**: 4-17.

Andrews JT, Eberl DD. 2011. Surface (sea floor) and near-surface (box cores) sediment mineralogy in Baffin Bay as a key to sediment provenance and ice sheet variations. Canadian Journal of Earth Sciences **48**: 1307-1328.

Andrews JT, Eberl DD. 2012a. Determination of sediment provenance by unmixing the mineralogy of source-area sediments: The “SedUnMix” program. Marine Geology **291–294**: 24-33.

Andrews JT, Barber DC, Jennings AE, et al. 2012b. Varying sediment sources (Hudson Strait, Cumberland Sound, Baffin Bay) to the NW Labrador Sea slope between and during Heinrich events 0 to 4. Journal of Quaternary Science **27**: 475-484.

Azetsu-Scott K, Clarke A, Falkner K. 2010. Calcium carbonate saturation states in the waters of the Canadian Arctic Archipelago and the Labrador Sea. Journal of Geophysical Research **115**: C11021.

Blott SJ, Pye K. 2001. GRADISTAT: a grain size distribution and statistics package for the analysis of unconsolidated sediments. Earth Surface Processes and Landforms **26**: 1237-1248.

Bigg GR. 1999. An estimate of the flux of iceberg calving from Greenland. Arctic, Antarctic, and Alpine Research, **31**: 174– 178.

Bigg GR, Wadley MR. 2001. The origin and flux of icebergs released into the Last Glacial Maximum Northern Hemisphere oceans: the impact of ice-sheet topography. Journal of Quaternary Science **16**: 565-573.

Bond GC, Lotti R. 1995. Iceberg Discharges into the North Atlantic on Millennial Time Scales During the Last Glaciation. Science **267**: 1005-1010.

Bond GC, Showers W, Elliot M, et al. 1999. The North Atlantic's 1–2 kyr climate rhythm: relation to Heinrich Events, Dansgaard/Oeschger cycle and the Little Ice Age. In Clark, P.; Webb, R.; Keigwin, L.. Mechanisms of Global Climate Change at Millennial Time Scales. Geophysical Monograph Series. 112. Washington, DC: American Geophysical Union. pp. 35–58.

Briner JP, Miller GH, Davis PT, et al. 2003. Last Glacial Maximum ice sheet dynamics in Arctic Canada inferred from young erratics perched on ancient tors. Quaternary Science Reviews **22**: 437-444.

Briner JP, Miller GH, Davis PT, et al. 2006. Cosmogenic radionuclides from fiord landscapes support differential erosion by overriding ice sheets. Geological Society of America Bulletin **118**: 406-420.

Briner JP, Overeem I, Miller G, et al. 2007. The deglaciation of Clyde Inlet, northeastern Baffin Island, Arctic Canada. Journal of Quaternary Science **23**(3): 223-232.

Campbell DC, de Vernal A. 2009. CCGS Hudson Expedition 2008029: Marine geology and paleoceanography of Baffin Bay and adjacent areas, Nain, NL to Halifax, NS, August 28- September 23; Geological Survey of Canada, Open File 5989, 1 DVD

Clark PU, Mix AC. 2002. Ice Sheets and sea level of the Last Glacial Maximum. Quaternary Science Reviews **21**: 1-7.

Davis JC. 2002. Statistics and Data Analysis in Geology, 3rd Edition. John Wiley and Sons, New York, 656 pp.

Dowdeswell JA, Maslin MA, Andrews JT, et al. 1995. Iceberg production, debris rafting, and the extent and thickness of Heinrich layers (H-1, H-2) in North Atlantic sediments. Geology **23**: 301-304.

Dowdeswell JA, Hagen J, Björnsson H, et al. 1997. The Mass Balance of Circum-Arctic Glaciers and Recent Climate Change. Quaternary Research **48**: 1-14.

Dowdeswell JA, Elverhøi A, Andrews JT, et al. 1999. Asynchronous deposition of ice-rafted layers in the Nordic seas and North Atlantic Ocean. Nature **400**: 348-351.

Dyke AS, Andrews JT, Clark PU, et al. 2002. The Laurentide and Innuitian Ice Sheets during the Last Glacial Maximum. Quaternary Science Reviews **21**: 9–31.

Dyke A. 2004. An outline of North American deglaciation with emphasis on central and northern Canada. Developments in Quaternary Science **2**: 373-424.

Eberl DD. 2003. User Guide to RockJock: A program for determining quantitative mineralogy from X-ray diffraction data. United States Geological Survey, Open File Report 03-78, Washington, DC, 40 p.

Eberl DD. 2004. Quantitative mineralogy of the Yukon River system: Variations with reach and season, and determining sediment provenance. American Mineralogist **89**: 1784-1794.

England JH, Atkinson N, Bednarski, J, et al. 2006. The Innuitian Ice Sheet: configuration, dynamics and chronology. Quaternary Science Reviews **25**: 689-703.

England JH, Furze MFA, Doupé JP. 2009. Revision of the NW Laurentide Ice Sheet: implications for paleoclimate, the northeast extremity of Beringia, and Arctic Ocean sedimentation. Quaternary Science Reviews **28**: 1573–1596.

Ehrhardt A, Gohl K, Neben S, et al. 2008. Davis Strait and Ungava Fault Zone: First results from a recent geophysical survey. Eos Trans. AGU, 89(53), Fall Meet. Suppl., AGU Fall Meeting, San Francisco.

Funder S, Kjellerup K, Kjær K, et al. 2011. The Greenland Ice Sheet, the last 300,000 years: A review. In Quaternary Glaciations, Extent and Chronology. Part IV. A Closer Look. Developments in Quaternary Science 16. Elsevier, Amsterdam.

Ganopolski A, Calov R, Clausen M. 2010. Simulation of the last glacial cycle with a coupled climate ice-sheet model of intermediate complexity. Climate of the Past **6**: 229-244.

Harrison JC, St-Onge MR, Petrov O, et al. 2011. Geological map of the Arctic. Geological Survey of Canada, Map 2159A, scale 1:5000000.

Hemming SR. 2004. Heinrich events: Massive late Pleistocene detritus layers of the North Atlantic and their global climate imprint. Rev. Geophys. **42**: RG1005.

Hillaire-Marcel C, de Vernal A, Aksu A, et al. 1989. High-resolution isotopic and micropaleontological studies of upper Pleistocene sediment at ODP site 645, Baffin Bay. In: Srivastava, S.P. et al. (Eds), Proceedings of the Ocean Drilling Program, Scientific Results leg 105-B, 599-616.

Hiscott RN, Aksu AE, Nielsen OB. 1989. Provenance and dispersal patterns, Pliocene-Pleistocene section at site 645, Baffin Bay. In: Srivastava, S.P. et al. (Eds), Proceedings of the Ocean Drilling Program, Scientific Results leg 105, 31-52. Doi:10.2973/odp.proc.sr.105.117.1989.

Hogan KA, Dowdeswell JA, Ó Cofaigh C. 2012. Glacimarine sedimentary processes and depositional environments in an embayment fed by West Greenland ice streams. Marine Geology **311–314**: 1-16.

Holland DM, Thomas RH, De Young B, et al. 2008. Acceleration of Jakobshavn Isbrae triggered by warm subsurface ocean waters. Nature Geoscience **1**: 659-664.

Hulbe CL, MacAyeal DR, Denton GH, et al. 2004. Catastrophic ice shelf breakup as the source of Heinrich event icebergs, Paleoceanography **19**: PA1004.

Jennings AE, Sheldon C, Cronin TM, et al. 2011. The Holocene history of Nares Strait: Transition from glacial bay to Arctic-Atlantic throughflow. Oceanography **24**: 26–41.

Laskar JP, Robutel F, Joutel F, et al. 2004.A long term numerical solution for the insolation quantities of the Earth. Astronomy & Astrophysics **428**: 261-285.

Li G, Piper DJW, Campbell DC. 2011. The Quaternary Lancaster Sound trough-mouth fan, NW Baffin Bay. Journal of Quaternary Science **26**: 511-522.

MacAyeal DR. 1993. Binge-purge oscillations of the Laurentide Ice Sheet as a cause of the North Atlantic's Heinrich events. Paleoceanography **8**: 775–784.

Maclean B, Williams GL, Srivastava SP. 1990. Geology of Baffin Bay and Davis Strait. In Geology of Canada No.2: Geology of the continental margin of eastern Canada, M.j. Keen and G.L. Williams (eds.). Geological Survey of Canada, p. 293-348.

MacLean B, Blasco S, Bennett R, et al. 2010. Ice keel seabed features in marine channels of the central Canadian Arctic Archipelago: evidence for former ice streams and iceberg scouring. Quaternary Science Reviews **29**: 2280–2301.

Marcott SA, Clark PU, Padman L, et al. 2011. Ice-shelf collapse from subsurface warming as a trigger for Heinrich events. Proceedings of the National Academy of Sciences **108**: 13415-13419.

Marshall SJ, Koutnik M.R. 2006. Ice sheet action versus reaction: Distinguishing between Heinrich events and Dansgaard-Oeschger cycles in the North Atlantic. Paleoceanography **21**: PA2021.

Ó Cofaigh C, Andrews JT., Jennings AE, et al. 2012. Glacimarine lithofacies, provenance and depositional processes on a West Greenland trough-mouth fan. Journal of Quaternary Science. doi:10.1002/jqs.2569.

Ó Cofaigh C, Dowdeswell JA, Jennings AE, et al. 2013. An extensive and dynamic ice sheet on the West Greenalnd shelf during the last glacial cycle. Geology **41**: 219-222.

Parnell J, Bowden S, Andrews JT, et al. 2007. Biomarker determination as a provenance tool for detrital carbonate events (Heinrich events?): Fingerprinting Quaternary glacial sources into Baffin Bay. Earth and Planetary Science Letters **257**: 71-82.

Rignot E, Mouginot J. 2012, Ice flow in Greenland for the International Polar Year 2008. Geophysical Research Letters **39**: L11501.

Seidenkrantz MS, Kuijpers A, Aagaard-Sørensen S, et al. 2010. Glacial ocean circulation and shelf edge glaciation offshore SW Greenland during the past 75.000 years. Geophysical Research Abstract, vol. 12, EGU2010-4721.

Sheldon C. 2012. The deglacial history and paleoceanography of the Uummannaq System, West Greenland. MSc thesis, University of Colorado.

Simon, Q., G. St-Onge, C. Hillaire-Marcel (2012), Late Quaternary chronostratigraphic framework of deep Baffin Bay glaciomarine sediments from high-resolution paleomagnetic data, *Geochemistry, Geophysics, Geosystems*, 13, Q0AO03, doi:10.1029/2012GC004272.

Simon Q, Hillaire-Marcel C, St-Onge G. submitted. Detrital carbonate events in Baffin Bay during the last climatic cycle: Their timing vs. the Greenland Dansgaard-Oeschger cycles and North Atlantic Heinrich events. Paleoceanography.

Srivastava SP, Arthur M, Clement B. 1987. Introduction, In:Proc. ODP, Init. Repts., 105. Eds: Srivastava, S.P., Arthur, M., Clement, B., College Station, TX (Ocean Drilling Program), 5-20.

Srivastava SP. 1989. Proceedings of the Ocean Drilling Program, Scientific Results. Baffin Bay and Labrador Sea. Leg 105, Sites 645-647.

St-Onge G, Mulder T, Francus P, et al. 2007. Continuous physical properties of cored marine sediments, in Developments in Marine Geology. Proxies in late Cenozoic paleoceanography, vol. 1, edited by C. Hillaire-Marcel, and A. de Vernal, Elsevier, Amsterdam, The Netherlands, 63-98.

Stokes CR, Clark CD. 2001. Palaeo-ice streams. Quaternary Science Reviews **20**: 1437–1457.

Stokes CR, Tarasov L. 2010. Ice streaming in the Laurentide Ice Sheet: a first comparison between data-calibrated numerical model output and geological evidence. Geophysical Research Letters **37**: L01501.

Stokes CR, Tarasov L, Dyke AS. 2012. Dynamics of the North American Ice Sheet Complex during its inception and build-up to the Last Glacial Maximum. Quaternary Science Reviews **50**: 86-104.

Tang C, Ross C, Yao T, et al. 2004. The circulation, water masses and sea-ice of Baffin Bay. Progress in Oceanography **63** : 183-228.

Thorez J. 2003. L'argile, minéral pluriel, Bulletin de la Société Royale des Sciences de Liège, **72**: 19-70.

Waelbroeck C, Labeyrie L, Michel E, et al. 2002. Sea-level and deep water temperature changes derived from benthic foraminifera isotopic records. Quaternary Science Reviews **21**: 295-305.

Wang Z, Cochelin ASB, Mysak LA, et al. 2005. Simulation of the last glacial inception with the green McGill Paleoclimate Model. Geophysical Research Letters **32**: L12705.

Weidick A, Bennike O. 2007. Quaternary glaciation history and glaciology of Jakobshavn Isbræ and the Disko Bugt region, West Greenland: a review, Geological Survey of Denmark and Greenland Bulletin 14, 78 pp.

Wolff EW, Chappellaz J, Blunier T, et al. 2010. Millennial-scale variability during the last glacial: The ice core record. Quaternary Science Review **29**: 2828-2838.

Young NE, Briner JP, Rood DR, et al. 2012. Glacier extent during the Younger Dryas and 8.2-ka event on Baffin Island, Arctic Canada. Science **337**: 1330-1333.

Table 1. Principal component analysis (PCA) data and Pearson correlation coefficients.

Loading	PC1	PC2	PC3	PC1	PC2
Eigenvalues	10.57	2.94	2.6		
Variance (%)	40.68	11.34	9.99		
Variance (cumulative %)	40.68	52.02	62.01		
				r	r
Quartz	0.10	0.10	0.34	0.32	0.17
K-Feldspar	0.10	0.42	0.03	0.33	0.73
Plagioclase	0.20	0.25	-0.03	0.66	0.42
Amphibole	0.23	0.15	-0.08	0.76	0.26
Pyroxene	0.26	0.01	0.04	0.83	0.01
Calcite	-0.20	-0.33	-0.16	-0.66	-0.56
Dolomite	-0.24	-0.18	-0.16	-0.79	-0.32
Smectite	0.13	0.02	0.34	0.42	0.04
Illite	0.11	0.23	-0.46	0.35	0.40
Kaolinite	-0.05	-0.18	0.46	-0.16	-0.31
Chlorite	-0.19	-0.23	0.18	-0.63	-0.39
Gravel%	-0.13	0.24	-0.05	-0.42	0.41
Sand%	-0.27	0.09	0.06	-0.89	0.15
>63 μm (%)	-0.27	0.16	0.03	-0.87	0.28
Silt (0-63 μm) (%)	0.20	-0.07	0.18	0.64	-0.12
Clay (0-2μm) (%)	0.24	-0.20	-0.23	0.77	-0.34
Very fine silts (2-4 μm) (%)	0.29	-0.08	0.00	0.94	-0.14
"Glacial Flour" (0-4 μm) (%)	0.27	-0.17	-0.17	0.87	-0.29
Pseudo-Sortable Silt (8-63 μm) (%)	-0.11	0.04	0.24	-0.35	0.07
CT# (density)	-0.19	-0.07	-0.14	-0.61	-0.11
Ti (peak surface)	0.25	0.09	0.14	0.81	0.16
Uummannaq weight%	0.14	-0.34	-0.07	0.45	-0.59
Eastern Baffin Island weight%	-0.19	0.28	0.05	-0.60	0.48
Northen Baffin Bay weight%	0.11	-0.10	0.13	0.36	-0.17
Not Resolved weight%	0.01	0.22	0.04	0.04	0.37

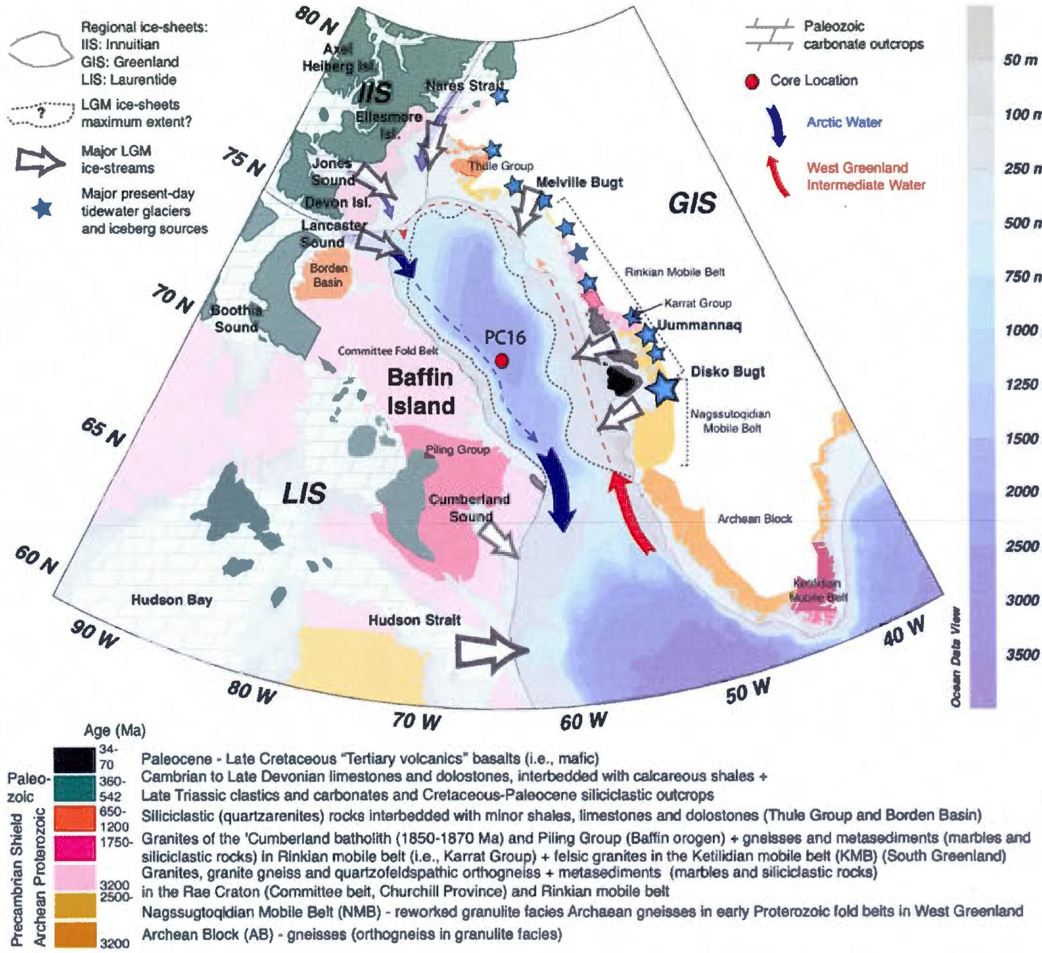

Figure 1. Baffin Bay general map and core location. The bathymetry, oceanic circulation and simplified bedrock geology are from http://www.geus.dk; Harrison *et al.* (2011) and Tang *et al.* (2004). Major present-day tidewater glacier locations are from Bigg (1999). Last Glacial Maximum limits of the Greenland (GIS), Innuitian (IIS) and Laurentide (LIS) ice sheets and major ice stream locations are adapted from Funder *et al.* (2011), Ó Cofaigh *et al.*, (2012), Dyke (2004), England *et al.* (2006), Li *et al.* (2011).

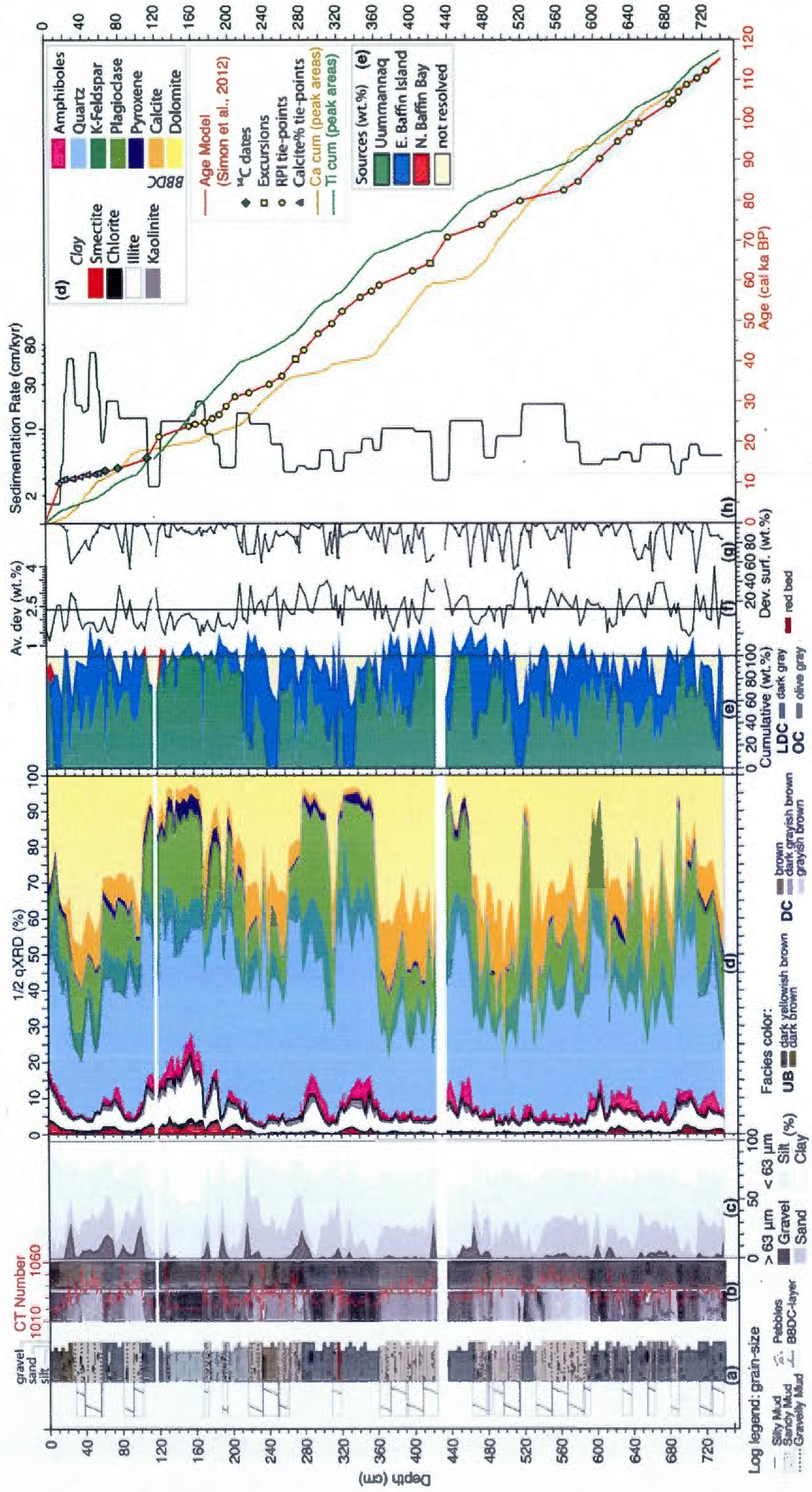
Depth (cm)
gravel
sand
silt
CT Number
1010
1060
1/2 qXRD (%)
Av. dev (wt.%)
Sedimentation Rate (cm/kyr)
(a)
(b)
(c)
(d)
(e)
(f)
(g)
(h)
Clay
Smectite
Chlorite
Illite
Kaolinite
Amphiboles
Quartz
K-Feldspar
Plagioclase
Pyroxene
Calcite
Dolomite
BBDC
Age Model
(Simon et al., 2012)
¹⁴C dates
Excursions
RPI tie-points
Calcite% tie-points
Ca cum (peak areas)
Ti cum (peak areas)
Sources (wt.%)
Uummannaq
E. Baffin Island
N. Baffin Bay
not resolved
Age (cal ka BP)
Cumulative (wt.%)
Dev. surf. (wt.%)
Log legend: grain-size
Silty Mud
Sandy Mud
Gravelly Mud
Pebbles
BBDC-layer
> 63 µm
Gravel
Sand
< 63 µm
Silt
Clay
(%)
Facies color:
UB
dark yellowish brown
dark brown
DC
brown
dark grayish brown
grayish brown
LDC
dark grey
OC
olive gray
red bed

Figure 2. (page 148). Core PC16 lithostratigraphy and age model. (a) Simplified stratigraphy log (see legend for details). (b) CAT-Scan image (X-ray) of the core (left) and associated CT number (density proxy). High-resolution digital image (right). (c) Grain size distribution (%) for clay (0-2 μm), silt (2-63 μm), sand (63 μm-2 mm) and gravel (>2 mm). (d) Relative XRD mineralogical assemblages (calculated on the most abundant minerals and summed to 100%). (e) Cumulative wt% contributions from the 3 major sediment-sources (Uummannaq, E. Baffin Island and Northern Baffin Bay) calculated from the mineralogical assemblages using SedUnMix (Andrews and Eberl, 2012a). "Not resolved" indicates that the sum wt% was <100 %. (f) Average deviations. (g) Mineralogical-assemblage deviation (wt%) between surface and down-core samples. Large deviations from 100% indicate major changes in mineral composition. (h) core PC16 age model (red curve; Simon *et al.*, 2012) and associated sediment accumulation rates (SAR). The Ti (green) and Ca (orange) cumulative curves represent the cumulative addition of titanium and calcium relative concentrations (peak areas measured with the μXRF ITRAX™ core scanner). Gradient changes give independent information about sedimentary depositional process variability.

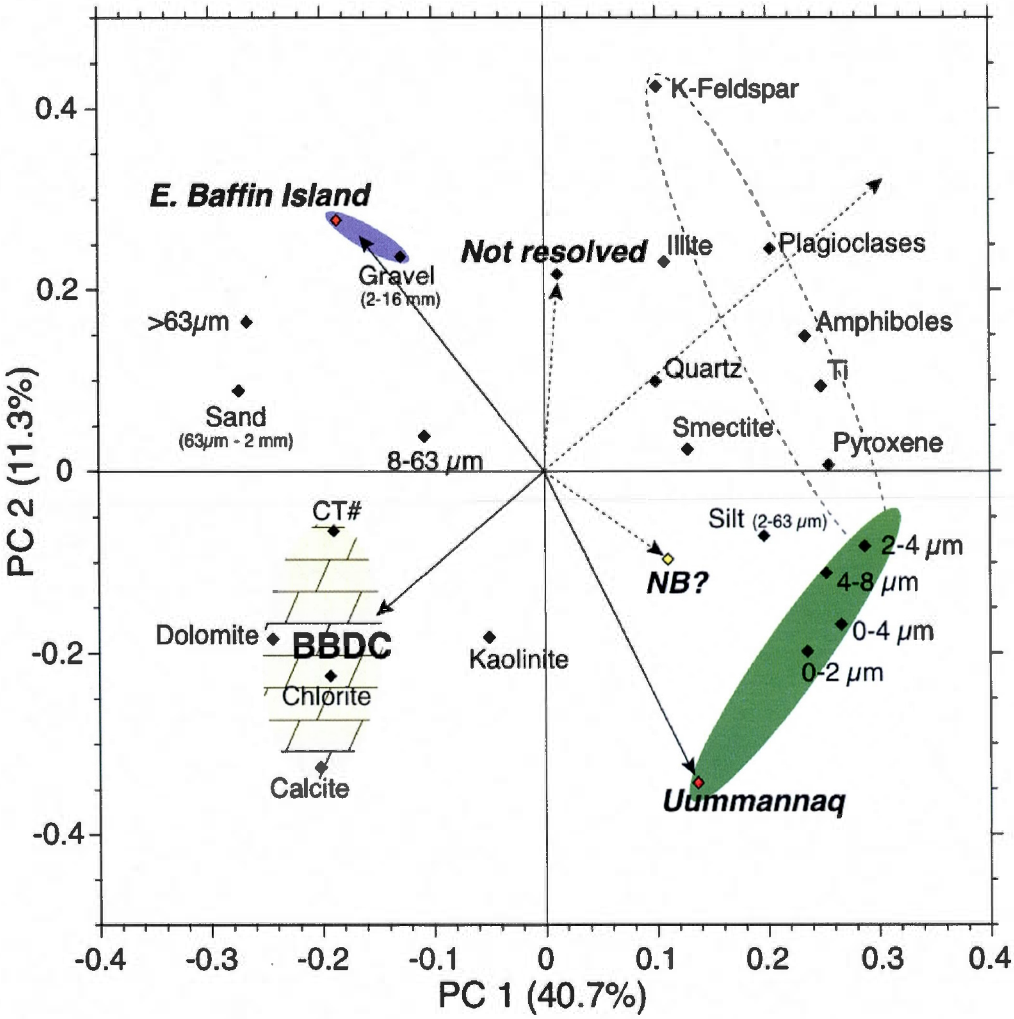

Figure 3. Principal component analysis (PCA) of the mineralogical and grain-size dataset. The loading scores for PC1 vs. PC2 explain respectively 40.7% and 11.3% of the total variance. PCA analysis illustrates the two sedimentary modes in Baffin Bay during the last glacial cycle.

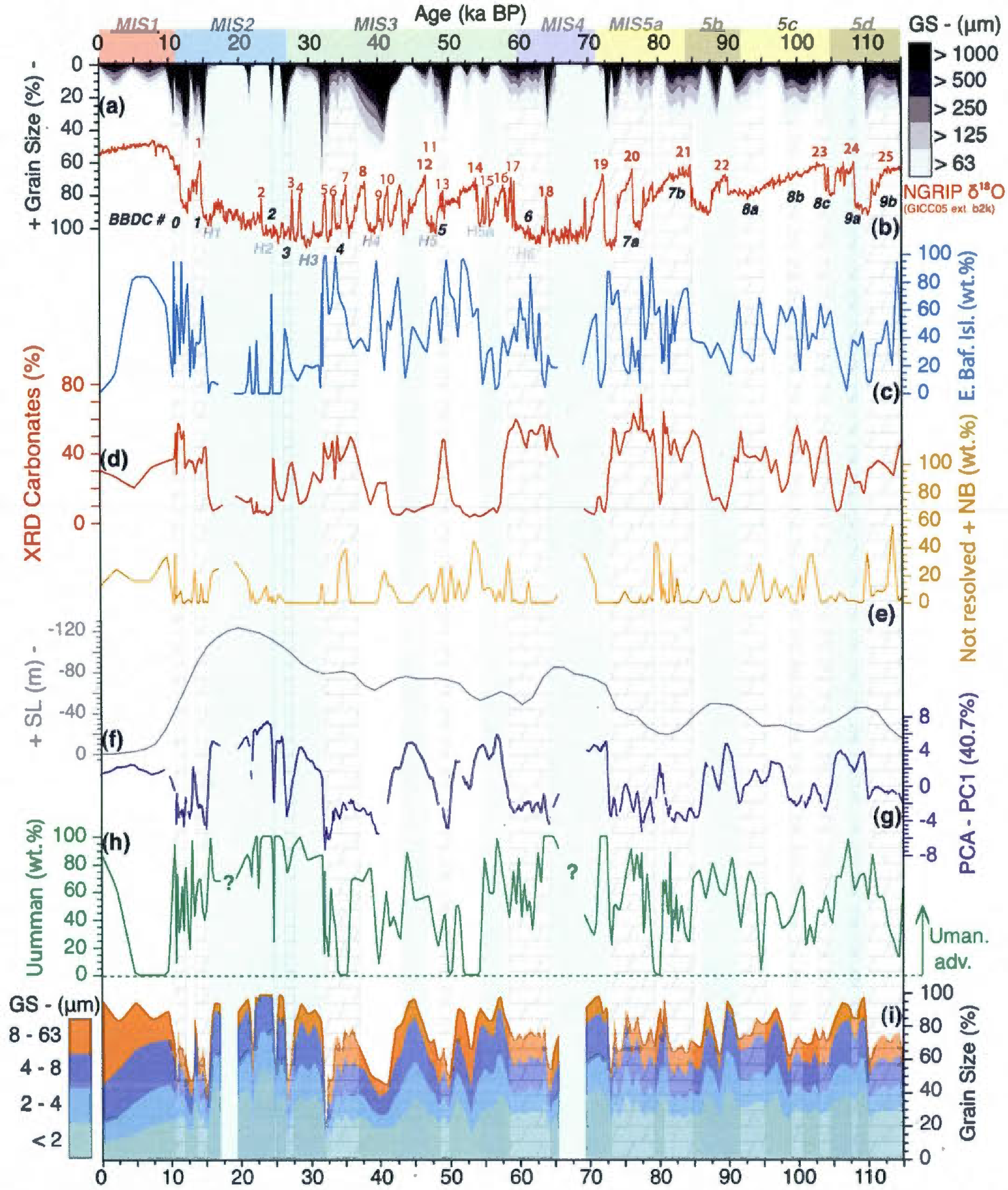
Age (ka BP)
MIS1
MIS2
MIS3
MIS4
MIS5a
5b
5c
5d
GS - (µm)
> 1000
> 500
> 250
> 125
> 63
+ Grain Size (%) -
NGRIP δ18O
(GICC05 ext. b2k)
BBDC #
E. Baf. Isl. (wt.%)
XRD Carbonates (%)
Not resolved + NB (wt.%)
+ SL (m) -
PCA - PC1 (40.7%)
Uumman (wt.%)
Uman. adv.
GS - (µm)
8 - 63
4 - 8
2 - 4
< 2
Grain Size (%)

Figure 4. (page 151). Grain size and sediment provenance variability during the last glacial cycle. (a) Coarse grain size distribution (%) per size fraction (see legend). (b) NGRIP $\delta^{18}O$ and Greenland interstadials (1-25) are from www.icecores.dk (Wolff *et al.*, 2010). (c) Eastern Baffin Island wt% contribution. (d) XRD carbonate (dolomite and calcite) relative percentages. (e) "Not resolved" + northern Baffin Bay wt% contribution. (f) Sea level record (SL, y-axis reverse) from Waelbroeck *et al.* (2002). (g) First component (40.7%) of the PCA analysis. (h) Uummannaq wt% contribution. (i) Grain size distribution (%) of clay and silt fractions. Marine isotopic stages (MIS1 to MIS5d) are represented by color boxes along the age axis. Baffin Bay Detrital Carbonate (BBDC) layers are represented by a vertical brick pattern and numbered according to Simon *et al.* (subm.).

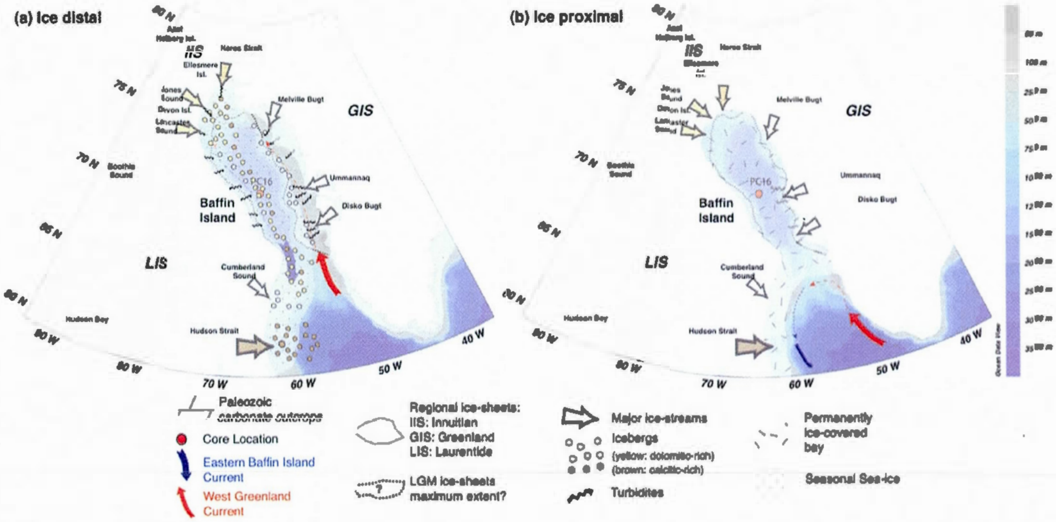

Figure 5. Simplified Baffin Bay paleogeography during the last glacial cycle. (a) Ice distal “axial” mode characterized by ice rafted debris sediments originating from the northern ice streams, and by lateral turbidites from Baffin Island ice streams. (b) Ice proximal "lateral" mode characterized by Greenland and Baffin Island glacial flour sediments corresponding to a permanently ice-covered bay, and by large ice stream extents.

Supplementary material

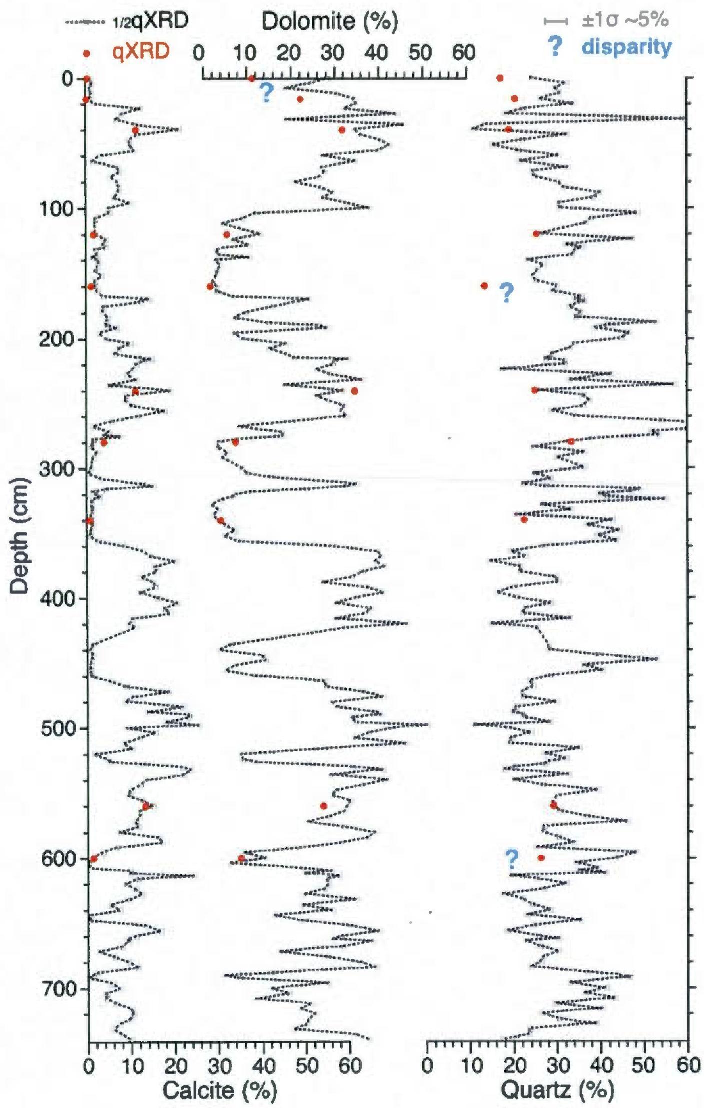

S1. Mineralogical estimates comparison between semi-quantitative XRD and quantitative XRD methods. Estimate weight% of calcite, dolomite and quartz are presented. 201 samples were measured routinely by the semi-quantitative XRD method, while 10 samples were measured by the quantitative XRD method (see text for details). The error bars represent ±1σ ~5%. The interrogative dots represent depth where major disparities between the results were found.

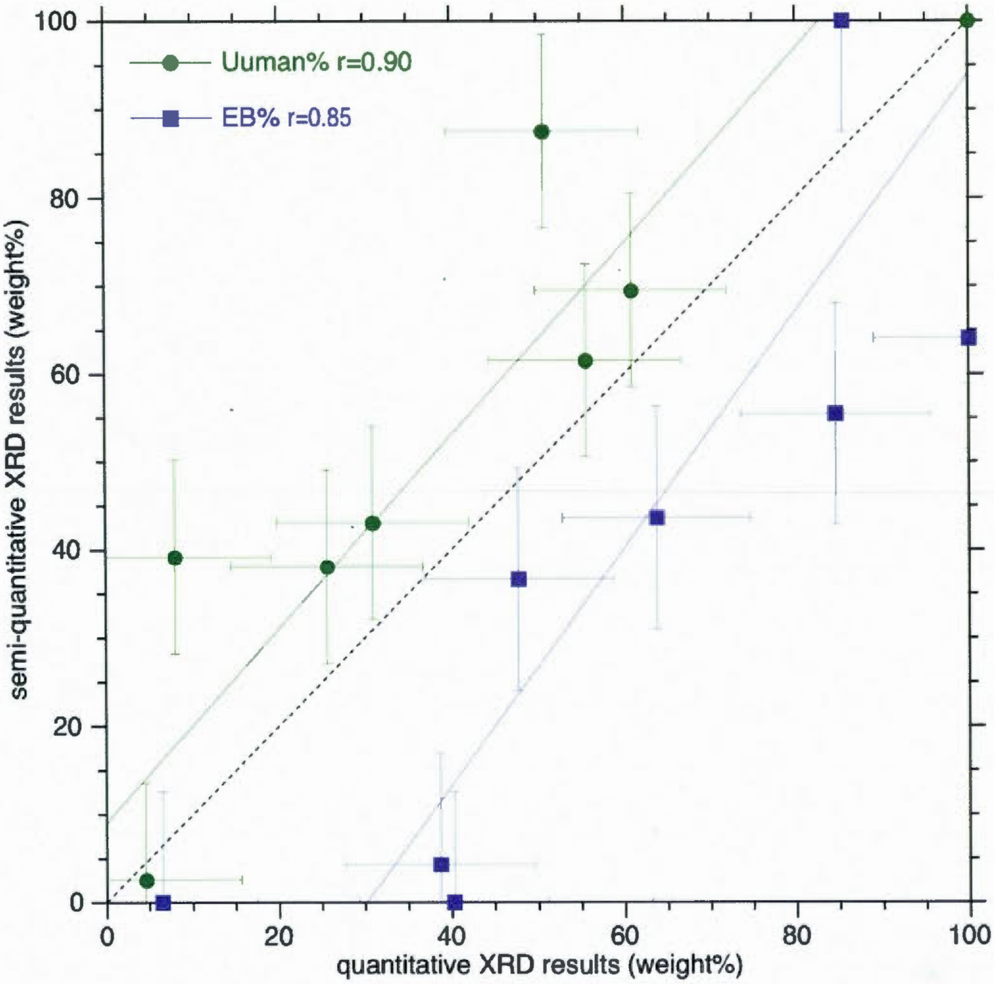

S2. Comparison of SedUnMix provenance weight% results for Uummannaq and eastern Baffin Island based on mineralogical assemblages measured by both XRD techniques (see S1). The error bars represent the standard error.

CONCLUSION

Les résultats de l'approche multidisciplinaire présentés dans cette thèse ont permis de répondre à 2 objectifs majeurs, c'est-à-dire : (1) établir une chronostratigraphie fiable d'une séquence sédimentaire essentiellement glacio-marine et (2) reconstituer la variabilité des marges glaciaires sur le pourtour de la baie de Baffin durant le dernier cycle glaciaire. La reconstitution et la compréhension de la dynamique des marges glaciaires exigent une connaissance précise de leur activité dans le temps afin d'appréhender les mécanismes glaciaires intrinsèques. Cependant, l'érosion des traces géologiques directes des fluctuations des marges glaciaires (e.g., moraines, stries), contraint à l'étude d'empreintes indirectes enregistrées par les sédiments marins comme unique source d'information. Toutefois, l'analyse de ces séquences sédimentaires dans les bassins profonds arctiques (la baie de Baffin dans ce cas-ci) présente des difficultés supplémentaires de datation. En effet, les méthodes traditionnelles de chronostratigraphie, tels que la stratigraphie isotopique ($\delta^{18}O$ sur les tests de foraminifères) ou la datation par le radiocarbone (i.e., ^{14}C), ne permettent pas d'établir des modèles d'âge convaincants dans ces bassins (Hillaire-Marcel et de Vernal, 2008 ; Polyak et Jakobsson, 2011). L'approche paléomagnétique utilisée dans cette thèse a dès lors été prioritairement motivée par cette question chronostratigraphique, avant de permettre une lecture environnementale de la variabilité des lithofacies sédimentaires et de leur origine glaciaire éventuelle.

Les analyses paléomagnétiques de haute résolution, associées à l'examen approfondi des propriétés magnétiques des sédiments de la carotte HU2008-029-016PC, permettent d'établir que l'enregistrement de l'aimantation rémanente naturelle à travers la majeure partie de la carotte est principalement le fait des minéraux magnétiques de faible coercivité, tel que la magnétite ou la titanomagnetite, et de taille « *pseudo-single domain* » (PSD). Ces résultats sont particulièrement importants puisqu'ils autorisent l'utilisation des données paléomagnétiques comme outil chronostratigraphique (Tauxe, 1993). Cependant, une corrélation significative a également été établie entre la lithologique et les signatures magnétiques. Il s'agit d'un schéma classique dans un bassin sédimentaire confiné ayant été affecté de toutes parts par l'activité glaciaire. Ainsi, les couches carbonatées (i.e., *Baffin Bay Detrital Carbonate*, BBDC) sont-elles décrites par des grains grossiers (i.e., PSD à *Multi-Domain* - MD) et caractérisées par des valeurs plus faibles de la concentration des grains ferrimagnétiques; tandis que les unités stratigraphiques couvrant les périodes Holocène et du dernier maximum glaciaire sont caractérisées par des grains plus fins (i.e., PSD à *Single Domain* – SD) et des concentrations de grains ferrimagnétiques plus élevées. Il y a deux corollaires majeurs à ces résultats, premièrement l'utilisation directe des données paléomagnétiques ne peut être envisagée sans un "filtrage" préalable des données et, deuxièmement, la variabilité environnementale des propriétés magnétiques informe sur l'origine, le transport et le dépôt des sédiments glaciomarins (Stein, 2008).

Dans le premier chapitre de cette thèse nous avons reconstruit le signal de paléointensité relative (PIR) du champ magnétique terrestre enregistré dans les sédiments en enlevant les couches problématiques (e.g., grains magnétiques MD) et en normalisant le signal de l'aimantation rémanente naturelle par l'aimantation rémanente anhystérétique induite et mesurée sur la séquence sédimentaire. Cette dernière étape permet de s'affranchir de la variabilité de la concentration des grains magnétiques, tandis que le retrait des couches problématiques diminue significativement le bruit induit par les variations lithologiques (e.g., taille de grain). Afin d'établir un modèle d'âge pour la séquence sédimentaire étudiée, nous avons corrélé le signal de paléointensité relative de la carotte PC16 aux courbes de référence des changements du champ magnétique terrestre enregistrées et compilées (Laj et al., 2000) à travers le monde, grâce à des archives bien datées telles que les carottes de sédiments marins de bassins océaniques plus ouverts (Stoner et St-Onge, 2007). Sur base de 35 points de liaisons (i.e., pics et creux), nous avons établi une chronologie fiable recouvrant le dernier cycle climatique (i.e., depuis 115 ka BP). Les directions calculées (i.e., inclinaison et déclinaison) sur l'enregistrement de l'aimantation rémanente naturelle ont également permis de retracer les fluctuations millénaires de l'orientation du champ magnétique terrestre. Nous avons en outre clairement retracé deux excursions géomagnétiques bien connues et datées, soient les excursions de Laschamp et de la mer de Norvège-Groenland (Lund et al., 2006). Ces deux excursions ont permis de consolider notre modèle d'âge en ajoutant 2 points d'ancrages consistant à la corrélation basée sur la seule PIR. Enfin, nous avons obtenu 3 âges ^{14}C couvrant la déglaciation qui ont également confirmé la fiabilité du modèle d'âge établi. Ce modèle d'âge est conforme à certains modèles d'âge préalablement estimés (Andrews et al., 1998 ; de Vernal et al., 1987), mais il ajoute une précision temporelle accrue et, surtout, permet de s'affranchir des hypothèses émises pour les soutenir (permettant d'éviter des raisonnements circulaires dans l'interprétation des signaux climatiques). En effet, Andrews et al (1998) ont établi leur cadre chronostratigraphique sur la base d'un lien hypothétique entre les dépôts des couches carbonatées et les interstadiaires majeurs enregistrés dans les carottes de glace groenlandaises. La résolution temporelle proposée ici est essentielle pour interpréter les origines et les liens entre les dépôts sédimentaires et la variabilité climatique ou océanographique.

Dans le deuxième chapitre de cette thèse, nous avons démontré l'influence des glaciers du nord de la baie (i.e., calottes innuitienne et NE-laurentidienne) sur le "patron de sédimentation" de la baie de Baffin. Sur la base d'analyses minéralogiques des carbonates associées à des données granulométriques, de microfluorescence X et aux propriétés magnétiques des grains, nous avons identifié 14 couches carbonatées grossières. L'identification précise des couches carbonatées et l'utilisation d'une chronologie fiable a permis de renforcer l'interprétation en ce qui a trait à leur provenance, mais, surtout, a permis de proposer des relations causales entre leur dépôt, transport et origine. Des teneurs élevées en dolomite (>35%) et chlorite ont confirmé une provenance nordique (i.e., courants de glace situés dans les détroits de

Lancaster, Jones et Nares), tandis que la distribution des grains grossiers et la présence de graviers suggèrent un transport par la glace (i.e., glace de mer et icebergs) et par les courants d'eaux de fonte associés. Nos résultats appuient les modélisations récentes du mode de croissance des calottes glaciaires régionales (Ganopolski et al., 2010 ; Stokes et al., 2012). En effet, la première couche de sédiments carbonatés est liée à une croissance rapide des calottes NE-laurentidienne et innuitienne, immédiatement après le dernier interglaciaire (i.e., dès le MIS5d), et au développement rapide de leurs exutoires à bases marines, vers les détroits de Lancaster, Jones et Nares, dès 115 ka BP. Sur base de la chronologie établie précédemment, nous avons démontré que ces couches carbonatées n'étaient pas en phase avec les événements carbonatés de Heinrich enregistrés dans l'Atlantique Nord (Andrews et al., 1998; Hemming, 2004). Nous avons plutôt associé ces dépôts avec les phases de réchauffement des interstadiaires enregistrés dans les carottes de glaces groenlandaises (Dansgaard et al., 1993). Contrairement à l'hypothèse émise par Andrews et al. (1998), nous avons principalement associé le début des dépôts de ces couches avec des interstadiaires suivant de longues périodes de croissance glaciaires, plutôt que par les interstadiaires majeurs. Nous avons décrit deux types de couches BBDC : (1) des couches s'étant déposées durant de longues périodes, typiquement de 3 à 6 ka ; et (2) des dépôts brefs n'excédant pas 1.5 ka. Nous expliquons l'origine de ces dépôts par deux processus distincts : (1) un vélage persistant d'icebergs par des glaciers étendus, durant des périodes d'avancées glaciaires ou durant des lents retraits graduels de ces glaciers et (2) des phases abruptes de vêlage correspondant aux épisodes les plus chauds des interstadiaires. Nos données suggèrent que les marges glaciaires au nord de la baie de Baffin étaient sensibles aux changements et réorganisations climatiques/océaniques de haute fréquence telles que les oscillations de Dansgaard-Oescheger (Dansgaard et al., 1993; Wolff et al., 2010).

Dans la troisième partie de cette thèse, nous nous sommes intéressés à la provenance latérale des sédiments (i.e., Groenland et l'île de Baffin). Pour ce faire, nous avons étudié les assemblages minéralogiques de la carotte PC16 et les avons comparés aux sources potentielles au pourtour de la baie de Baffin établies par Andrews et Eberl (2011), sur base d'analyses des sédiments de surface. Nous avons utilisé le programme SedUnMix qui permet de calculer statistiquement les pourcentages en poids de chacune des sources. Les apports sédimentaires de l'Est de l'île de Baffin sont caractérisés par des sédiments grossiers déposés rapidement et correspondant à des débris transportés par la glace ou par des courants de turbidité. Nous avons interprété le synchronisme de ces dépôts haute fréquence avec les couches BBDC comme des réponses similaires des glaciers de sortie des calottes laurentidienne et innuitienne aux forçages climatiques durant des épisodes chauds des oscillations de type de Dansgaard-Oeschger. Les sédiments fins provenant de l'ouest groenlandais, notamment en provenance du système de glaciers d'Uummannaq, se sont quant à eux mis en place durant des périodes froides plus longues (i.e., MIS5d-5b, -4, -2). Une signature sédimentologique distincte durant la période correspondant à un LGM étendu (32-16 ka BP) suggère une avancée continue de la marge glaciaire jusqu'au bord du plateau continental groenlandais, comme le démontrent les observations récentes de Ó Cofaigh et al. (2012), tandis que les avancées précédentes étaient vraisemblablement de moindre envergure. Ces avancées glaciaires groenlandaises sont en phase avec des périodes de niveau marin relativement bas, confirmant le développement important des glaciers groenlandais sur un plateau continental moins profond et/ou la déstabilisation plus aisée des glaciers lors de hausses du niveau marin. La dissymétrie des réponses des glaciers ceinturant la baie de Baffin aux forçages climatiques et océanographiques est expliquée par des instabilités plus fréquentes des étroits glaciers nordiques et de l'île de Baffin, tandis que le large complexe glaciaires groenlandais a maintenu une inertie plus grande lors des réorganisations climatiques et océanographiques rapides.

Nous proposons deux modes principaux qui illustrent la sédimentation dans le centre de la baie de Baffin durant le dernier cycle glaciaire : (1) un mode « normal » constitué de sédiments grossiers transportés par la glace et provenant des glaciers nordiques et de l'île de Baffin correspondant à des périodes où les marges glaciaires étaient situées à proximité des embouchures, et (2) un mode « latéral » caractérisé par des sédiments fins d'origine groenlandaise correspondant à des périodes où les marges glaciaires avançaient loin sur le plateau continental groenlandais (et dans une moindre mesure sur le plateau de l'île de Baffin).

D'un point de vue méthodologique, cette thèse a permis de mettre en évidence le potentiel de l'utilisation de l'approche paléomagnétique pour établir des chronostratigraphies fiables dans des environnements problématiques comme les bassins de l'Arctique.

En guise de perspective, il serait intéressant de préciser la durée de mise en place des différentes unités lithologiques, afin de mieux cerner les processus de dépôt et de transport, par exemple sur base d'approches isotopiques (e.g., U, Th) qui ont donné quelques résultats dans l'Arctique (e.g., Not et Hillaire-Marcel, 2010). Cela permettrait de mieux apprécier la durée des processus sédimentaires et, surtout, d'estimer la durée des phases d'activité glaciaire afin de comparer les taux passés, et récents de recul des glaciers groenlandais (cf. intro, Rignot et Mouginot, 2012). Aussi, il semble judicieux de mieux localiser les sources détritiques en utilisant, par exemple, les isotopes radiogéniques (e.g., Nd, Pb, Sr) des sédiments et ainsi affiner les résultats obtenus sur base de la minéralogie. Enfin, une corrélation de la carotte PC16 avec les séquences sédimentaires disponibles dans la baie de Baffin permettrait probablement l'amélioration du modèle d'âge et établirait un cadre chronostratigraphique régional cohérent afin de mieux chronométrer les différents processus dans le temps et l'espace.

Finalement, les résultats de cette thèse serviront à vérifier et alimenter les modèles afin d'améliorer notre compréhension, et ainsi, aider à pronostiquer l'évolution future des marges glaciaires.

Références

Andrews, J. T., M. Kirby, A. E. Aksu, D. G. Barber, and D. Meese, D. (1998), Late Quaternary Detrital Carbonate (DC-) layers in Baffin Bay marine sediments (67°-74° N): correlation with Heinrich events in the North Atlantic?, *Quat. Sci. Rev.*, 17, 1125-1137.

Andrews, J. T. and D. D. Eberl (2011), Surface (sea floor) and near-surface (box cores) sediment mineralogy in Baffin Bay as a key to sediment provenance and ice sheet variations, *Can. J. Earth Sci.*, 48, 1307-1328.

Dansgaard, W., S. J. Johnsen, H. B. Clausen, D. Dahl-Jensen, N. S. Gundestrup, C. U. Hammer, C. S. Hvidberg, J. P. Steffensen, A. E. Sveinbjörnsdottir, J. Jouzel, and G. Bond (1993), Evidence for general instability of past climate from a 250-kyr ice-core record, Nature 363(6434), 218-220.

de Vernal, A., C. Hillaire-Marcel, A. E. Aksu, and P. Mudie (1987), Palynostratigraphy and chronostratigraphy of Baffin Bay deep sea cores: climatostratigraphic implications, *Palaeogeogr., Palaeoclimatol., Palaeoecol.*, 61, 97-105.

Ganopolski, A., R. Calov, and M. Clausen (2010), Simulation of the last glacial cycle with a coupled climate ice-sheet model of intermediate complexity, *Climate of the Past* 6, 229-244.

Hemming, S. R. (2004), Heinrich events: Massive late Pleistocene detritus layers of the North Atlantic and their global climate imprint, *Reviews of Geophysics* 42(1), RG1005, doi:10.1029/2003RG000128.

Hillaire-Marcel, C., and A. de Vernal (2008), Stable isotope clue to episodic sea ice formation in the glacial North Atlantic, *Earth Planet. Sci. Lett*, 268, 143-150.

Laj, C., C. Kissel, A. Mazaud, J. E. T. Channell, and J. Beer (2000), North Atlantic palaeointensity stack since 75 ka (NAPIS-75) and the duration of the Laschamp event, *Phil. Trans. R. Soc. London, Series B*, 358, 1009-1025.

Lund, S. P., J. S. Stoner, J. E. T. Channell, and G. Acton (2006), A summary of Brunhes paleomagnetic field variability recorded in Ocean Drilling Program cores, *Phys. Earth Planet. Inter.*, 156, 194-204.

Not, C., and C. Hillaire-Marcel (2010), Time constraints from ^{230}Th and ^{231}Pa data in late Quaternary, low sedimentation rate sequences from the Arctic Ocean: An example from the northern Mendeleev Ridge, *Quaternary Science Review*, 29(25-26), 3665-3675.

Ó Cofaigh, C., J. T. Andrews, A. E. Jennings, J. A. Dowdeswell, K. Hogan, A. A. Kilfeather, and C. Sheldon (2012), Glacimarine lithofacies, provenance and depositionnal processes on a West Greenland trough-mouth fan, *Journal of Quaternary Science*, doi:10.1002/jqs.2569.

Polyak, L., and M. Jakobsson (2011), Quaternary sedimentation in the Arctic Ocean: Recent advances and further challenges, *Oceanography* 24(3), 52–64, http://dx.doi.org/10.5670/oceanog.2011.55.

Rignot, E., and J. Mouginot (2012), Ice flow in Greenland for the International Polar Year 2008, *Geophys. Res. Lett.*, 39(11), L11501.

Stein, R. (2008), Arctic Ocean Sediments: Processes, Proxies, and Paleoenvironment, Developments in Marine Geology 2, Elsevier, Amsterdam, The Netherlands, pp. 592.

Stokes, C. R., L. Tarasov, and A. S. Dyke (2012), Dynamics of the North American Ice Sheet Complex during its inception and build-up to the Last Glacial Maximum, *Quaternary Science Reviews* 50, 86-104, doi:10.1016/j.quascirev.2012.07.009.

Stoner, J. S., and G. St-Onge (2007), Magnetic stratigraphy in paleoceanography: reversals, excursions, paleointensity and secular variation, in *Developments in Marine Geology. Proxies in late Cenozoic paleoceanography*, vol. 1, edited by C. Hillaire-Marcel, and A. de Vernal, Elsevier, Amsterdam, The Netherlands, 99-137.

Tauxe, L. (1993), Sedimentary records of relative paleointensity of the geomagnetic field: theory and practice, *Rev. Geophys.*, 31, 319-354.

Wolff, E. W., J. Chappellaz, T. Blunier, S. O. Rasmussen, and A. Svensson (2010), Millennial-scale variability during the last glacial: The ice core record, *Quaternary Science Review*, 29, 2828-2838, doi:10.1016/j.quascirev.2009.10.013.